ENGINEERING NANOPOROUS MATERIALS FOR APPLICATION IN GAS SEPARATION MEMBRANES

A Thesis
Presented to
The Academic Faculty

by

Tae-Hyun Bae

In Partial Fulfillment
of the Requirements for the Degree
Doctor of Philosophy in Chemical Engineering
in the School of Chemical & Biomolecular Engineering

Georgia Institute of Technology
December 2010

ENGINEERING NANOPOROUS MATERIALS FOR APPLICATION IN GAS SEPARATION MEMBRANES

Approved by:

Dr. Christopher W. Jones, Co-advisor
School of Chemical & Biomolecular Engineering
Georgia Institute of Technology

Dr. Sankar Nair, Co-advisor
School of Chemical & Biomolecular Engineering
Georgia Institute of Technology

Dr. William J. Koros
School of Chemical & Biomolecular Engineering
Georgia Institute of Technology

Dr. J. Carson Meredith
School of Chemical & Biomolecular Engineering
Georgia Institute of Technology

Dr. Zhong Lin Wang
School of Materials Science and Engineering
Georgia Institute of Technology

Date Approved: August 3, 2010

To my wife, Jieun

ACKNOWLEDGEMENTS

I would like to express my sincere gratitude to my advisors, Prof. Christopher Jones and Prof. Sankar Nair, for providing me an opportunity to work with them at Georgia Tech, and for extending continuous encouragement, support and guidance. I am also grateful to my committee members, Prof. William J. Koros, Prof. J. Carson Meredith and Prof. Zhong Lin Wang, for providing valuable suggestions and for their critical reading of this thesis.

I would like to thank my co-workers for their kind helps. Junqing and Jong Suk in Dr. Koros group helped me to get gas permeation results of my membranes. Josh Francis, an undergraduate researcher, helped me a lot by making large amount of zeolites, a time-consuming job. I want to thank all members of Jones and Nair research groups. They have helped me a lot in my research work and made me enjoy the time at Georgia Tech for the last four years. I'm also very grateful to many Korean friends in ChBE Korean Student Association. They have provided my wife and me of very joyful time in this foreign country since 2006.

The important support has come from my parents, who have always stood beside me. Lastly and most importantly, I would like to thank my wife, Jieun. This accomplishment could not be made without her support and sacrifice.

TABLE OF CONTENTS

LIST OF TABLES

Page

LIST OF FIGURES

Page

SUMMARY

The main theme of this dissertation is to engineer nanoporous materials and nanostructured surfaces for applications in gas separation membranes. Tunable methods have been developed to create inorganic hydroxide nanostructures on zeolite surfaces, and used to control the inorganic/polymer interfacial morphology in zeolite/polymer composite membranes. The study of the structure-property relationships in this material system showed that appropriate tuning of the surface modification methods leads to quite promising structural and permeation properties of the membranes made with the modified zeolites.

First, a facile solvothermal deposition process was developed to prepare roughened inorganic nanostructures on zeolite pure silica MFI crystal surfaces. The functionalized zeolite crystals resulted in high-quality 'mixed matrix' membranes, wherein the zeolite crystals were well-adhered to the polymeric matrix. Substantially enhanced gas separation characteristics were observed in mixed matrix membranes containing solvothermally modified MFI crystals. Gas permeation measurements on membranes containing nonporous uncalcined MFI revealed that the performance enhancements were due to significantly enhanced MFI-polymer adhesion and distribution of the MFI crystals. Solvothermal deposition of inorganic nanostructures was successfully applied to aluminosilicate LTA surfaces. Solvothermal treatment of LTA was tuned to deposit smaller/finer $Mg(OH)_2$ nanostructures, resulting in a more highly roughened zeolite surface. Characterization of particles and mixed matrix membranes

revealed that the solvothermally surface-treated LTA particles were promising for application in mixed matrix membranes.

Zeolite LTA materials with highly roughened surfaces were also successfully prepared by a new method: the ion-exchange-induced growth of $Mg(OH)_2$ nanostructures using the zeolite as the source of the Mg^{2+} ions. The size/shape of the inorganic nanostructures was tuned by adjusting several parameters such as the pH of the reagent solution and the amount of magnesium in the substrates and systematic modification of reaction conditions allowed generation of a good candidate for application in mixed matrix membranes. Zeolite/polymer adhesion properties in mixed matrix membranes were improved after the surface treatment compared to the untreated bare LTA. Surface modified zeolite 5A/6FDA-DAM mixed matrix membranes showed significant enhancement in CO_2 permeability with slight increases in CO_2/CH_4 selectivity as compared to the pure polymer membrane. The CO_2/CH_4 selectivity of the membrane containing surface treated zeolite 5A was much higher than that of membrane with untreated zeolite 5A.

In addition, the use of metal organic framework (MOF) materials has been explored in mixed matrix membrane applications. ZIF-90 crystals with submicron and 2-μm sizes were successfully synthesized by a nonsolvent induced crystallization technique. Structural investigation revealed that the ZIF-90 particles synthesized by this method had high crystallinity, microporosity and thermal stability. The ZIF-90 particles showed good adhesion with polymers in mixed matrix membranes without any compatibilization. A

significant increase in CO_2 permeability was observed without sacrificing CO_2/CH_4 selectivity when Ultem® and Matrimd® were used as the polymer matrix. In contrast, mixed matrix membranes with the highly permeable polymer 6FDA-DAM showed substantial enhancement in both permeability and selectivity, as the transport properties of the two phases were more closely matched.

CHAPTER 1

INTRODUCTION

1.1 Gas Separation Using Membranes

Membrane-based gas separation offers several advantages over conventional gas separation processes, including lower energy requirement and lower operating costs [1]. With the increased cost of energy, membrane technology has become a more attractive option for gas separations [2]. To be more useful for separation or purification process, membranes must exhibit a number of characteristics such as high permeability, high selectivity, mechanical stability and low cost. The progress made in development of new membrane materials has played an important role in adoption of membranes for separation and purification in many industrial fields. Well-known examples are natural gas purification by removal of carbon dioxide, hydrogen separation from nitrogen in ammonia purge gas stream and nitrogen production from air. [3].

1.1.1 Polymeric Membranes

The most commonly used gas separation membranes are made with polymeric materials such as silicone rubber, cellulose acetate, polysulfone for O_2/N_2 separation and polyimides for O_2/N_2 and CO_2/CH_4 separations [3]. It is known that the gas separation in nonporous polymer membranes is based on solution-diffusion mechanism, involving molecular scale interactions of the permeating gas molecule with the membrane polymer [3-6]. It is assumed that gas molecules are sorbed by the membrane at one interface, transported by diffusion across the membrane through the free volume of polymer, and desorbed at the other interface. According to the solution-diffusion model, the permeation

of molecules through membranes is controlled by two major parameters, diffusivity and solubility coefficient. Diffusivity is a measure of the mobility of individual molecules passing through the free volume of the polymer and the solubility equals the ratio of sorption uptake normalized by some measure of uptake potential, such as partial pressure [4-5]. In general, the diffusion coefficient decreases and the solubility coefficient increases with an increase in the molecular size of the gas [4, 7]. For high-performance polymer membranes, both high permeability and selectivity are desirable. The higher the permeability, the lower membrane area required to treat a given throughput rate of the feed gas mixture; and the higher the selectivity, the higher the purity of the product gas under equivalent feed and permeate conditions [4].

Polymers provide a range of desirable properties that are important for gas separation processes including low cost, good mechanical stability and processability [1]. A polymer material with a high glass transition temperature (T_g), high melting point, and high crystallinity is generally preferred [4]. Glassy polymers (i.e., polymers below their T_g) have stiffer polymer backbones and therefore let smaller molecules such as H_2 and He pass more quickly, and larger molecules such as hydrocarbons permeate the membrane more slowly [5, 7]. To increase the membrane selectivity, either the diffusivity or the solubility should be enhanced; however, polymers that are more permeable are generally less selective and vice versa. A rather general trade-off exists between permeability and selectivity, resulting in polymer upper bound limit [2, 8]. This is illustrated in Fig. 2-1, which shows an upper bound in the relationships between the CO_2/CH_4 selectivity and the permeability of CO_2 for various glassy and rubbery polymers. A substantial

research effort has been directed at overcoming the limit imposed by the upper bound. Several successes have been reported over the past two decades and the upper bound has been redrawn recently as a result. The most prominent new work is thermally rearranged (TR) polymers [9-10], capable of molecular sieving. But the trade-off behavior is still valid for most polymeric membranes, as long as gas transport depends on the solution-diffusion mechanism.

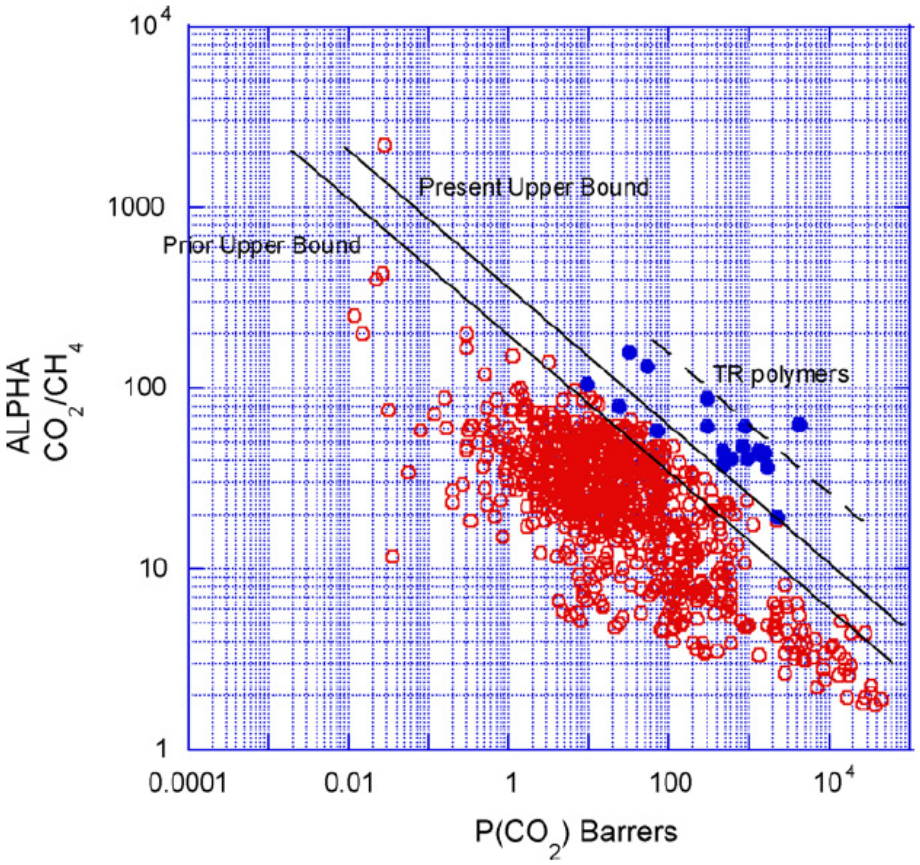

Fig.1-1 Upper bound correlation for CO_2/CH_4 separation (TR, thermally rearranged). Prior and present upper bounds were drawn in 1991 and 2008, respectively [2].

1.1.2 Inorganic Molecular Sieve Membranes

Extensive work on inorganic membranes, such as zeolite membranes and carbon molecular sieve membranes [11-22], has been done over the past 25 years and the state of the art of inorganic molecular sieve membranes has been reviewed elsewhere [4, 11, 23-29]. So far, zeolite membranes with various frameworks, such as MFI [30-49], DDR [50-53], LTA [54-68], CHA [69-71], FAU [72-81] and MOR [82-90], and with various compositions, such as silicate, aluminosilicate, aluminophosphate [91-92] and silicoaluminosilicate [93-105], have been synthesized on porous supports. In most cases, the performance of zeolite membranes is much better than that of polymeric membranes due to the accurate size/shape discrimination of gas molecules through micropores of zeolites. In addition, because the thermal and chemical stabilities of the materials are generally outstanding, the potential applications of zeolite membranes are wide ranging. These zeolite membranes, however, often have poor processability and may be difficult to fabricate with defect-free morphologies for large-scale applications. Although some successful applications of inorganic membranes have been reported in liquid phase separations such as dehydration of organics, gas separation is less tolerant to membrane imperfections. Furthermore, zeolites membranes are brittle and the manufacturing cost is also very high compared to polymeric membranes [24].

1.1.3 Mixed Matrix Membranes

In spite of good processability and mechanical stability, the performance of polymeric membranes is generally limited by trade-off between permeability and

selectivity. On the other hand, some inorganic membranes, such as zeolite and carbon molecular sieve membranes, offer much higher permeability and selectivity than polymeric membranes, but are expensive and difficult for large-scale manufacture. Therefore, it is highly desirable to provide an alternate, cost effective membrane in a position above the trade-off curves between permeability and selectivity.

Due to the desire for a more easily manufacturable yet highly selective membranes, a new type of membranes (referred to as "mixed matrix membranes" or "MMMs" in this work), has been developed. MMMs are hybrid membranes containing nanoporous materials such as zeolites, carbon molecular sieves or metal organic frameworks embedded in a polymeric membrane matrix. MMMs have the potential to achieve higher selectivity with greater permeability compared to existing polymer membranes, due to the good size/shape selectivity of the dispersed nanoporous molecular sieve material, while maintaining several of the advantages of polymeric materials such as relative ease of processing and good mechanical stability.

The performance of a MMM can be estimated to a first approximation by the Maxwell model [1, 4, 106]. This model is well-understood and accepted as a simple, but effective, tool for estimating MMM properties. The Maxwell model equation is:

$$P_{MM} = P_C \left(\frac{P_D + 2P_C - 2\Phi_D (P_C - P_D)}{P_D + 2P_C + \Phi_D (P_C - P_D)} \right) \quad (1)$$

In this equation, P is permeability, Φ_D is the volume fraction of the dispersed (molecular

sieving) material, the MM subscript refers to the mixed matrix membrane, the C subscript refers to the continuous polymeric matrix, and the D subscript refers to the dispersed material phase. Provided the volume fraction of the dispersed phase and the permeability of a gas through the two pure materials are known, the performance of the resultant MMM can be readily predicted by Equation 1.

Highlighted potential applications for MMMs include separation and purification of gas mixtures such as O_2/N_2 separation [107-110] and CO_2 removal from natural gas [109, 111-112] as well as pervaporation of liquid mixtures [113-123]. However research has shown that the interfacial region, which is a transition phase between the continuous polymer matrix and the dispersed sieve phase, is of particular importance in successful mixed matrix membrane formation [124-128]. The type of morphology that forms at the interfacial region has a direct impact on the membrane's separation properties, and its ability to reach the predicted Maxwell model properties. As shown in Fig. 1-2, the ideal membrane will exhibit both an increase in selectivity and permeability as the dispersed phase volume fraction is increased, and the Maxwell model can be used to estimate these separation properties.

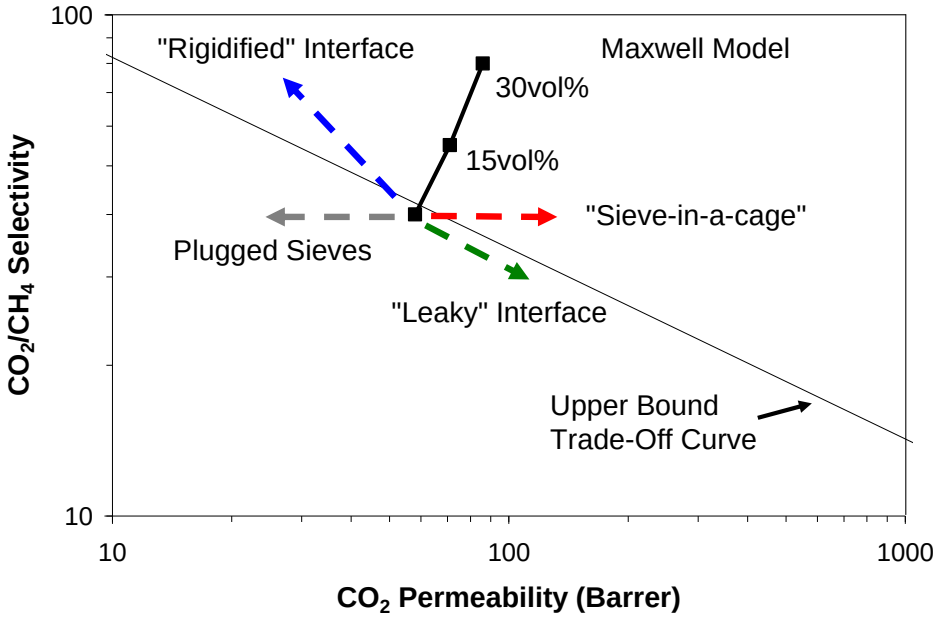

Fig.1-2 Possible interfacial morphologies for mixed matrix membranes and their effect on CO_2/CH_4 gas transport properties; center point represents a polymer membrane with no sieving [4].

Poor interfacial adhesion can result in interfacial voids that are much larger than the penetrating molecules. The morphology of such a composite has been described as "sieve-in-a-cage" (Fig. 1-3). These voids are non-selective and permit the transport of both the slow and fast penetrant, thereby preventing the membrane from reaching the performance enhancement predicted by the Maxwell model. This was a common problem reported when glassy polymers were used as a matrix without considering its compatibility with the dispersed material. Likewise, an interface with molecular-scale or sub-molecular scale excess free volume between polymer chains can also occur, and this produces a small decrease in selectivity below that of the pure polymer while still demonstrating an increase in permeability. This non-ideal case has been called a "leaky

interface" [128].

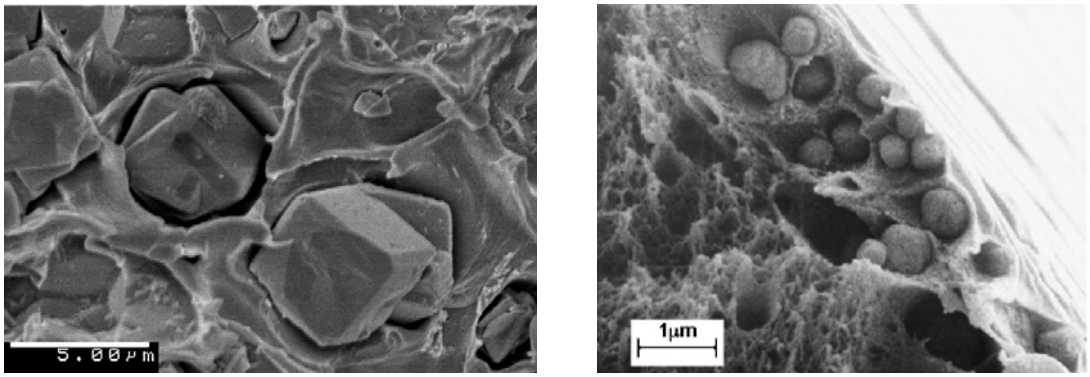

Fig. 1-3 SEM of a typical "sieve-in-a-cage" morphology; (a) dense film [128] and (b) asymmetric hollow fiber membrane [129].

Although several approaches have previously been reported to lead to good sieve/polymer interfacial adhesion, a reduction in mobility and free volume in the polymer is also believed to occur near the sieve surface. This case has been called a "rigidified interface" [128]. The layer of rigidified polymer that surrounds the molecular sieves displays a lower permeability than the bulk polymer matrix. Thus, the overall membrane permeability is lowered, as shown in Fig. 1-2. The enhancement in selectivity caused by molecular sieves dispersed may not be affected significantly unless the rigidified polymer layer prevents permeation inside the molecular sieves. Potential plugging of molecular sieve pores with solvents, water, contaminants, or other transport-limiting entities is also a concern. If the pores are completely blocked, permeability of the membrane decreases significantly, with no change in selectivity, as shown in Fig. 1-2.

1.1.4 Engineering Interfacial Morphology in Mixed Matrix Membranes

Compatibilization of the molecular sieve and polymer is indispensable for successful fabrication of mixed matrix membranes. For this purpose, the surfaces of zeolites have been modified by various methods. Silane chemistry is a well-studied method to functionalize the surface of zeolites or silica, and can also be used for coupling of the filler and the polymer matrix in the composites. In general, silane coupling agents have two functional moieties: reactive surface groups such as alkoxides at one end, and a functional group intended to interact with the polymer at the other end. The coupling agents are anchored on the zeolite surface by condensation reactions between the silanol groups on the zeolite surface and the alkoxides in the silane reagent. By covalent (or other) bonding of the pendant functional group at the other end of the coupling agent with the functional groups in the polymer chains, the coupling process between inorganic fillers and polymers is accomplished. For example, as shown in Fig. 1-4, silane coupling agents with amine functionalities can be used to fabricate mixed matrix membranes with polyimides since the pendant amine group can react with the imide rings in the polymer to form covalent bonds [125]. However, this method often resulted in other non-ideal morphologies, such as rigidified polymer layers [126] and leaky interfaces [125]. In other studies, polyimides with carboxylic acid groups were synthesized to generate chemical bonding sites for the amine groups in silane coupling agents [130]. Adhesion between the zeolite and polymer can also be enhanced without chemical bonding between the coupling agent and polymer, for example, by van der Waals or hydrogen bonding interactions [129, 131]. However, Husain et al. reported that there can be non-selective

gas permeation through gaps between the zeolite and polymer due to insufficient organic loading [129]. Similarly, enhancement of gas separation performance of mixed matrix membranes made with zeolite LTA and a polysulfone was not satisfactory when a silane coupling agent with amine functionalities was used [131].

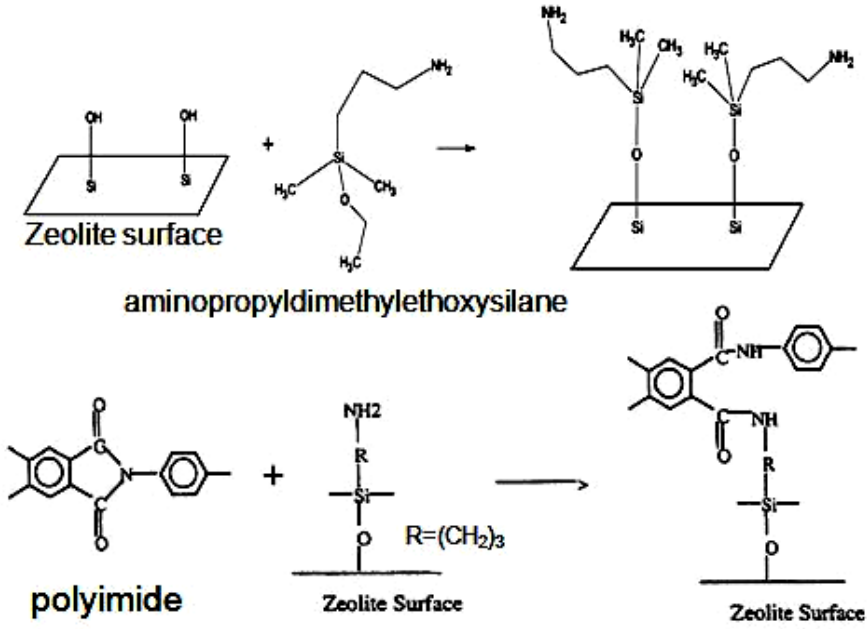

Fig. 1-4 Chemical coupling between zeolite and polyimide using a silane coupling reagent [125].

Recently, a new method to improve adhesion between zeolites and polymers has been suggested. Shu et al. reported that a "nano-whisker structure" could be created on the surface of zeolite LTA via a halide/Grignard route, as shown in Fig. 1-5 [132-133]. Highly roughened surfaces created by formation of $Mg(OH)_2$ nanocrystals on the zeolite surface provided enhanced interactions at the polymer/particle interface, via possible adsorption and interlocking of polymer chains in the whisker structure. In contrast, a

membrane with untreated zeolite showed a typical “sieve-in-a-cage” morphology. The resultant mixed matrix membrane demonstrated significant improvement in both O_2/N_2 and CO_2/CH_4 separation performance. However, this method utilizes a complicated procedure, a series of reactions of the aluminosilicate zeolite with $SOCl_2$, CH_3MgBr, isopropyl alcohol and water. Furthermore, $SOCl_2$ and CH_3MgBr are unstable and should be handled in inert environment. Thus, the development of rational methods to create such nanostructures, using more benign chemistry would be highly attractive.

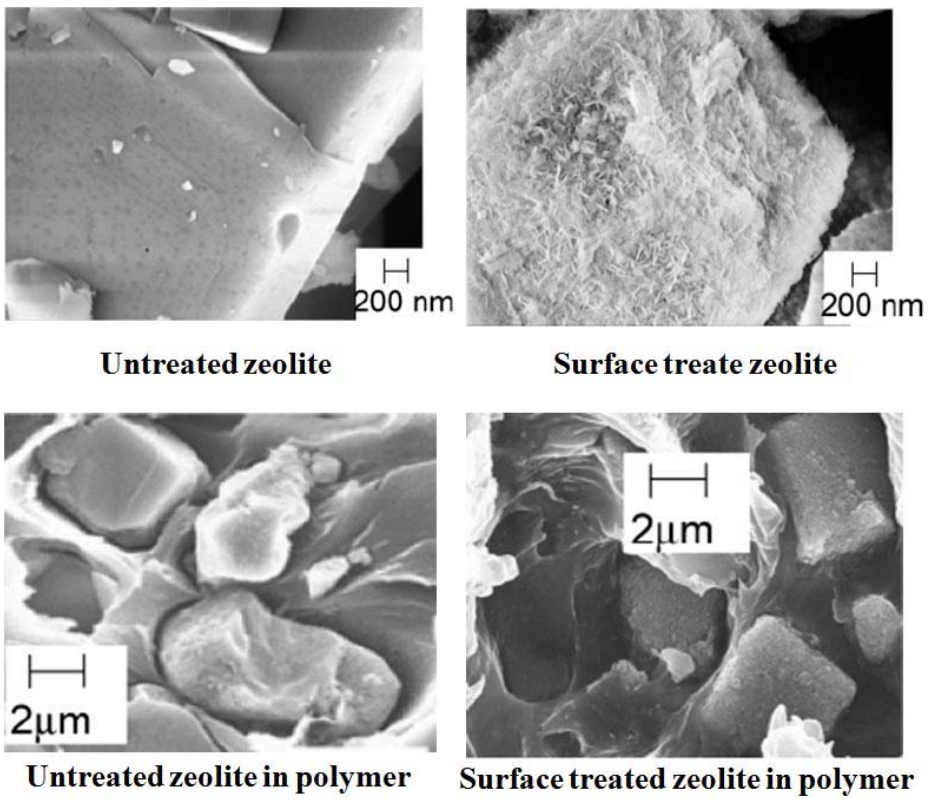

Fig. 1-5 The control of sieve/polymer interfacial morphology in mixed matrix membranes by the formation of $Mg(OH)_2$ nano-whisker structures on zeolite LTA via a halide/Grignard route [132].

1.2 Zeolite Molecular Sieves

1.2.1 Introduction to Zeolites

Zeolites are microporous crystalline aluminosilicates, composed of TO_4 tetrahedra (T=Si, Al) with O atoms connecting neighboring tetrahedral [23]. Zeolites composed of pure silica (SiO_2) are uncharged solids. However, the incorporation of Al (+3 charge) into the silica framework makes the framework negatively charged and requires the presence of extraframework cations to keep the overall framework neutral. The extraframework cations are reversibly exchangeable and give rise to the ion-exchange chemistry of these materials. The applications of zeolites stem from their highly ordered nanometer-scale pores and channels, which are a result of the topology of the framework.

The amount of Al within the framework can vary over a wide range, with Si/Al=1 to infinity (pure silicates). The lower limit of Si/Al=1 of a zeolite framework arises because the bonding of adjacent AlO_4^- tetrahedra is not favored due to electrostatic repulsion [23]. The framework composition depends on the synthesis conditions and postsynthesis modifications, such as dealumination, have also been developed. As the Si/Al ratio of the framework increases, the hydrothermal stability as well as the hydrophobicity increases. The concentration and strength of acid sites (when H^+ are the cations) are also determined by the Si/Al ratio, and are a very important property for applications in catalysis.

Fig. 1-6 shows the framework projections and the sizes of the pores for

commonly studied frameworks. The crystalline nature of the framework ensures that the pore openings are uniform throughout the crystal and can readily discriminate against molecules with dimensional difference less that 0.1 nm, giving rise to the name molecular sieves.

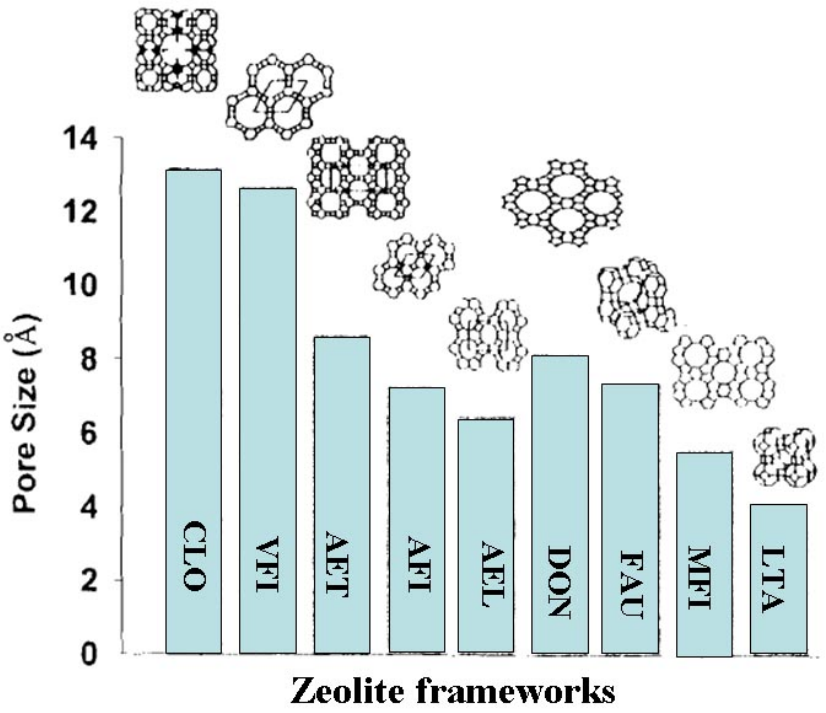

Fig. 1-6 Comparison of pore sizes of different framework structures [23].

Other elements such as B, Ge, Zn, P and transition metals, can also be incorporated into the framework, and the resulting solids are referred to as crystalline molecular sieves [23]. Aluminophosphates (AlPOs) have strictly altering AlO_2^- and PO_2^+ units, and the framework is neutral, organophilic and nonacidic. Substitution of P by Si

leads to silicoaluminophosphates (SAPOs), with extraframework cations for charge balance. Metal cations can also be introduced into the framework, including transition metal ions such as Co, Fe, Mn and Zn. Discovery of these solids has led to the development of several new structures [134].

Zeolites are extensively used in many applications. As adsorbents, zeolites are used for removal of small polar or polarizable molecules (kinetic selectivity) usually by aluminum rich zeolites, and (sorption selective) bulk separations based on molecular sieving process. Examples are drying, CO_2 and sulfur compound removals n-/iso-paraffin separation, xylene separation and air separation [23, 135]. Zeolites are industrially important catalysts promoting size/shape selective chemical reactions [23, 135]. Hydrocarbon transformation by zeolites, such as alkylation, cracking, hydrocracking and isomerization, is promoted by the strong acidity of zeolites. Zeolites are also widely used in various inorganic and organic chemical reactions. Advantages of zeolites include heterogenization of catalysts for easy separation, doping with metals for selective oxidation chemistry and easy of regeneration of catalysts [23]. As ion-exchange agents, the major use of zeolites is for water softening in detergent industry [23]. Zeolites can also be used for removal of Cs^+ and Sr^{2+} radioisotopes by ion exchange from radioactive waste streams [23, 135]. As discussed in the previous section, zeolites in membrane forms (film or mixed matrix) are used in kinetic separations of molecules based on their size/shape selectivity.

1.2.2 Synthesis of Zeolites

Hydrothermal reaction has been the major method to synthesize zeolites [136]. A typical hydrothermal zeolite synthesis can be described in briefest terms as follows [137]:

1. Amorphous reactants containing silica and alumina are mixed together with a cation source or structure directing agents (SDA), usually in a basic (high pH) medium.
2. The aqueous reaction mixture is heated, often (for reaction temperatures above 100 ^{o}C) in a sealed autoclave.
3. For some time after reaching to the synthesis temperature, the reactants remain amorphous.
4. After the above "induction period", crystalline zeolite product can be detected.
5. Gradually, essentially all amorphous material is replaced by an approximately equal mass of zeolite crystals, which are recovered by filtration, washing and drying.

A prominent series of work investigating the crystallization mechanism of zeolites has been conducted with pure silica-MFI (Silicalite-1) as a model zeolite [138-141]. In a very significant paper, Chang and Bell [138] studied the formation of pure silica-MFI from precursor gels containing tetrapropylammonium (TPA) as a SDA at 90-95 °C using combined characterization by XRD, ^{29}Si MAS NMR and ion exchange. The NMR and ion exchange study suggested that major changes in the gel structure occur during the early stages of reaction. As shown Fig. 1-7, embryonic structures with Si/TPA = 20-24 was formed rapidly upon heating. These first-formed units, approximating to channel intersections and each containing essentially one TPA^{+} cation, were initially

randomly connected but in time became ordered through repeated cleavage and recombination of siloxane bonds, mediated by hydroxide ion. The hydrophobic effect and the isomorphism between water and the silicate structure were invoked to provide a possible mechanism for ZSM-5 nucleation with the following steps: (a) formation of clathrate-like water structure around the template, (b) isomorphous substitution of silicate for water in these cages that resemble MFI channel intersections and (c) progressive ordering of these entities into the final crystal structure. Then crystal growth occurred through diffusion of the same species to the surface of the growing crystallites to give a layer-by-layer growth mechanism as shown in Fig. 1-7 [139-141].

For many applications, not only the framework type and chemical composition but also the size/shape of the zeolite crystals is an important factor affecting overall performance of the processes [23]. For example, the size of the zeolite affects the rate of ion-exchange at a given specific exchange capacity. Gas adsorption kinetics are also a function of the particle size at a given equilibrium adsorption capacity. For the fabrication of mixed matrix composite membranes, size control of zeolites is indispensible, since the zeolite particles should fit in the thin selective skin layer of the membrane. Despite the large number of zeolite types having different structures and chemical compositions, the general features of zeolite crystal growth do not depend on the type of zeolite and a single type of zeolite may be synthesized under variety of conditions [23, 142]. Well known factors influencing on zeolite crystal growth and the size of the resultant crystals are reaction temperature [23, 143-144], synthesis time [143-144], pre-aging [145-146] and the composition of the reagent mixtures, such as pH [23, 145, 147], SDA concentration

[148] and the Si/Al ratio [149-150] .

This thesis describes the hydrothermal synthesis of zeolites MFI and LTA and the resulting solids were used as substrates for surface treatments. The size of the zeolite crystals was controlled by adjusting the parameters mentioned above.

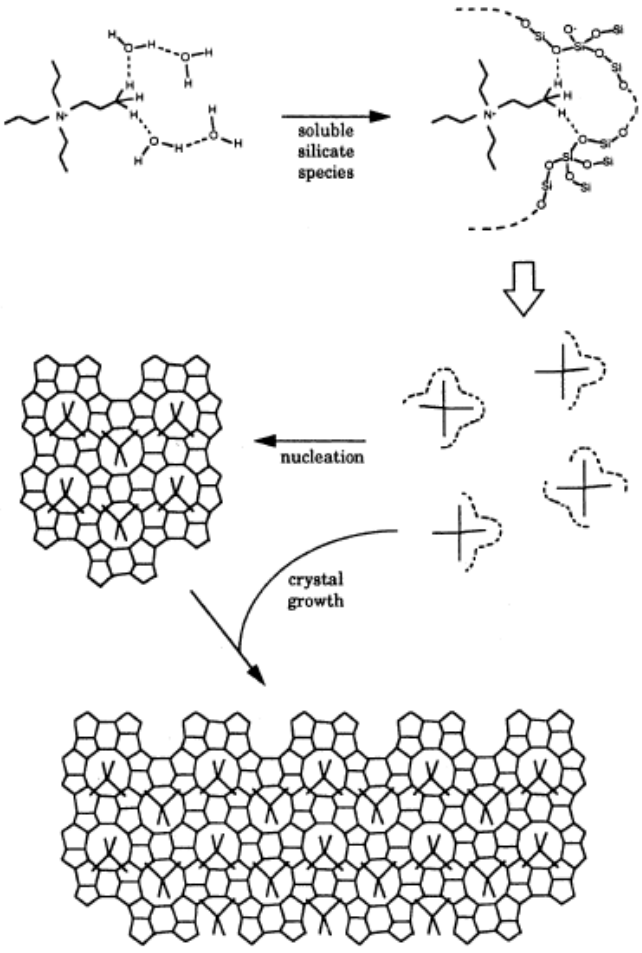

Fig. 1-7 Mechanism of structure direction and crystal growth in the synthesis of TPA-Si-ZSM-5 as envisaged by Burkett and Davis. This view highlights the interactions between TPA and silicate within inorganic-organic composite precursor species [137].

1.3 Metal Organic Frameworks

Metal organic frameworks (MOFs) or porous coordination polymers (PCPs) are new class of nanoporous materials comprised of metal centers connected by various organic linkers to create 1-d, 2-d and 3-d porous structures [151]. In comparison to zeolite-related inorganic materials, MOFs can be more readily synthesized near room temperature [151]. Moreover, the existence of inorganic and organic moieties in the structure allows hydrophilic and hydrophobic parts to coexist within the pores and may have some influence on the adsorption properties [151].

Another interesting feature of MOFs concerns the great variety of cations that can participate in the framework. Indeed, compared to inorganic zeolites which are more based on a few cations, MOFs can accept a wider range of cations that are di-, tri-, and tetravalent. This provides a huge number of possibilities for creating new MOFs. The number of possible MOF materials is drastically increased considering the large choice of functionalized organic linkers that can be associated with the inorganic parts. The most well-known organic linkers contain O or N donors. Typical O donors are carboxylates, phosphonates and rarely sulfonates. All of them, even combined, can provide different possibilities for linkage with the inorganic cations via chelating or single bonds. The nitrogen derivatives such as cyanides, pyridines and imidazoles, are fixed directly to the cation via a single bond. Moreover, the carbon sub-lattice of the linker and the unsaturated metal centers can both be functionalized by post-synthesis approaches, depending on the required applications [152]. For example, the CO_2 adsorption properties of MOFs can be tuned by functionalization with amine groups [153].

MOFs have a wide range of potential applications such as selective gas adsorption [154-155], hydrogen storage [156], catalysis [157] and sensors [158] and are very attractive due to their large pore volumes, surface areas and tunable chemical properties. MOFs are also good materials for application in gas separation membranes because MOFs with various structures are available and the size of the pores and chemical properties of MOFs are tunable. For example, as shown in Fig. 1-8, the IRMOF (isorecticular-MOF) series developed by Yaghi et al. has a wide range of pore dimensions depending on the length of the organic linkers, although all MOFs have the same framework structure [159-160]. ZIF (Zeolitic imidazolate framework)-8, ZIF-65 and ZIF-90 have different functionalities in their imidazole linkers, methyl, nitro and carbonyl groups, respectively, although the framework structure and pore dimension of all of them are identical [161-164]. However, a rational screening process to find promising materials out of the numerous MOFs is a prerequisite for rapid success at a given separation.

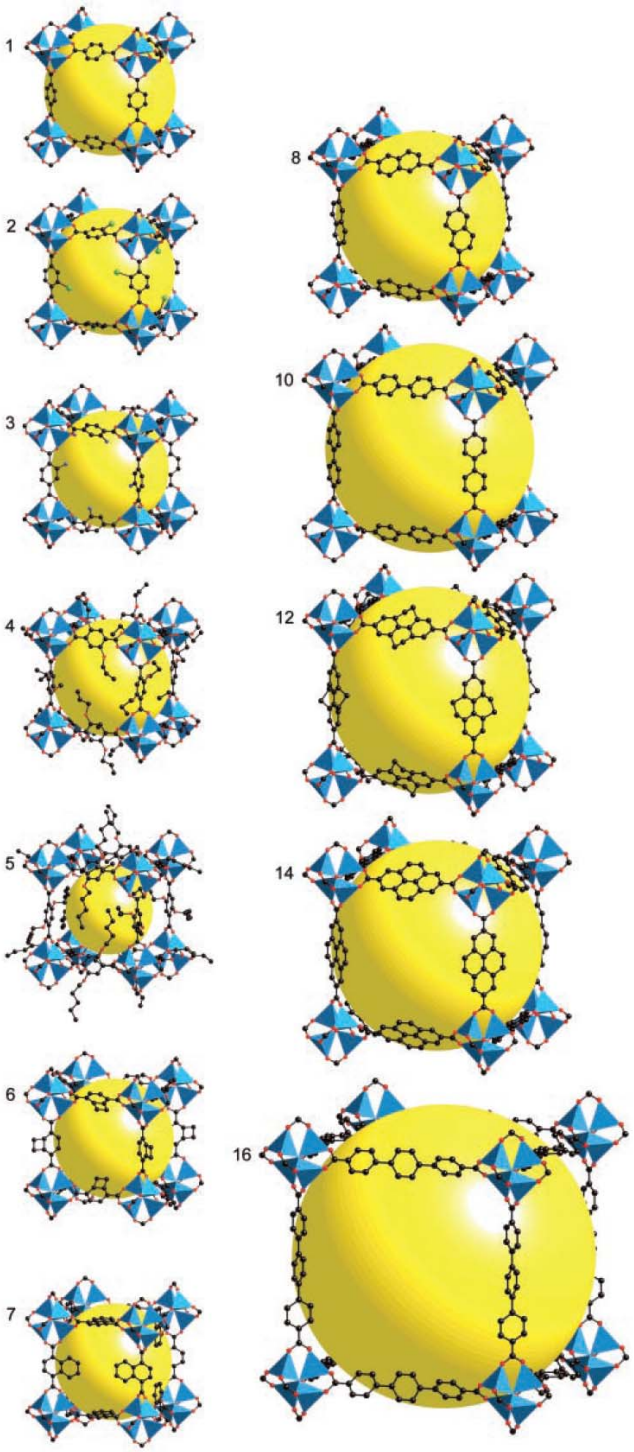

Fig. 1-8 The structures of IRMOF-n (n=1 through 7, 8, 10, 12, 14, and 16), labeled respectively. Zn (blue polyhedra), O (red spheres), C (black spheres), Br (green spheres in **2**), amino-groups (blue spheres in **3**) [160].

1.4 Overall Objective and Strategy

This thesis is focused on engineering the interface between polymers and nanoporous materials such as zeolites and metal organic frameworks and their application in MMMs. So far, zeolites have been widely used for MMM fabrication, and one of key the issues for success is controlling the zeolite/polymer interfacial morphology. As discussed in Section 1.1, micro/nanoscale gaps can be formed at the zeolite/polymer interfaces when bare zeolites are added to polymeric membranes. Functionalization of the zeolite surface using silane chemistry has been used to address this problem but this method is limited in scope, being confined to specific sieve/polymer pairs, often giving rise to other non-ideal morphologies such as leaky interfaces and rigidified polymer chains. Another approach is to create inorganic nanostructures on the surface of the zeolite crystals using benign chemistry to improve the physical interaction between the zeolite and the polymer. In Chapter 2, a method for facile solvothermal deposition of inorganic nanostructures on zeolite surfaces is presented. In this study, pure silica-MFI zeolites were solvothermally modified to create roughened nanostructures at the surface. After the thorough investigation of the structural properties of the surface-modified zeolites, the zeolite/polymer adhesion properties in mixed matrix membranes were rigorously assessed by visual observation with SEM and gas permeation tests. Finally, the CO_2/CH_4 separation performance of mixed matrix membranes containing surface modified MFI was measured. The solvothermal treatment was applied to aluminosilicate LTA surfaces in Chapter 3. The reaction conditions were modified to tune the size/shape of the inorganic nanostructures on the LTA surfaces. Then the structural properties of

these modified zeolites relevant to their application in mixed matrix membranes were thoroughly investigated. In Chapter 4, an ion-exchange induced growth of inorganic nanostructures on zeolite LTA surfaces is reported. This method is designed to create nanostructures on zeolite surfaces in a controlled manner by an aqueous phase reaction. The size/shape of the inorganic nanostructures was successfully tuned by adjusting the reaction conditions. Then, the gas separation performance of the mixed matrix membranes containing surface modified zeolites was tested.

In Chapter 5, a study of mixed matrix membranes containing MOFs is presented. From a screening process, ZIF-90 was selected for the fabrication of mixed matrix membranes since its pore dimensions and functionalities in the organic linker are attractive for CO_2/CH_4 separations. ZIF-90 crystals suitable for application in composite membranes were synthesized by a novel method, namely non-solvent induced crystallization. The structural properties of the ZIF-90 crystals prepared were thoroughly investigated. Mixed matrix membranes were fabricated using various polyimides as the polymer matrix and their CO_2/CH_4 separation properties were investigated. Chapter 6 summarizes the work and discusses suggested future directions to engineer nanoporous materials for application in gas separation membranes.

1.5 References

[1] T.-S. Chung, L.Y. Jiang, Y. Li and S. Kulprathipanja, Prog. Polym. Sci., 32 (2007) 483.

[2] L.M. Robeson, J. Membr. Sci., 320 (2008) 390.

[3] R.W. Baker, Membrane technology and applications, J. Wiley, Chichester ;, 2004.

[4] Advanced membrane technology and applications, Wiley, Hoboken, N.J. :, 2008.

[5] R.E. Kesting, Polymeric gas separation membranes, Wiley, New York :, 1993.

[6] M. Mulder, Basic principles of membrane technology, Kluwer Academic, Dordrecht, Netherlands ;, 1991.

[7] T. Matsuura, Synthetic membranes and membrane separation processes, CRC Press, Boca Raton :, 1994.

[8] L.M. Robeson, J. Membr. Sci., 62 (1991) 165.

[9] H.B. Park, C.H. Jung, Y.M. Lee, A.J. Hill, S.J. Pas, S.T. Mudie, E. Van Wagner, B.D. Freeman and D.J. Cookson, Science, 318 (2007) 254.

[10] J.I. Choi, C.H. Jung, S.H. Han, H.B. Park and Y.M. Lee, J. Membr. Sci., 349 (2010) 358.

[11] K. Briceno, R. Garcia-Valls and D. Montane, Asia-Pac. J. Chem. Eng., 5 (2010) 169.

[12] M.C. Campo, S. Lagorsse, F.D. Magalhaes and A. Mendes, J. Membr. Sci., 346 (2010) 26.

[13] M.C. Campo, F.D. Magalhaes and A. Mendes, J. Membr. Sci., 346 (2010) 15.

[14] B. Zhang, T.G. Wang, Y.H. Wu, Q.L. Liu, S.L. Liu, S.H. Zhang and H.S. Qiu, Sep. Purif. Technol., 60 (2008) 259.

[15] S.H. Han, G.W. Kim, C.H. Jung and Y.M. Lee, Desalination, 233 (2008) 88.

[16] Y.K. Kim, J.M. Lee, H.B. Park and Y.M. Lee, J. Membr. Sci., 235 (2004) 139.

[17] Y.K. Kim, H.B. Park and Y.M. Lee, J. Membr. Sci., 226 (2003) 145.

[18] Y.K. Kim, H.B. Park and Y.M. Lee, J. Membr. Sci., 243 (2004) 9.

[19] Y.K. Kim, H.B. Park and Y.M. Lee, J. Membr. Sci., 251 (2005) 159.

[20] H.B. Park, C.H. Jung, Y.K. Kim, S.Y. Nam, S.Y. Lee and Y.M. Lee, J. Membr. Sci., 235 (2004) 87.

[21] H.B. Park, I.Y. Suh and Y.M. Lee, Chem. Mater., 14 (2002) 3034.

[22] A. Singh-Ghosal and W.J. Koros, J. Membr. Sci., 174 (2000) 177.

[23] S.M. Auerbach, K.A. Carrado and P.K. Dutta (Editors), Handbook of zeolite science and technology, Marcel Dekker, 2003.

[24] J. Caro, M. Noack, P. Kolsch and R. Schafer, Micropor Mesopor Mater., 38 (2000) 3.

[25] A. Tavolaro and E. Drioli, Adv. Mater., 11 (1999) 975.

[26] Z.L. Cheng, Z.S. Chao and H.L. Wan, Prog. Chem., 16 (2004) 61.

[27] Y.S. Li and W.S. Yang, J. Membr. Sci., 316 (2008) 3.

[28] E.E. McLeary, J.C. Jansen and F. Kapteijn, Micropor Mesopor Mater., 90 (2006) 198.

[29] M.A. Snyder and M. Tsapatsis, Angew. Chem. Int. Ed., 46 (2007) 7560.

[30] J. Hedlund, M. Noack, P. Kolsch, D. Creaser, J. Caro and J. Sterte, J. Membr. Sci., 159 (1999) 263.

[31] J.C. Poshusta, R.D. Noble and J.L. Falconer, J. Membr. Sci., 160 (1999) 115.

[32] H.H. Funke, M.G. Kovalchick, J.L. Falconer and R.D. Noble, Ind. Eng. Chem. Res., 35 (1996) 1575.

[33] K. Kusakabe, A. Murata, T. Kuroda and S. Morooka, J. Chem. Eng. Jpn., 30 (1997) 72.

[34] K. Kusakabe, S. Yoneshige, A. Murata and S. Morooka, J. Membr. Sci., 116 (1996) 39.

[35] Z. Vroon, K. Keizer, M.J. Gilde, H. Verweij and A.J. Burggraaf, J. Membr. Sci., 113 (1996) 293.

[36] J. Choi, H.K. Jeong, M.A. Snyder, J.A. Stoeger, R.I. Masel and M. Tsapatsis, Science, 325 (2009) 590.

[37] G.T.P. Mabande, S. Ghosh, Z.P. Lai, W. Schwieger and M. Tsapatsis, Ind. Eng. Chem. Res., 44 (2005) 9086.

[38] Z.P. Lai, G. Bonilla, I. Diaz, J.G. Nery, K. Sujaoti, M.A. Amat, E. Kokkoli, O. Terasaki, R.W. Thompson, M. Tsapatsis and D.G. Vlachos, Science, 300 (2003) 456.

[39] Z.P. Lai and M. Tsapatsis, Ind. Eng. Chem. Res., 43 (2004) 3000.

[40] Z.P. Lai, M. Tsapatsis and J.R. Nicolich, Adv. Funct. Mater., 14 (2004) 716.

[41] M.A. Snyder, Z. Lai, M. Tsapatsis and D.G. Vlachos, Micropor Mesopor Mater., 76 (2004) 29.

[42] Y.H. Chiou, T.G. Tsai, S.L. Sung, H.C. Shih, C.N. Wu and K.J. Chao, J. Chem. Soc. Faraday Trans., 92 (1996) 1061.

[43] E.R. Geus, M.J. Denexter and H. Vanbekkum, J. Chem. Soc. Faraday Trans., 88 (1992) 3101.

[44] T. Sano, M. Hasegawa, Y. Kawakami and H. Yanagishita, J. Membr. Sci., 107 (1995) 193.

[45] A.J. Burggraaf, Z. Vroon, K. Keizer and H. Verweij, J. Membr. Sci., 144 (1998) 77.

[46] M.C. Lovallo, A. Gouzinis and M. Tsapatsis, AIChE J., 44 (1998) 1903.

[47] Z. Vroon, K. Keizer, A.J. Burggraaf and H. Verweij, J. Membr. Sci., 144 (1998) 65.

[48] R. Lai, Y.S. Yan and G.R. Gavalas, Micropor Mesopor Mater., 37 (2000) 9.

[49] M. Noack, P. Kolsch, J. Caro, M. Schneider, P. Toussaint and I. Sieber, Micropor Mesopor Mater., 35-6 (2000) 253.

[50] S. Himeno, T. Tomita, K. Suzuki, K. Nakayama, K. Yajima and S. Yoshida, Ind. Eng. Chem. Res., 46 (2007) 6989.

[51] M. Kanezashi, J. O'Brien-Abraham, Y.S. Lin and K. Suzuki, AIChE J., 54 (2008) 1478.

[52] T. Tomita, K. Nakayama and H. Sakai, Micropor Mesopor Mater., 68 (2004) 71.

[53] J. van den Bergh, A. Tihaya and F. Kapteijn, Micropor Mesopor Mater., 132 (2010) 137.

[54] T. Kyotani, T. Mizuno, Y. Katakura, S. Kakui, N. Shimotsuma, J. Saito and T. Nakane, J. Membr. Sci., 296 (2007) 162.

[55] Y.S. Li, H.L. Chen, J. Liu and W.S. Yang, J. Membr. Sci., 277 (2006) 230.

[56] Y.S. Li, J. Liu and W.S. Yang, J. Membr. Sci., 281 (2006) 646.

[57] Y.S. Li, H. Zhou, G.Q. Zhu, J. Liu and W.S. Yang, J. Membr. Sci., 297 (2007) 10.

[58] Z.B. Wang, Q.Q. Ge, J. Shao and Y.S. Yan, J. Am. Chem. Soc., 131 (2009) 6910.

[59] S. Aguado, J. Gascon, J.C. Jansen and F. Kapteijn, Micropor Mesopor Mater., 120 (2009) 170.

[60] Q.Q. Ge, Z.B. Wang and Y.S. Yan, J. Am. Chem. Soc., 131 (2009) 17056.

[61] Y. Hasegawa, T. Nagase, Y. Kiyozumi, T. Hanaoka and F. Mizukami, J. Membr. Sci., 349 (2010) 189.

[62] A.S. Huang and W.S. Yang, Mater. Lett., 61 (2007) 5129.

[63] A.S. Huang and W.S. Yang, Micropor. Mesopor. Mater., 102 (2007) 58.

[64] A.S. Huang and W.S. Yang, Sep. Purif. Technol., 61 (2008) 175.

[65] A. Malekpour, M.R. Millani and M. Kheirkhah, Desalination, 225 (2008) 199.

[66] M. Pera-Titus, M. Bausach, J. Llorens and F. Cunill, Sep. Purif. Technol., 59 (2008) 141.

[67] K. Sato and T. Nakane, J. Membr. Sci., 301 (2007) 151.

[68] K. Sato, K. Sugimoto and T. Nakane, J. Membr. Sci., 307 (2008) 181.

[69] Y. Hasegawa, H. Hotta, K. Sato, T. Nagase and F. Mizukami, J. Membr. Sci., 347 (2010) 193.

[70] H. Kalipcilar, T.C. Bowen, R.D. Noble and J.L. Falconer, Chem. Mater., 14 (2002) 3458.

[71] H. Lee and P.K. Dutta, Micropor Mesopor Mater., 38 (2000) 151.

[72] C. Algieri, P. Bernardo, G. Barbieri and E. Drioli, Micropor. Mesopor. Mater., 119 (2009) 129.

[73] Z.L. Cheng, E.Q. Gao and H.L. Wan, Chem. Commun., (2004) 1718.

[74] C. Covarrubias, R. Garcia, R. Arriagada, J. Yanez, H. Ramanan, Z.P. Lai and M. Tsapatsis, J. Membr. Sci., 312 (2008) 163.

[75] I.G. Giannakopoulos, K. Kalambaliki, V. Dracopoulos and V. Nikolakis, Molecular Sieves: From Basic Research to Industrial Applications, Pts a and B, 158 (2005) 137.

[76] F. Guillou, L. Rouleau, G. Pirngruber and V. Valtchev, Micropor. Mesopor. Mater., 119 (2009) 1.

[77] Y. Hasegawa, T. Tanaka, K. Watanabe, B.H. Jeong, K. Kusakabe and S. Morooka, Korean J. Chem. Eng., 19 (2002) 309.

[78] B.H. Jeong, Y. Hasegawa, K. Sotowa, K. Kusakabe and S. Morooka, J. Chem. Eng. Jpn., 35 (2002) 167.

[79] K. Weh, M. Noack, I. Sieber and J. Caro, Micropor. Mesopor. Mater., 54 (2002) 27.

[80] G.Q. Zhu, Y.S. Li, H.L. Chen, J. Liu and W.S. Yang, J. Mater. Sci., 43 (2008) 3279.

[81] G.Q. Zhu, Y.S. Li, H. Zhou, J. Liu and W.S. Yang, J. Membr. Sci., 337 (2009) 47.

[82] M.P. Bernal, J. Coronas, M. Menendez and J. Santamaria, Ind. Eng. Chem. Res., 41 (2002) 5071.

[83] M.P. Bernal, E. Piera, J. Coronas, M. Menendez and J. Santamaria, Catal. Today, 56 (2000) 221.

[84] L. Casado, R. Mallada, C. Tellez, J. Coronas, M. Menendez and J. Santamaria, J. Membr. Sci., 216 (2003) 135.

[85] G. Li, E. Kikuchi and M. Matsukata, Sep. Purif. Technol., 32 (2003) 199.

[86] X. Lin, E. Kikuchi and M. Matsukata, Chem. Commun., (2000) 957.

[87] A. Navajas, R. Mallada, C. Tellez, J. Coronas, M. Menendez and J. Santamaria, J. Membr. Sci., 299 (2007) 166.

[88] N. Nishiyama, K. Ueyama and M. Matsukata, J. Chem. Soc. Chem. Commun., (1995) 1967.

[89] K. Sawamura, T. Shirai, T. Ohsuna, T. Hagino, M. Takada, Y. Sekine, E. Kikuchi and M. Matsukata, J. Chem. Eng. Jpn., 41 (2008) 870.

[90] A. Tavolaro, A. Julbe, C. Guizard, A. Basile, L. Cot and E. Drioli, J. Mater. Chem., 10 (2000) 1131.

[91] G.Q. Guan, T. Tanaka, K. Kusakabe, K.I. Sotowa and S. Morooka, J. Membr. Sci., 214 (2003) 191.

[92] A.S. Huang, F.Y. Liang, F. Steinbach, T.M. Gesing and J. Caro, J. Am. Chem. Soc., 132 (2010) 2140.

[93] M. Hong, S.G. Li, J.L. Falconer and R.D. Noble, J. Membr. Sci., 307 (2008) 277.

[94] S.G. Li, G. Alvarado, R.D. Noble and J.L. Falconer, J. Membr. Sci., 251 (2005) 59.

[95] S.G. Li, M.A. Carreon, Y.F. Zhang, H.H. Funke, R.D. Noble and J.L. Falconer, J. Membr. Sci., 352 (2010) 7.

[96] S.G. Li, J.L. Falconer and R.D. Noble, J. Membr. Sci., 241 (2004) 121.

[97] S.G. Li, J.L. Falconer and R.D. Noble, Adv. Mater., 18 (2006) 2601.

[98] S.G. Li, J.L. Falconer and R.D. Noble, Micropor. Mesopor. Mater., 110 (2008) 310.

[99] S.G. Li and C.Q. Fan, Ind. Eng. Chem. Res., 49 (2010) 4399.

[100] J.C. Poshusta, R.D. Noble and J.L. Falconer, J. Membr. Sci., 186 (2001) 25.

[101] J.C. Poshusta, V.A. Tuan, J.L. Falconer and R.D. Noble, Ind. Eng. Chem. Res., 37 (1998) 3924.

[102] J.C. Poshusta, V.A. Tuan, E.A. Pape, R.D. Noble and J.L. Falconer, AIChE J., 46 (2000) 779.

[103] Y.Y. Tian, L.L. Fan, Z.Y. Wang, S.L. Qiu and G.S. Zhu, J. Mater. Chem., 19 (2009) 7698.

[104] T.G. Tsai, H.C. Shih, S.J. Liao and K.J. Chao, Micropor. Mesopor. Mater., 22 (1998) 333.

[105] W.S. Yang, B.Q. Zhang and X.F. Liu, Micropor. Mesopor. Mater., 117 (2009) 391.

[106] S.A. Hashemifard, A.F. Ismail and T. Matsuura, J. Membr. Sci., 350 (2010) 259.

[107] S.B. Tantekin-Ersolmaz, C. Atalay-Orala, M. Tather, A. Erdem-Senatalar, B. Schoeman and J. Sterte, J. Membr. Sci., 175 (2000) 285.

[108] M.G. Suer, N. Bac and L. Yilmaz, J. Membr. Sci., 91 (1994) 77.

[109] J.M. Duval, B. Folkers, M.H.V. Mulder, G. Desgrandchamps and C.A. Smolders, J. Membr. Sci., 80 (1993) 189.

[110] T.M. Gur, J. Membr. Sci., 93 (1994) 283.

[111] J.M. Duval, A.J.B. Kemperman, B. Folkers, M.H.V. Mulder, G. Desgrandchamps and C.A. Smolders, J. Appl. Polym. Sci., 54 (1994) 409.

[112] T. Battal, N. Bac and L. Yilmaz, Sep. Sci. Technol., 30 (1995) 2365.

[113] S.G. Adoor, L.S. Manjeshwar, S.D. Bhat and T.M. Aminabhavi, J. Membr. Sci., 318 (2008) 233.

[114] S.G. Adoor, B. Prathab, L.S. Manjeshwar and T.A. Aminabhavi, Polymer, 48 (2007) 5417.

[115] S. Amnuaypanich, J. Patthana and P. Phinyocheep, Chem. Eng. Sci., 64 (2009) 4908.

[116] S.D. Bhat and T.M. Aminabhavi, J. Membr. Sci., 306 (2007) 173.

[117] T.C. Bowen, R.G. Meier and L.M. Vane, J. Membr. Sci., 298 (2007) 117.

[118] B.B. Liu, Y.M. Cato, T.H. Wang and Q. Yuan, J. Appl. Polym. Sci., 106 (2007) 2117.

[119] E. Okumus, T. Gurkan and L. Yilmaz, Sep. Sci. Technol., 29 (1994) 2451.

[120] M.B. Patil and T.M. Aminabhavi, Sep. Purif. Technol., 62 (2008) 128.

[121] H.L. Sun, L.Y. Lu, X. Chen and Z.Y. Jiang, Appl. Surf. Sci., 254 (2008) 5367.

[122] R.S. Veerapur, M.B. Patil, K.B. Gudasi and T.M. Aminabhavi, Sep. Purif. Technol., 58 (2008) 377.

[123] X.L. Zhang, L.P. Qian, H.T. Wang, W. Zhong and Q.G. Du, Sep. Purif. Technol., 63 (2008) 434.

[124] R. Mahajan and W.J. Koros, Ind. Eng. Chem. Res., 39 (2000) 2692.

[125] R. Mahajan and W.J. Koros, Polym. Eng. Sci., 42 (2002) 1420.

[126] R. Mahajan and W.J. Koros, Polym. Eng. Sci., 42 (2002) 1432.

[127] T.T. Moore, Chem. Eng., PhD thesis, University of Texas, 2004.

[128] T.T. Moore and W.J. Koros, J. Mol. Struct., 739 (2005) 87.

[129] S. Husain and W.J. Koros, J. Membr. Sci., 288 (2007) 195.

[130] T.W. Pechar, S. Kim, B. Vaughan, E. Marand, M. Tsapatsis, H.K. Jeong and C.J. Cornelius, J. Membr. Sci., 277 (2006) 195.

[131] Y. Li, H.-M. Guan, T.-S. Chung and S. Kulprathipanja, J. Membr. Sci., 275 (2006) 17.

[132] S. Shu, S. Husain and W.J. Koros, J. Phys. Chem. C, 111 (2007) 652.

[133] S. Shu, S. Husain and W.J. Koros, Chem. Mater., 19 (2007) 4000.

[134] A.K. Cheetham, G. Ferey and T. Loiseau, Angew. Chem. Int. Ed., 38 (1999) 3268.

[135] E.M. Flanigen, Pure Appl. Chem., 52 (1980) 2191.

[136] C.S. Cundy and P.A. Cox, Chem. Rev., 103 (2003) 663.

[137] C.S. Cundy and P.A. Cox, Micropor. Mesopor. Mater., 82 (2005) 1.

[138] C.D. Chang and A.T. Bell, Catal. Lett., 8 (1991) 305.

[139] S.L. Burkett and M.E. Davis, J. Phys. Chem., 98 (1994) 4647.

[140] S.L. Burkett and M.E. Davis, Chem. Mater., 7 (1995) 920.

[141] S.L. Burkett and M.E. Davis, Chem. Mater., 7 (1995) 1453.

[142] R. Szostak, Molecular Sieves; principles of synthesis and identification, Van Nostrand Reinhold, New York, 1989.

[143] S. Bosnar, J. Bronic and B. Subotic, in I. Kiricsi, G. PalBorbely, J.B. Nagy and H.G. Karge (Editors), Porous Materials in Environmentally Friendly Processes, Vol. 125, 1999, p. 69.

[144] C. Falamaki, M. Edrissi and M. Sohrabi, Zeolites, 19 (1997) 2.

[145] Molecular sieves, American Chemical Society, Washington, 1973.

[146] Structure and reactivity of modified zeolites : proceedings of an international conference, Prague, July 9-13, 1984, Elsevier ;, Amsterdam ;, 1984.

[147] S. Bosnar and B. Subotic, Micropor. Mesopor. Mater., 28 (1999) 483.

[148] O. Regev, Y. Cohen, E. Kehat and Y. Talmon, Zeolites, 14 (1994) 314.

[149] E.I. Basaldella, A. Kikot and J.C. Tara, Mater. Lett., 31 (1997) 83.

[150] E.I. Basaldella and J.C. Tara, Mater. Lett., 34 (1998) 119.

[151] G. Ferey, Chem. Soc. Rev., 37 (2008) 191.

[152] Z.Q. Wang and S.M. Cohen, Chem. Soc. Rev., 38 (2009) 1315.

[153] A. Demessence, D.M. D'Alessandro, M.L. Foo and J.R. Long, J. Am. Chem. Soc., 131 (2009) 8784.

[154] J.R. Li, R.J. Kuppler and H.C. Zhou, Chem. Soc. Rev., 38 (2009) 1477.

[155] S. Choi, J.H. Drese and C.W. Jones, ChemSusChem, 2 (2009) 796.

[156] L.J. Murray, M. Dinca and J.R. Long, Chem. Soc. Rev., 38 (2009) 1294.

[157] J. Lee, O.K. Farha, J. Roberts, K.A. Scheidt, S.T. Nguyen and J.T. Hupp, Chem. Soc. Rev., 38 (2009) 1450.

[158] D. Zacher, O. Shekhah, C. Woll and R.A. Fischer, Chem. Soc. Rev., 38 (2009) 1418.

[159] O.M. Yaghi, M. O'Keeffe, N.W. Ockwig, H.K. Chae, M. Eddaoudi and J. Kim, Nature, 423 (2003) 705.

[160] M. Eddaoudi, J. Kim, N. Rosi, D. Vodak, J. Wachter, M. O'Keeffe and O.M. Yaghi, Science, 295 (2002) 469.

[161] A. Phan, C.J. Doonan, F.J. Uribe-Romo, C.B. Knobler, M. O'Keeffe and O.M. Yaghi, Acc. Chem. Res., 43 (2010) 58.

[162] W. Morris, C.J. Doonan, H. Furukawa, R. Banerjee and O.M. Yaghi, J. Am. Chem. Soc., 130 (2008) 12626.

[163] H. Hayashi, A.P. Cote, H. Furukawa, M. O'Keeffe and O.M. Yaghi, Nat. Mater., 6 (2007) 501.

[164] R. Banerjee, A. Phan, B. Wang, C. Knobler, H. Furukawa, M. O'Keeffe and O.M. Yaghi, Science, 319 (2008) 939.

CHAPTER 2

SOLVOTHERMAL DEPOSITION OF INORGANIC NANOSTRUCTURES ON ZEOLITE MFI FOR MIXED MATRIX MEMBRANE FABRICATION

2.1 Introduction

As discussed in Chapter 1, the creation of inorganic "nano-whisker structures" on zeolite surfaces is an effective way to control zeolite/polymer interfacial morphology in mixed matrix membranes [1-3]. Thus, the development of rational methods to form such nanostructures on zeolites, using a benign chemistry, would be highly attractive. In this work, $Mg(OH)_2$ was selected as an inorganic material to create nanostructured surfaces on zeolites since well-defined $Mg(OH)_2$ nanostructures can be synthesized by a simple reaction of inexpensive raw materials. Moreover, the morphologies of $Mg(OH)_2$ nanostructures can be readily tuned by adjusting the reaction conditions.

$Mg(OH)_2$ solids can be formed by reactions between a magnesium source, a base and water. There are several studies that demonstrate the formation of $Mg(OH)_2$ nanostructures via precipitation at moderate temperatures [4-7] or via hydrothermal processes [8-11]. The type and concentration of both the magnesium source and base [6-7], reaction time [9], pH (in aqueous processes) [6-7, 11] and reaction temperature [11] are important factors affecting crystallinity and morphology of the resulting nanomaterials.

Henrist et al. reported the effect of magnesium sources on the size/shape of resultant $Mg(OH)_2$ structures synthesized by precipitation in an aqueous phase [6]. Both magnesium nitrate and magnesium chloride gave rise to platelet-like $Mg(OH)_2$ nanocrystals. However, magnesium sulfate promoted particle intergrowth, resulting in randomly tangled particles interconnected to each other. They also studied the effect of the chemical nature of the base precipitant on the resultant $Mg(OH)_2$ morphology. The use of sodium hydroxide led to the cauliflower-like agglomerates, while synthesis driven with aqueous ammonia promoted the formation of platelet-shaped particles. Lv et al. studied the effect of surfactants on the $Mg(OH)_2$ structure in an aqueous phase reaction [4]. $Mg(OH)_2$ of needle-like morphology was formed when surfactants were added to the reagent mixtures. They also observed morphological evolution as the reaction temperature decreased. As the temperature decreased, platelet-like structures were gradually changed to a rod-shaped morphology. Yan et al. reported the growth of $Mg(OH)_2$ crystals as a function of time in a hydrothermal reaction at 160 ^oC [8]. As the reaction time increased from 2.5 to 20 hrs, the width of the needle structures increased from ~10 nm to ~1 μm. The combined effect of pH and temperature on the morphology of $Mg(OH)_2$ crystals was also studied in hydrothermal reactions [11]. As shown in Fig. 2-1, the crystal shape was successfully tuned by adjusting the pH and temperature of the hydrothermal reaction. It was also shown that $Mg(OH)_2$ synthesized at high temperatures (115 ^oC) had better crystallinity than the materials from low synthesis temperatures (95 ^oC).

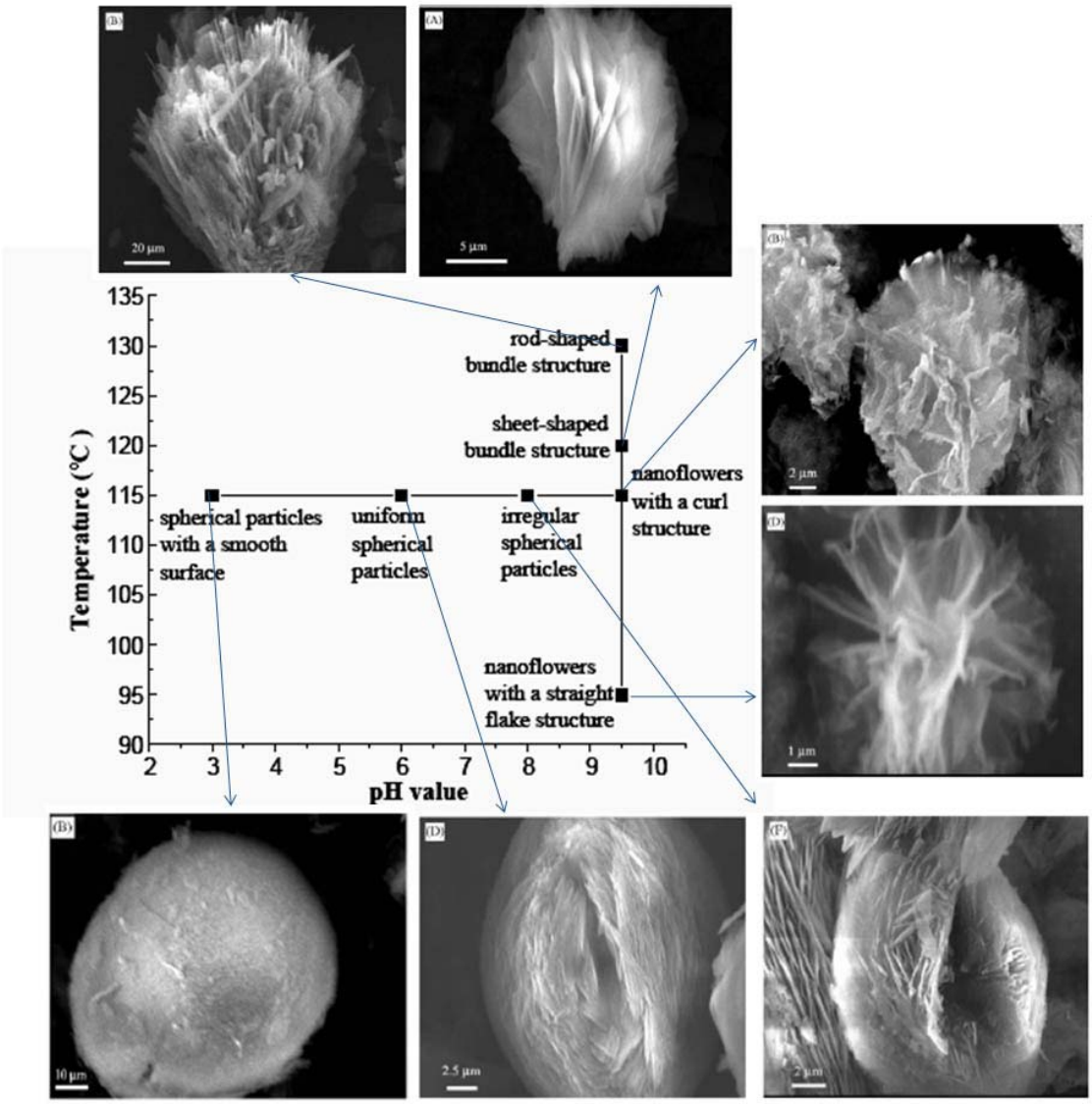

Fig. 2-1 Morphologies of $Mg(OH)_2$ synthesized by hydrothermal reaction at various temperatures and pHs [11].

Meanwhile, it was also shown that well-defined $Mg(OH)_2$ nanorods could be created solvothermally with a non-aqueous solvent [9, 12]. In this method, ethylenediamine acted as both reaction medium and base. Magnesium sources and a small amount of water were the other components of the reaction mixture. It was found that both the nature of the magnesium source and the ethylenediamine to water ratio were

key factors affecting the resultant crystal morphology. For instance, nanorods could be formed from magnesium powder and $MgSO_4$, but only platelets were obtained using $Mg(NO_3)_2$ as the metal source. A high ethylenediamine-to-water ratio was also essential to create nanoneedles or nanorods. When the ethylenediamine-to-water ratio was lower than 4:1 (volumetric ratio), $Mg(OH)_2$ lamellar structures were formed. Although the true role of ethylenediamine is unclear, the authors speculated that the selective interaction between the coordinating solvent (ethylenediamine) and surface ions (Mg^{2+}) slowed the growth of specific lattice planes, resulting in one dimensional growth of the nanocrystals (Fig. 2-2). A control experiment revealed that platelet-like structures were formed in an ammonia-water mixture, indicating the role of ethylenediamine is critical for 1-d growth of $Mg(OH)_2$.

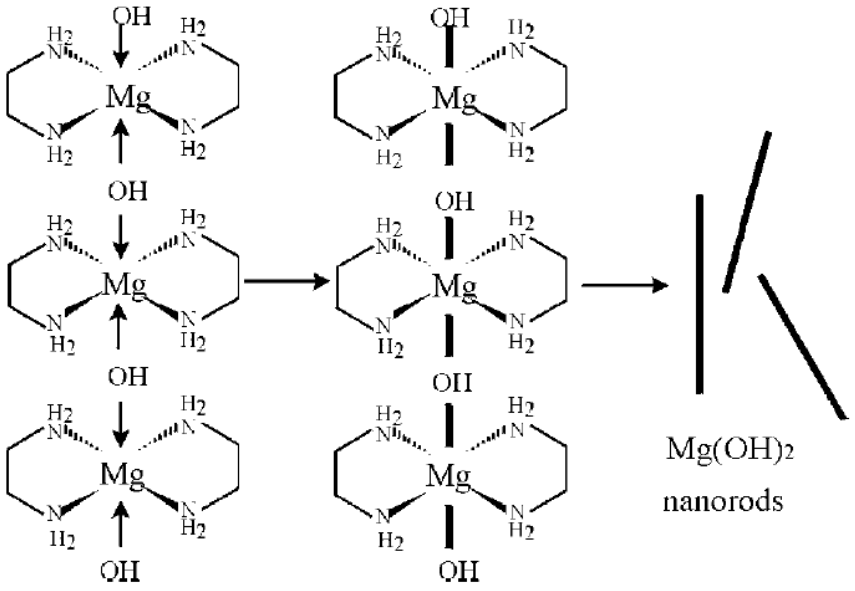

Fig. 2-2 Hypothetical mechanism of formation of $Mg(OH)_2$ nanorods from Mg^{2+}/ethylenediamine complexes [12].

To create nanostructured morphologies on the surfaces of zeolites based on the aforementioned methods, the synthesis conditions must be modified to allow the precipitation of inorganic crystals on the zeolite surface in a controlled manner, rather than precipitation in the solution independent of the zeolite surfaces. Thus, heterogeneous deposition, as well as heterogeneous nucleation and growth on the zeolite surface, are both desirable effects.

In Chapter 2, a facile solvothermal method to grow inorganic nanostructures on the surface of zeolites is reported. Pure Silica MFI crystals with various sizes were hydrothermally synthesized and used as model substrates. Solvothermal deposition of inorganic nanostructures was performed in a solvent mixture of ethylenediamine and water. For control studies, surface treatments were also performed using the Grignard route after seeding the zeolite surfaces with NaCl [3] . The structural properties of these modified zeolites relevant to their application in mixed matrix membranes were thoroughly investigated. Finally, gas permeation properties of mixed matrix membranes containing surface modified MFI were studied.

2.2 Experimental Section

2.2.1 Materials

The following chemicals were commercially available and were used as received: tetraethylorthosilicate (TEOS, 98% Sigma-Aldrich), tetrapropylammonium hydroxide (TPAOH, 40% w/w aqueous solution, Alfa Aesar), tetrapropylammonium bromide (TPABr, 98%, Sigma-Aldrich), ethylenediamine (EDA, 99%, Sigma-Aldrich),

methylmagnesium bromide (3 M in ether, Sigma-Aldrich), 2-propanol (Sigma-Aldrich), dichloromethane (DCM, 99.5%, Sigma-Aldrich), toluene (99.8%, Sigma-Aldrich), magnesium sulfate heptahydrate (Acros) and sodium chloride (Fisher Scientific). Two commercially available polyimides, Ultem® 1000 (SABIC) and Matrimid® 5218 (Vantico), were used for membrane fabrications (Fig. 2-3).

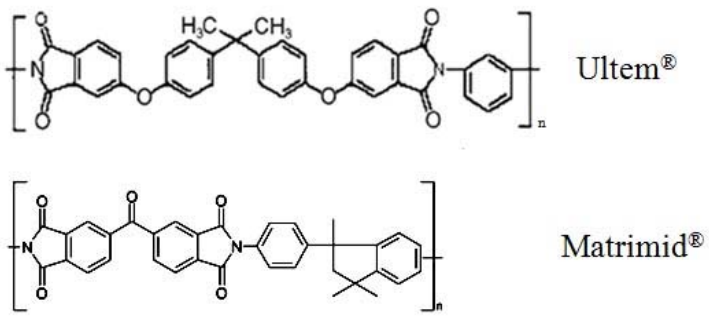

Fig. 2-3 Chemical structures of polyimides.

2.2.2 Synthesis of Zeolite MFI

Pure-silica MFI crystals were synthesized hydrothermally at 150 ^{o}C from TEOS/TPAOH/water solutions. The TEOS/TPAOH molar ratio was 1:0.36 or 1:0.24 and the water content was varied from 20 to 360 on a molar basis as part of a synthesis matrix that included variation in the reaction time (2 to 4 days). The general methodology otherwise followed a method described elsewhere [13]. Large crystal MFI was also prepared a the method described in the literature [14]. The solution with a molar ratio of 1TEOS:0.1TPABr:0.1NaOH:98H_2O was aged at 50 ^{o}C for 7 days and crystallized at 120 ^{o}C for 2 days. After the synthesis, the zeolite particles were washed with DI water by repetitions of centrifuge and dispersion at least 5 times, and dried at 80 ^{o}C. Calcination

was performed at 550 ^{o}C for 8 hr in air.

2.2.3 Grignard Treatment

After dispersing 0.5 g of zeolites in 3 M aqueous NaCl solution, the suspension was filtered using a microfiltration membrane with 0.1 μm pores to collect the particles. To remove some of the residual water, the particles were dried at 80 ^{o}C overnight. The NaCl seeded zeolites were placed in round bottom flask and 8 ml of toluene was added. After purging the flask with nitrogen, 1.5 ml of 3 M CH_3MgBr in ether was added using transfer needles. The suspension was sonicated for 4hr and then stirred for 12hr at room temperature under nitrogen. 2-propanol was added drop-wise to quench the Grignard reagent and the mixture was centrifuged to collect the particles. To remove residual solvents, the particles were washed with 2-propanol several times. After that, 40 ml of DI water was added to the particles and the mixture was sonicated for 2 hr. During the sonication, the temperature increased to 43-45 ^{o}C spontaneously. The particles were washed with DI water by several repetitions of centrifuge and dispersion and dried at 80 ^{o}C.

2.2.4 Solvothermal Treatment

After dispersing 0.2 g of zeolites in 10 ml of ethylenediamine by sonication, 1 ml of 1 M aqueous $MgSO_4$ solution was added dropwise to the dispersion while applying vigorous stirring. After further stirring for 1hr, the mixture was transferred to Teflon-lined autoclave and solvothermal treatment was performed at 160 ^{o}C in the synthesis oven for 12 hr. The particles were washed with DI water by several repetitions of sonication and

centrifuge and dried at 80 ^{o}C.

2.2.5 Mixed Matrix Membrane Fabrication

Zeolite/polymer composite films were prepared using a solution casting technique. Zeolite particles were dispersed in DCM using a sonication horn. Polymer was added to the suspension, which was then stirred overnight. After pouring the solution on a glass plate, a nascent film was cast using a "doctor's knife". Finally, a dense film was obtained after drying at room temperature.

2.2.6 Characterization

Morphologies of both zeolite particles and mixed matrix membranes were observed with a scanning electron microscope (SEM, LEO 1530). To prevent any morphological changes, zeolite particles were observed without coating with gold. On the other hand, to observe cross-sections, mixed matrix membranes were coated with gold after being cryogenically fractured in liquid nitrogen. Energy dispersive X-ray spectroscopy (EDS) was used to investigate the elemental composition of zeolites. Bulk compositions were also measured with ICP-AES (inductively coupled plasma atomic emission spectroscopy) with an outside vendor, Columbia Analytical Services Inc. Micropore volume by t-plot method and BET (Brunauer-Emmett-Teller) surface area were calculated from nitrogen physisorption measurements performed on a Micromeritics ASAP 2020 or 2010. Powder X-ray diffraction (XRD) patterns were obtained on a Philips X'pert diffractometer equipped with X'celerator using Cu Kα radiation. Differential scanning calorimetry (DSC) was performed on a Netzsch STA409. Samples

were initially heated under a nitrogen-diluted air stream from 30°C to 300°C at 10 °C/min and cooled to room temperature. DSC curves were obtained during the second run at a heating rate of 10 °C/min.

2.2.7 Permeation Tests

Single gas permeation tests were performed in a constant volume apparatus. In the system, feed and permeate reservoirs were separated by a cell that holds the membrane. It includes appropriate instrumentation for measuring the pressure in both reservoirs and necessary valves, all within a constant temperature box. The detailed experimental procedure is described in the literature [15]. Permeation tests were performed with 2.0 or 4.5 atm upstream pressure at 35°C. Numerous measurements were performed for the thickness of each sample by using a micrometer, and their arithmetic average values were used for permeation data analysis.

2.2.8 Theoretical Prediction of Membrane Performance

The permeabilities of gases in mixed matrix membranes with ideal morphology can be estimated by the Maxwell model. Since uncalcined MFI is non-porous, oxygen and nitrogen permeabilities in uncalcined MFI were assumed to be zero. The permeabilities in the polymer phase were obtained from the permeation tests of a pure Ultem® dense film. A modified-Maxwell model, which is a three-phase (polymer, sieve and voids) Maxwell model, was utilized to predict the performance of mixed matrix membranes with sieve-in-a-cage morphology [16-17]. The Knudsen diffusion of the gas molecules in the voids between MFI and Ultem® was assumed.

2.3 Results and Discussion

2.3.1 Zeolite MFI Synthesis and Characterization

In this study, pure silica MFI was used as a model substrate. Fig. 2-4 shows the framework structure of zeolite MFI. There are two channel systems in MFI: a straight channel running parallel to (010) with 10-membered ring openings of 0.54 x 0.56 nm, and a sinusoidal channel parallel to the (100) axis with 10-membered ring openings of dimension 0.51 x 0.55 nm [18]. Examples of the MFI particles synthesized for this study are shown in Fig. 2-5. The largest crystals were made using TPABr as a structure-directing agent (SDA) and were approximately 5 μm (Fig. 2-5a). The particles showed a broad size distribution. In contrast, crystals synthesized with TPAOH as the SDA showed uniform sizes. Crystals of 100 nm, 300 nm and 2 μm size were synthesized by adjusting the reaction time, and the amount of SDA or water. As the particle size increased, the morphology of particles changed from spherical (100 nm) to prismatic (2 and 5 μm). As shown in Fig. 2-6, all synthesized crystals exhibited typical XRD patterns of zeolite MFI.

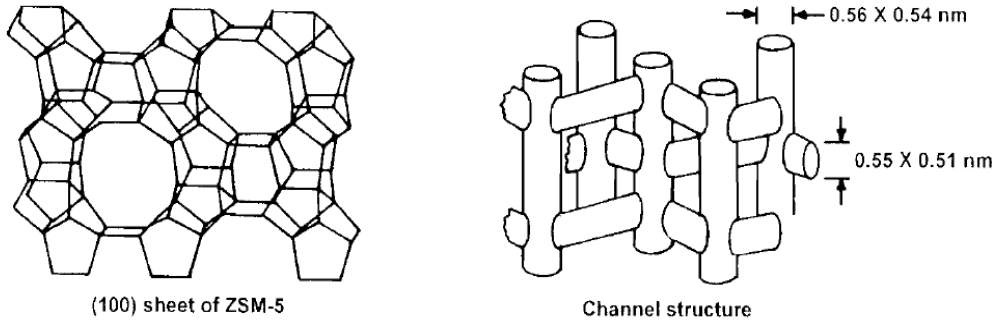

Fig. 2-4 Framework structures of zeolite MFI.

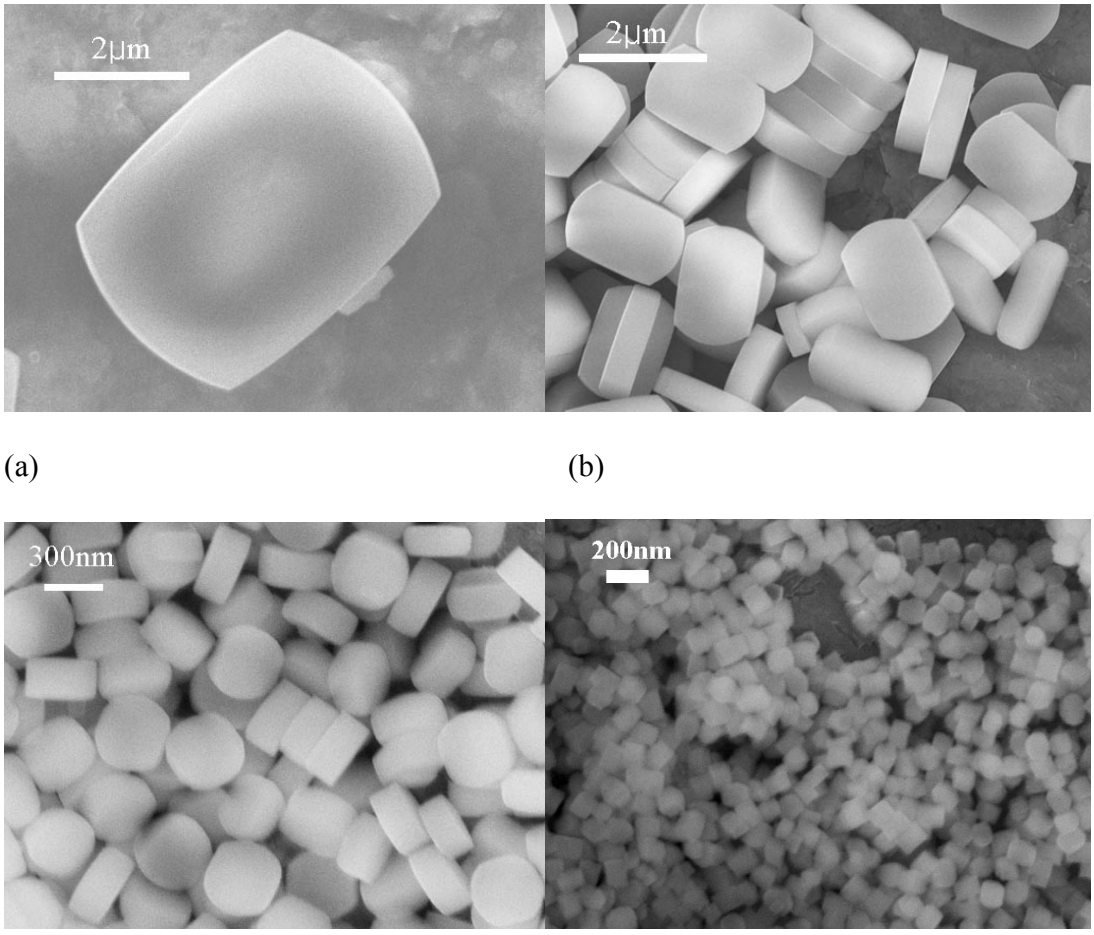

Fig. 2-5 SEM images of PS-MFI particles; (a) 5 μm large crystal; (b)-(c) crystals synthesized from the precursor solution composition of 1 TEOS: x TPAOH: y H2O for z days. (b) 2 μm, x = 0.24, y = 360 and z = 4; (c) 300 nm, x = 0.36, y = 180 and z = 2; (d) 100 nm, x = 0.36, y = 20 and z = 4.

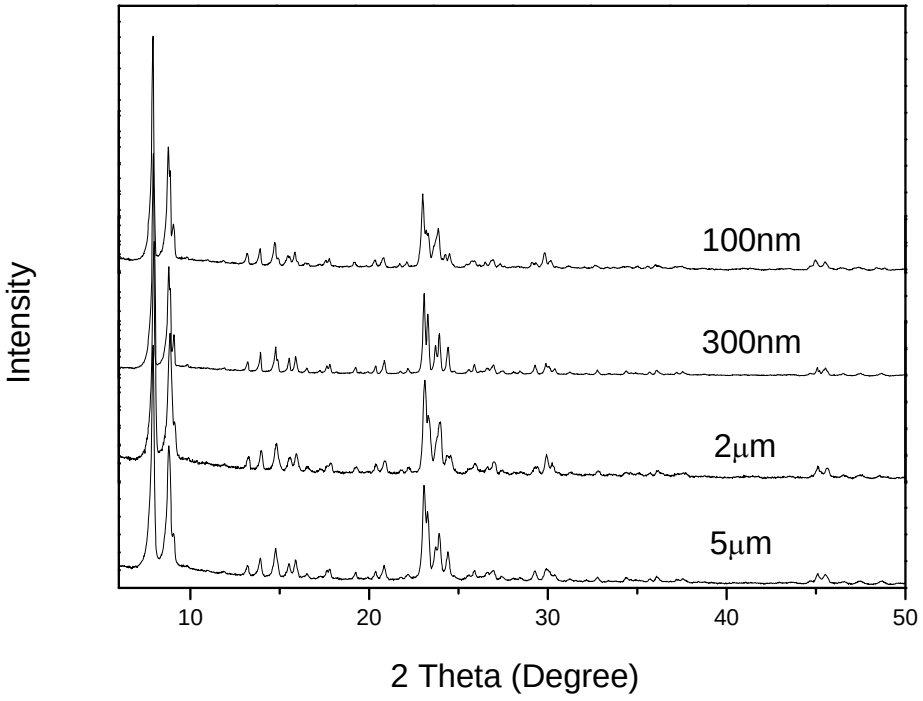

Fig. 2-6 Powder XRD patterns of untreated PS-MFI.

2.3.2 Morphology of Surface Treated PS-MFI

Fig. 2-7 shows the morphology of MFI particles surface-treated with both the solvothermal and Grignard routes. Roughened surfaces were created by the formation $Mg(OH)_2$ nanostructures on the surface of MFI. As shown in the Fig. 2-7a and 2-7c, the solvothermal treatments created well-defined whisker structures on the surface of prismatic 5 μm and 2 μm crystals, since the particles provide a large planar surface for the inorganic nanostructures to be immobilized. However, the morphology of 300 nm MFI particles was changed to a "cotton-ball" structure, as the size of the particles became closer to the size of the nanostructures created. This phenomenon was also reported in the

Grignard treatment by Shu et al [2]. Meanwhile, for 100 nm MFI crystals, the surfaces were coated with very fine structures without a distinguishable whisker-like morphology. Furthermore, particle aggregation was significant when compared to other larger MFI particles, as shown in Fig. 2-7g. In contrast, Grignard treatment created nano-whisker structures on the zeolite surfaces as well as inorganic platelet structures in solution. The amount of surface nanostructures created was smaller than that in solvothermally treated MFI, as seen initially by visual comparison.

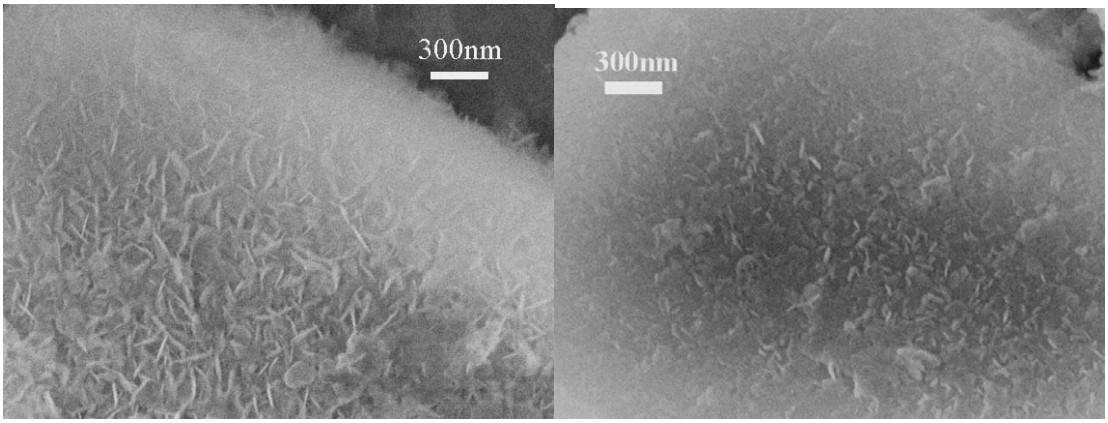

(a) (b)

Fig. 2-7 SEM images of the surface treated PS-MFI; (a) Solvothermal_5 μm, (b) Grignard_5 μm, (c) Solvothermal_2 μm, (d) Grignard_2 μm, (e) Solvothermal_300 nm, (f) Grignard_300 nm, (g) Solvothermal_100 nm, (h) Grignard_100 nm

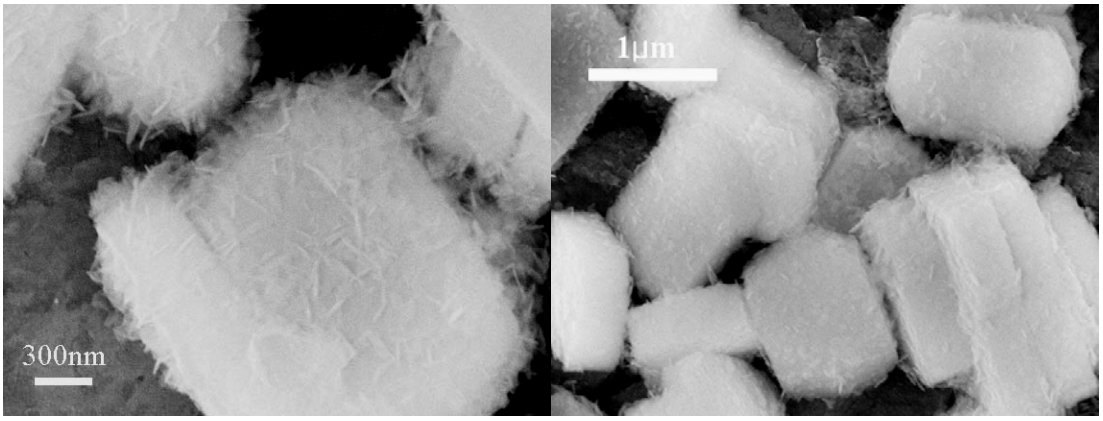

(c) (d)

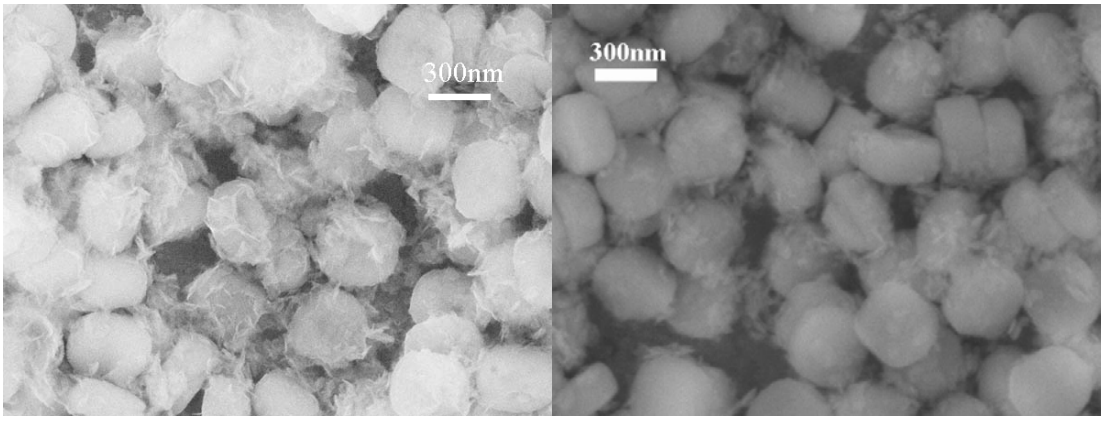

(e) (f)

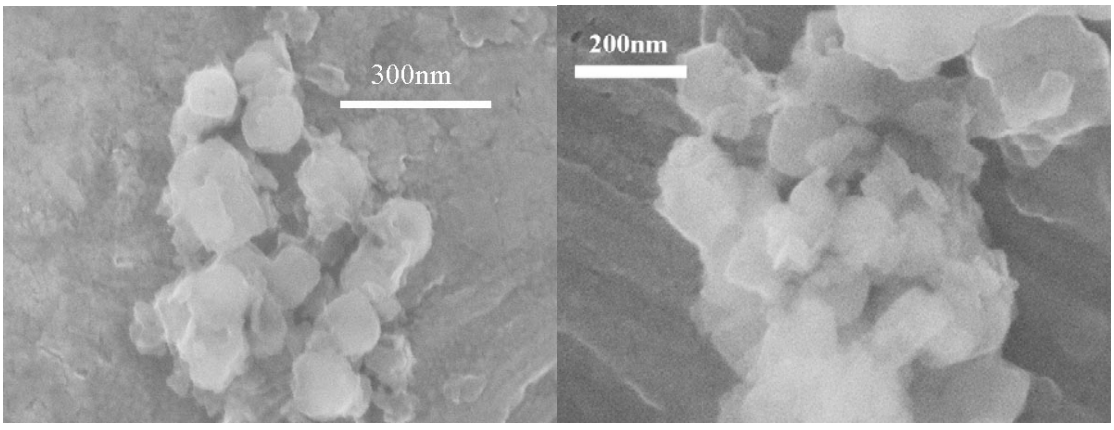

(g) (h)

continued

2.3.3 Mass Fraction of $Mg(OH)_2$

Bulk compositions of surface-treated MFI particles were measured by ICP-AES. From the Si and Mg contents, the mass fraction of $Mg(OH)_2$ was calculated after assuming the samples are comprised only of SiO_2 and $Mg(OH)_2$. The mass fraction of $Mg(OH)_2$ could also be estimated by TGA. A sharp endothermic peak in the range of 370-430 ^oC appears in the DSC curve (Fig. 2-8) due to the dehydration of $Mg(OH)_2$ to MgO. The mass of $Mg(OH)_2$ was calculated from the H_2O loss in this temperature region, and the results are summarized in Table 2-1. In general, results from both types of measurements showed good agreement. The mass fraction of $Mg(OH)_2$ in Grignard treated PS-MFI increased as the particle size decreased, since the smaller particles provide larger surface area per unit mass. However, in contrast to Grignard treatment, there was no relationship between the amount of $Mg(OH)_2$ and the MFI particle size in solvothermally treated MFI crystals, since the reaction continued until all the magnesium source in the reactant solution was consumed. The yield from the solvothermal reaction was so high that the mass fractions of $Mg(OH)_2$ were close to the theoretical maximum for all batches of particles.

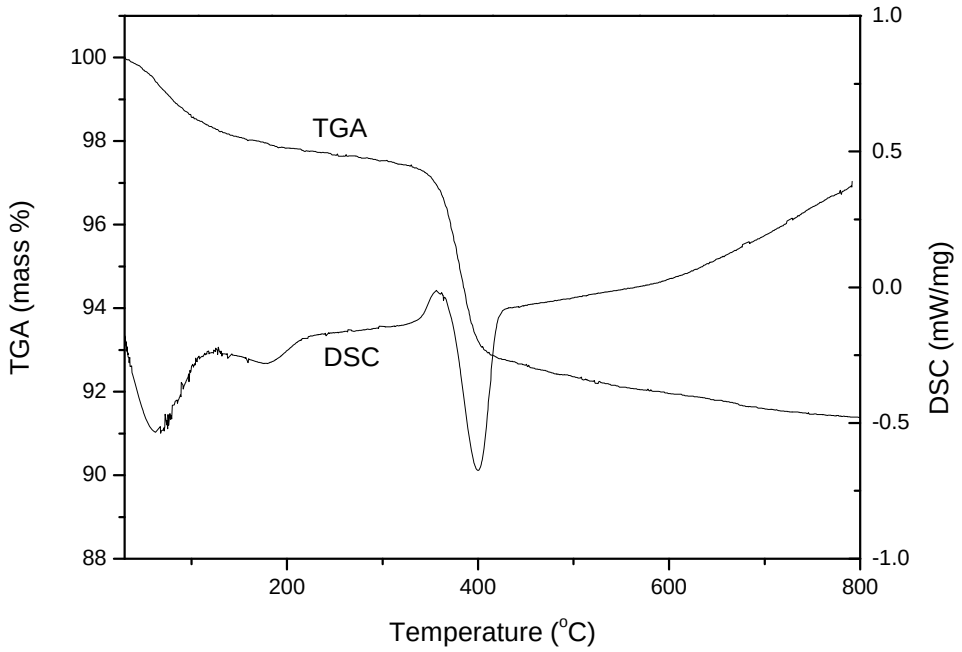

Fig. 2-8 TGA and DSC curves of 300 nm solvothermally treated PS-MFI.

Table 2-1 Mass fraction of $Mg(OH)_2$ in the surface treated PS-MFI measured by ICP-AES and TG analysis (%).

	Grignard			Solvothermal		
	Maximum*	ICP	TGA	Maximum	ICP	TGA
100 nm	34	37	34	23	19	21
300 nm	34	17	16	23	22	21
2 μm	34	8	5	23	22	21

*Theoretical calculations based on Mg source input assuming $Mg(OH)_2$ reaction yield is 100%.

2.3.4 Surface Roughness

Visual observation of SEM photographs indicates a high surface roughness of the nanostructures created by solvothermal treatment. However, the surface roughness can be quantified, since it is strongly related to the external surface area. The BET surface area after surface treatment on uncalcined MFI particles (whose internal micropores are blocked because of the presence of the SDA in them) was measured. In this study, 300 nm and 2 μm MFI crystals were chosen as representative samples, and the surface areas obtained from nitrogen physisorption measurements were normalized by the masses of zeolite and $Mg(OH)_2$ (which are obtained from ICP-AES measurements). Table 2-2 shows the BET surface area of bare and surface-treated uncalcined MFI particles. For both 300 nm and 2 μm MFI, surface roughness increased significantly after surface treatment. In addition, solvothermally treated MFI particles showed higher surface areas than Grignard treated samples, consistent with SEM observations. Normalization with the mass of $Mg(OH)_2$ showed that finer nanostructures were formed on 300 nm crystals in comparison to the 2 μm MFI crystals, via both the surface treatment methods. On the surface of 2 μm MFI crystals, the size of $Mg(OH)_2$ nanostructures created by both treatments was quite similar. However, for 300 nm particles, the nanostructures from the solvothermal treatment were smaller than those from the Grignard treatment.

Table 2-2 BET surface area of untreated and surface treated uncalcined PS-MFI normalized by the masses of zeolite and $Mg(OH)_2$.

	300 nm MFI (m^2/g zeolite)	300 nm MFI (m^2/g $Mg(OH)_2$)	2 μm MFI (m^2/g zeolite)	2 μm MFI (m^2/g $Mg(OH)_2$)
Untreated	7.5	-	3.7	-
Solvothermal	75	340	35	130
Grignard	40	190	11	130

2.3.5 Powder X-ray Diffraction

Powder XRD patterns of solvothermally surface-treated PS-MFI were measured. As shown in Fig. 2-9a, all particles maintained the MFI structure after the solvothermal treatment. Even though the treatment was performed in a basic environment at 160 ^oC, the MFI framework was observed to be robust. It was initially expected that peaks from $Mg(OH)_2$ could be detected by powder XRD measurements. However, there were no distinguishable peaks from $Mg(OH)_2$ except a broad peak at 38° 2θ. XRD patterns of MFI particles treated with Grignard reagent are also shown in Fig. 2-9b. All particles also maintained the MFI framework structure after the treatment. For large crystals such as 5 and 2 μm particles, only peaks from MFI were observed due to the high crystallinity of the zeolite. However, as the particle size decreased to 100 nm, the relative contribution of diffraction from the surface nanostructures became distinguishable, and the positions of these new XRD peaks were well matched with those of crystalline $Mg(OH)_2$ (brucite) [4, 6, 8]. Hence, it is concluded that nanostructures obtained by Grignard treatment are more

crystalline whereas those obtained by solvothermal treatment are likely X-ray amorphous (i.e., either composed of very small crystalline domains, or entirely amorphous). At the present time, there is no indication of the respective advantages of amorphous versus crystalline surface nanostructures.

2.3.6 Micropore Volume of Surface Treated MFI

It is possible that species involved in the surface nanostructure formation can plug/block the micropores of MFI, resulting in substantial pore volume reduction. If the nanostructure deposition is accompanied by a significant loss of microporosity, use of the surface-treated zeolites to fabricate membranes for separations will be complicated. To elucidate the effects of the surface treatments on the MFI pore structure, the micropore volumes of bare and surface-treated PS-MFI were measured by nitrogen physisorption. The isotherms are shown in Fig. 2-10, and the micropore volumes calculated by the t-plot method are summarized in Table 2-3. The apparent micropore volume was reduced after both Grignard and solvothermal treatments. In particular, the nitrogen adsorption capacity of 100 nm MFI in the low pressure region appears to decrease significantly after surface treatment, as shown in Fig. 2-10b. However, the apparent micropore volume should be normalized by the mass of the zeolite fraction, since the total mass increases after the growth of $Mg(OH)_2$ nanostructures on the surface. The appropriately normalized results show that the pore volume reduction by both surface treatments was marginal. For 100 nm particles, the pore volume decreased from 0.15 (bare MFI) to 0.12 (0.13) cm^3/g zeolite by solvothermal (Grignard) treatment, respectively. The pore volume reduction was negligible for larger crystals.

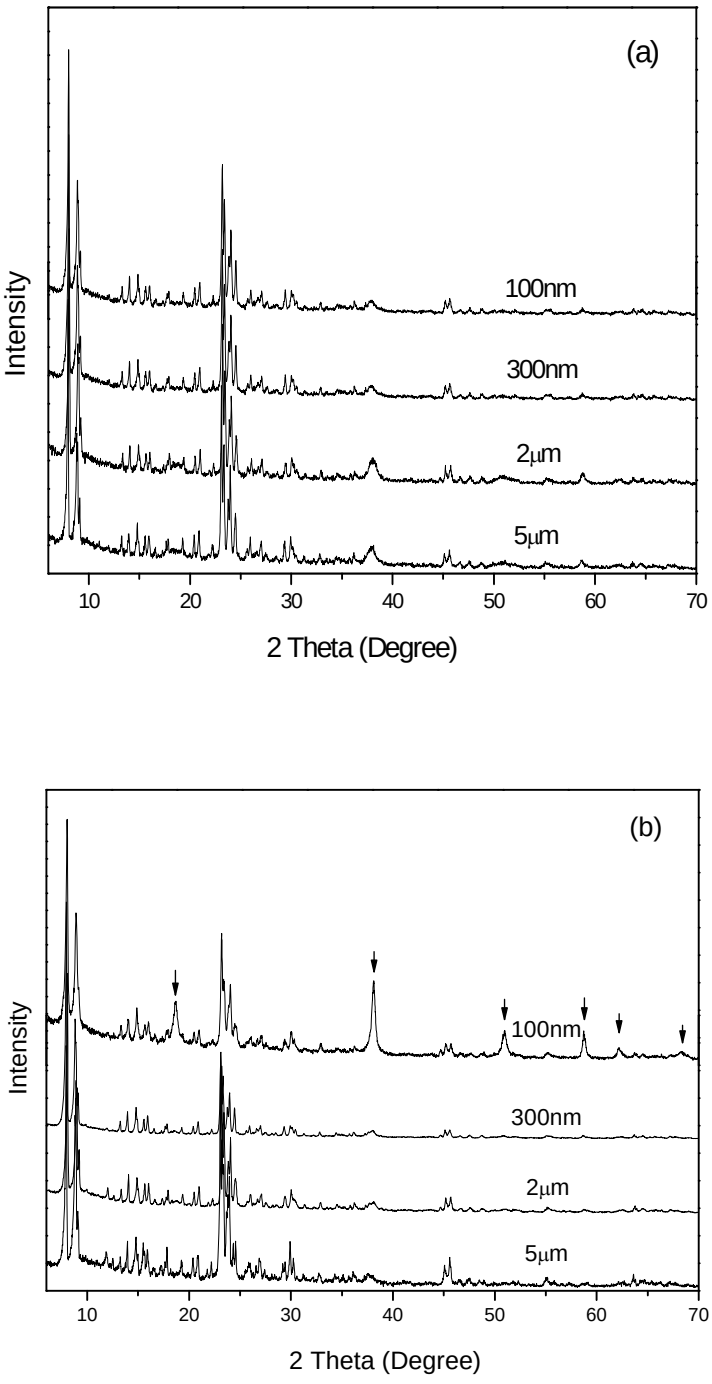

Fig. 2-9 XRD patterns of surface treated PS-MFI particles; (a) solvothermal treatment and (b) Grignard treatment. Peaks denoted by arrows are due to crystalline $Mg(OH)_2$.

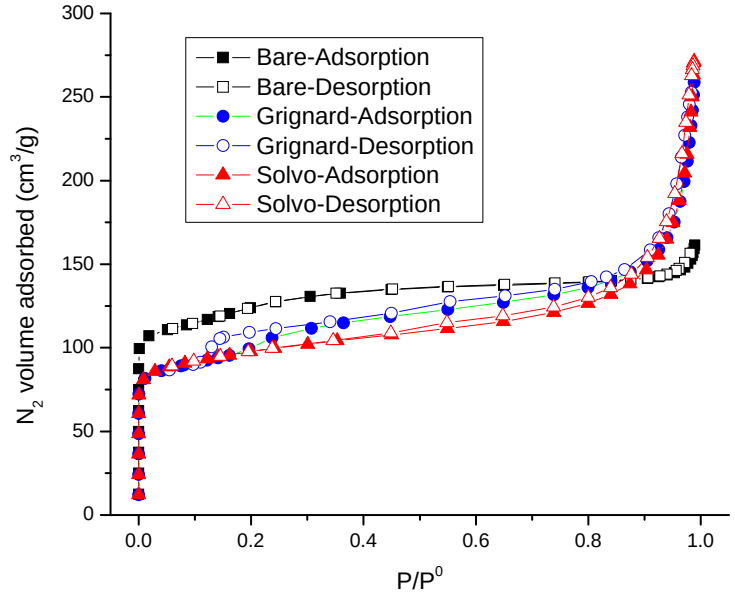

(a)

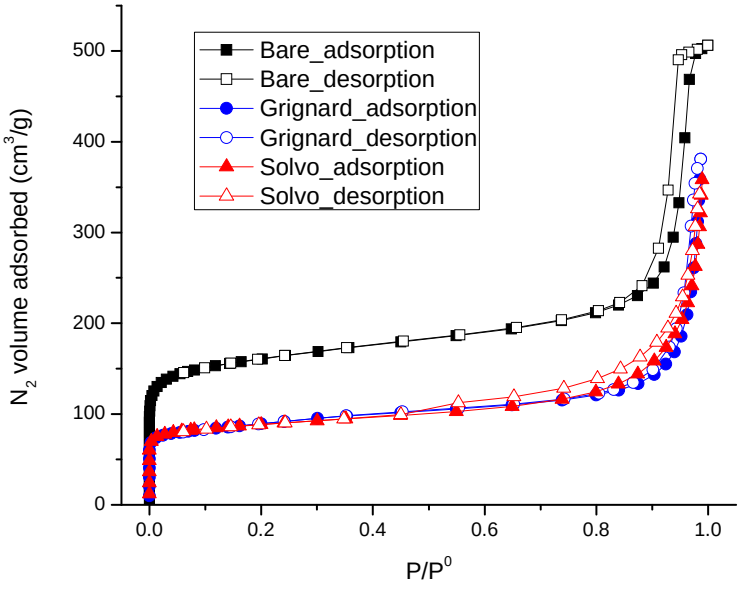

(b)

Fig. 2-10 Nitrogen physisorption isotherm of PS-MFI particles; (a) 300 nm and (b) 100 nm

Table 2-3 Micropore volumes of untreated and surface treated PS-MFI.

	100 nm		300 nm	
	cm^3/g sample	cm^3/g SiO_2	cm^3/g sample	cm^3/g SiO_2
Untreated	0.15		0.14	
Solvothermal	0.09	0.12	0.11	0.14
Grignard	0.08	0.13	0.11	0.13

2.3.7 Morphology of Mixed Matrix Composite Membranes

To investigate the compatibility of the surface-treated MFI particles with polymers, mixed matrix films were prepared using Ultem® as a polymer matrix and the zeolite loading was fixed to 10 wt% for all membranes. Fig. 2-11 shows SEM images of the cross-sections of Ultem®/untreated (bare) MFI. Voids at the interface are clearly seen in composite membranes fabricated with bare MFI. These "sieve-in-a-cage" morphologies have been reported in many previous studies [1, 15, 17, 19]. Furthermore, the particles formed clusters in the polymer matrix, resulting in a non-uniform distribution.

On the other hand, the film morphology was substantially improved by the use of MFI with nanostructured surfaces. As shown in Fig. 2-12, mixed matrix membranes fabricated with solvothermally treated MFI showed practically no interfacial voids by visual observation of the SEM images. Furthermore, all particles were uniformly distributed in the polymer matrix, in contrast to the membrane prepared with bare MFI - a

further indication of favorable interfacial adhesion between the molecular sieve and the polymer. MFI crystals modified with Grignard reagents also showed good zeolite/polymer interfacial morphology (Fig. 2-13).

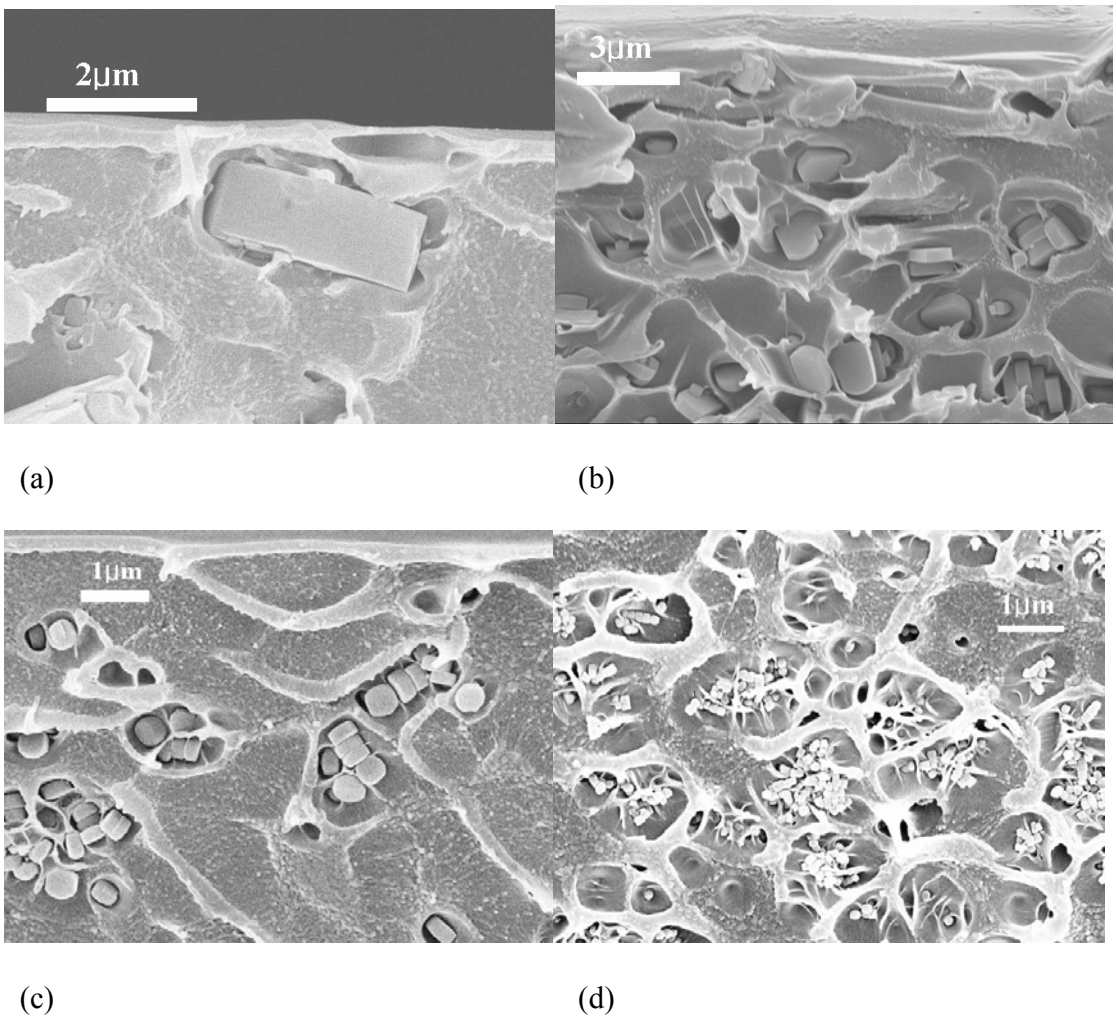

Fig. 2-11 SEM images of cross section of mixed matrix dense films made with bare MFI and Ultem®; (a) 5 μm, (b) 2 μm, (c) 300 nm and (d) 100 nm crystals.

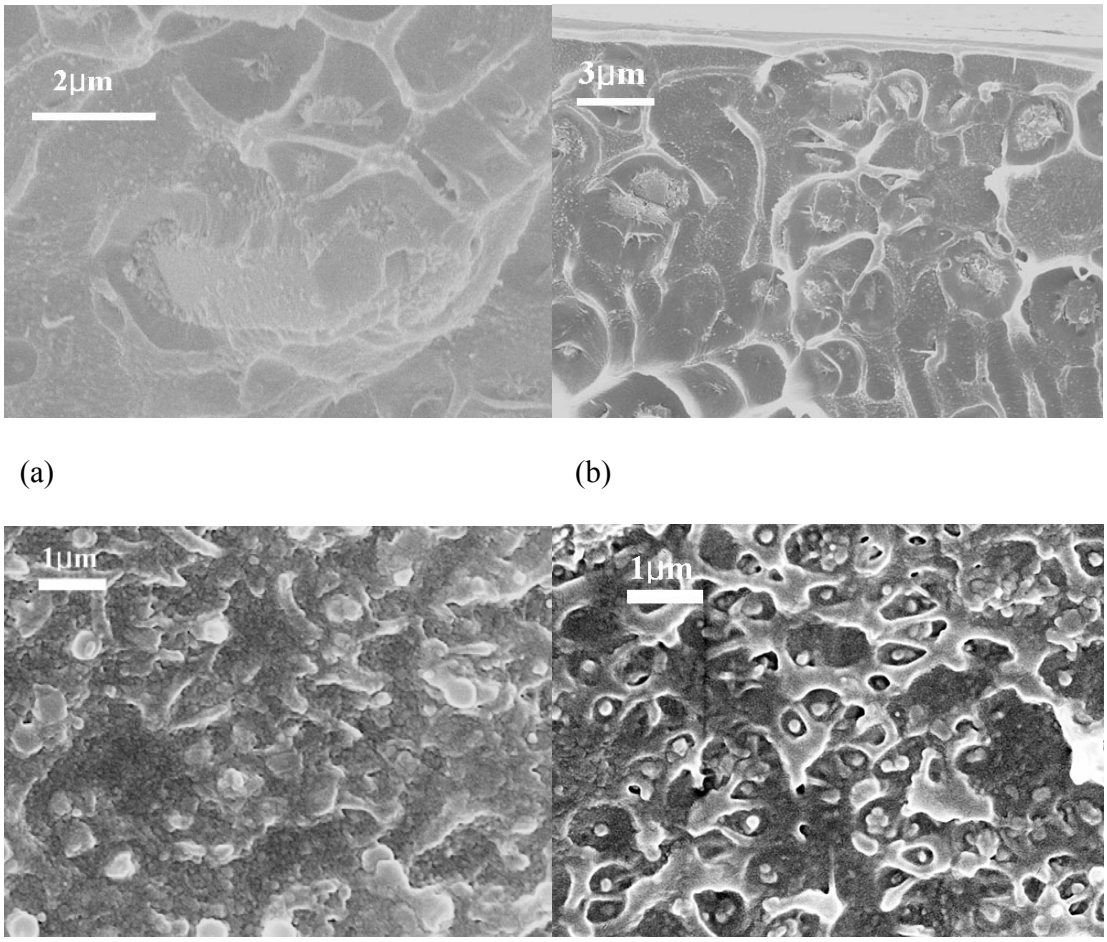

Fig. 2-12 SEM images of cross section of mixed matrix dense films made with solvothermally treated MFI and Ultem®; (a) 5 μm, (c) 2 μm, (c) 300 nm and (d) 100 nm crystals.

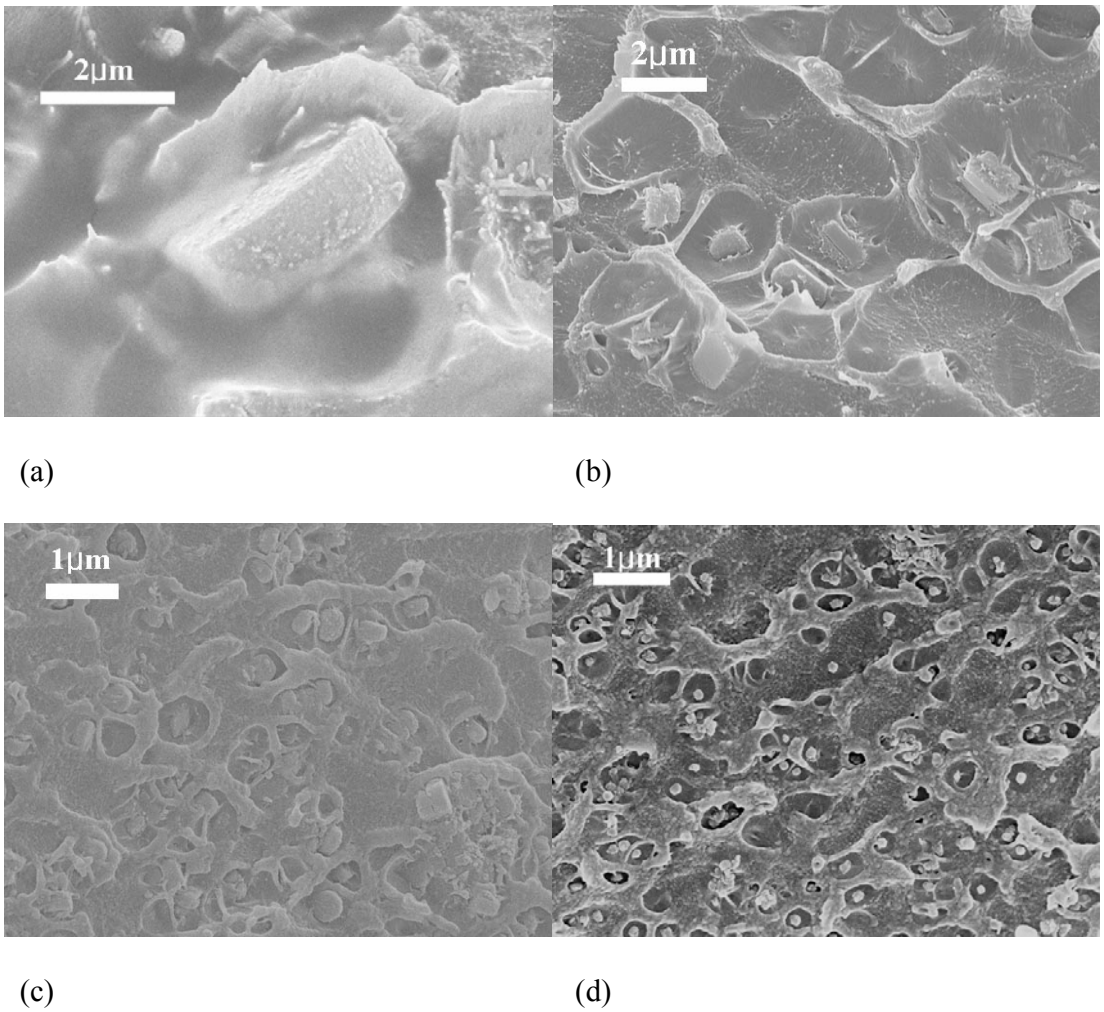

Fig. 2-13 SEM images of cross section of mixed matrix dense films made with Grignard treated MFI and Ultem®; (a) 5 μm, (b) 2 μm, (c) 300 nm and (d) 100 nm crystals.

2.3.8 Gas Prmeation Property of Mixed Matrix Membranes

Mixed matrix membranes with moderately high MFI loadings were fabricated using Ultem® and Matrimid® as polymer matrix. Table 2-4 summarizes the pure-component CO_2 and CH_4 gas permeation performance of mixed matrix membranes made with Ultem® and solvothermally modified MFI. High-quality membranes of this type

would give large increases in throughput without sacrificing selectivity. Ultem®/20 wt% MFI membranes showed a 60% enhancement in CO_2 permeability along with a 15% increase in CO_2/CH_4 selectivity compared to pure Ultem®. The use of 30 wt% MFI showed a further increase in selectivity with no significant change in CO_2 permeability, which remains much higher than that of pure Ultem®.

Table 2-4 Pure-component gas permeation properties of mixed matrix membranes containing 300 nm solvothermally treated MFI crystals at 35°C and 2 atm upstream pressure[(a)].

Membranes	CO_2 permeability (Barrer)	CH_4 permeability (Barrer)	CO_2/CH_4 selectivity
Pure Ultem[(b)]	1.4±0.1	0.036±0.001	38±1
20 wt% MFI in Ultem	2.2±0.1	0.051±0.001	43±2
30 wt% MFI in Ultem	2.0±0.1	0.044±0.001	45±2

[(a)] measured by Junqiang Liu in Dr. Koros research group
[(b)] averaged value from the literature [1, 20-21]

Matrimid®/MFI membranes showed a dramatic enhancement in CO_2 permeability and also a modest selectivity enhancement (Table 2-5). CO_2 permeability of 20 wt% MFI membranes increased to 23 from 7.6 of pure Matrimid® membranes with slight enhancement in CO_2/CH_4 selectivity. As the MFI loading increased to 35%, CO_2

permeability increased further. Since zeolite MFI has relatively large pore size (0.55 nm), it is reasonable for high quality mixed matrix membranes to show substantial enhancement in permeability with modest increase in selectivity.

Table 2-5 Pure-component gas permeation properties of mixed matrix membranes containing 300 nm solvothermally treated MFI crystals at 35°C and 2 atm upstream pressure[(a)].

Membrane	CO_2 permeability (Barrer)	CH_4 permeability (Barrer)	CO_2/CH_4 selectivity
Pure Matrimid[(b)]	7.6±2.3	0.21±0.07	35±1
20 wt% MFI in Matrimid	23±1	0.59±0.02	39±3
35 wt% MFI in Matrimid	31±2	0.78±0.04	39±4
20 wt% untreated MFI in Matrimid	42±1	1.5±0.1	28±2

[(a)] measured by Junqiang Liu in Dr. Koros research group
[(b)] averaged value from the literature [19-20, 22]

To rigorously show that the enhanced gas separation performance is due to the high quality of the polymer/modified-MFI interface, gas permeation measurements with

nonporous (uncalcined) MFI crystals were used, employing O_2 and N_2 as probes. Table 2-6 shows O_2 and N_2 single-component permeabilities of mixed matrix membranes fabricated with impermeable MFI crystals. In this case, the Maxwell model accurately predicted the permeability of the mixed matrix membrane of the desired ideal morphology (i.e., Experimental results from membranes made with solvothermally treated MFI (e.g., Fig. 2-12c) are well matched with the theoretical prediction, indicating excellent adhesion and no significant interfacial polymer rigidification. The latter is also confirmed by DSC results (Fig. 2-14). The rigidification of polymer chains at interface region is an important issue, resulting in lower gas permeability than the theoretical estimate. However, in this study, there were no observable changes in the glass transition temperature of Ultem® in the mixed matrix dense films.

On the other hand, membranes made with untreated MFI (e.g., Fig. 2-9c) showed considerably higher permeability than that of the ideal microstructure, with no positive effect on selectivity. This result is consistent with modified-Maxwell model predictions that account for voids at the polymer/zeolite interfaces [17], but the highly non-ideal microstructure of Fig. 2-11c cannot be rigorously described by the model. The overall results clearly show that the solvothermal deposition process substantially enhances polymer/particle adhesion, and is a promising route for processing functional inorganic crystals for membrane applications.

Table 2-6 Pure-component gas permeation properties of Ultem® and Ultem®/MFI mixed matrix membranes at 35°C and 4.5 atm upstream pressure. Uncalcined MFI crystals were used in the membranes[(a)].

Membranes	O_2 permeability (Barrer)	N_2 permeability (Barrer)	O_2/N_2 selectivity
Pure Ultem (Experimental)	0.43±0.01	0.055±0.002	7.8±0.2
Mixed matrix[(b)] (Experimental; treated MFI)	0.35±0.01	0.041±0.002	8.5±0.6
Mixed matrix[(c)] (Theoretical; ideal morphology)	0.35	0.044	7.8
Mixed matrix[(d)] (Experimental; untreated MFI)	0.43±0.02	0.056±0.003	7.5±0.7

[(a)] measured by Jong Suk Lee in Dr. Koros research group
[(b)] 20 wt% of solvothermally treated 300 nm MFI in the membrane.
[(c)] Maxwell model; 20 wt% of 300 nm MFI in the membrane; density of uncalcined MFI: 1.93 g/cm^3; density of Ultem: 1.27 g/cm^3.
[(d)] 20 wt % of untreated 300 nm MFI in the membrane.

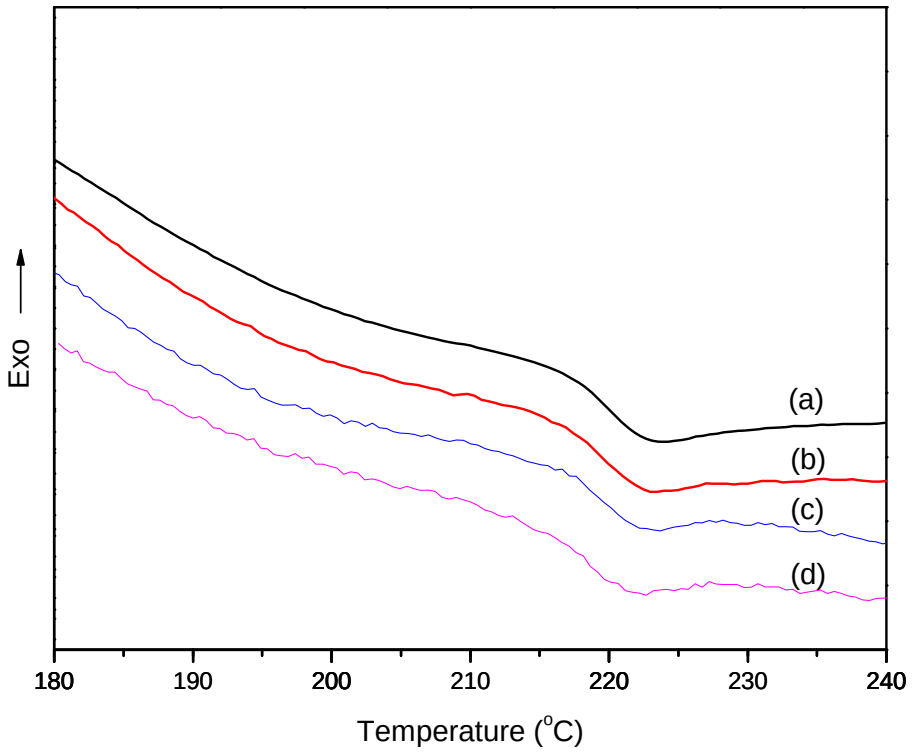

Fig. 2-14 DSC curves of pure and composite films; 50 wt % of 300 nm MFI loading; (a) pure Ultem®, (b) Bare MFI loading, (c) Grignard treated MFI loading, and (d) solvothermally treated MFI loading.

2.4 Conclusions

Pure-silica MFI was treated by solvothermal methods to deposit inorganic nanostructures on their surfaces. Surface roughness characterizations showed that solvothermal methods deposited small/fine $Mg(OH)_2$ nanostructures on the MFI surfaces, resulting in a highly roughened surface. The effect of surface treatment on the micropore volume of MFI was marginal or negligible. The functionalized zeolite crystals were used

in high-quality ‘mixed matrix’ membranes, wherein the zeolite crystals were well-adhered to the polymeric matrix. Substantially enhanced CO_2/CH_4 separation characteristics were observed in mixed matrix membranes containing solvothermally modified MFI crystals. Gas permeation measurements on membranes containing nonporous uncalcined MFI revealed that the performance enhancements were due to significantly enhanced MFI-polymer adhesion and distribution of the MFI crystals.

2.5 References

[1] S. Shu, S. Husain and W.J. Koros, J. Phys. Chem. C, 111 (2007) 652.

[2] S. Shu, S. Husain and W.J. Koros, Chem. Mater., 19 (2007) 4000.

[3] S. Shu, Chem. Eng. PhD Thesis, Georgia Institute of Technology, Atlanta, 2007.

[4] J. Lv, L.Z. Qu and B.J. Qu, J. Cryst. Growth, 267 (2004) 676.

[5] H. Yan, J.M. Wu, X.C. Zhang, Y. Zhang, L.Q. Wei, X.G. Liu and B.S. Xu, J. Mater. Res., 22 (2007) 2544.

[6] C. Henrist, J.P. Mathieu, C. Vogels, A. Rulmont and R. Cloots, J. Cryst. Growth, 249 (2003) 321.

[7] J.P. Hsu and A. Nacu, Colloid Surf. A., 262 (2005) 220.

[8] L. Yan, J. Zhuang, X.M. Sun, Z.X. Deng and Y.D. Li, Mater. Chem. Phys., 76 (2002) 119.

[9] Y. Ding, G.T. Zhang, H. Wu, B. Hai, L.B. Wang and Y.T. Qian, Chem. Mater., 13 (2001) 435.

[10] X.T. Lv, B. Hari, M.G. Li, X.K. Ma, S.S. Ma, Y. Gao, L.Q. Tang, J.Z. Zhao, Y.P. Guo, X. Zhao and Z.C. Wang, Colloid Surf. A., 296 (2007) 97.

[11] C.L. Yan, D.F. Xue, L.J. Zou, X.X. Yan and W. Wang, J. Cryst. Growth, 282 (2005) 448.

[12] Y.D. Li, M. Sui, Y. Ding, G.H. Zhang, J. Zhuang and C. Wang, Adv. Mater., 12 (2000) 818.

[13] C.H. Cheng, T.H. Bae, B.A. McCool, R.R. Chance, S. Nair and C.W. Jones, J. Phys. Chem. C, 112 (2008) 3543.

[14] J.R. Agger, N. Hanif, C.S. Cundy, A.P. Wade, S. Dennison, P.A. Rawlinson and M.W. Anderson, J. Am. Chem. Soc., 125 (2003) 830.

[15] T.T. Moore and W.J. Koros, J. Mol. Struct., 739 (2005) 87.

[16] T.-S. Chung, L.Y. Jiang, Y. Li and S. Kulprathipanja, Prog. Polym. Sci., 32 (2007) 483.

[17] R. Mahajan and W.J. Koros, Polym. Eng. Sci., 42 (2002) 1420.

[18] S.M. Auerbach, K.A. Carrado and P.K. Dutta (Editors), Handbook of zeolite science and technology, Marcel Dekker, 2003.

[19] S. Husain and W.J. Koros, J. Membr. Sci., 288 (2007) 195.

[20] D.Q. Vu, W.J. Koros and S.J. Miller, J. Membr. Sci., 211 (2003) 335.

[21] T.A. Barbari, W.J. Koros and D.R. Paul, J. Membr. Sci., 42 (1989) 69.

[22] H.Y. Zhao, Y.M. Cao, X.L. Ding, M.Q. Zhou, J.H. Liu and Q. Yuan, J. Membr. Sci., 320 (2008) 179.

CHAPTER 3

SOLVOTHERMAL TREATMENT OF ZEOLITE LTA FOR APPLICATION IN MIXED MATRIX MEMBRANES

3.1 Introduction

Zeolite LTA is an aluminosilicate zeolite having a 3-d micropore structure. The structure of LTA is shown in Fig. 3-1. A super-cage having 8-membered ring windows is constructed by assembly of sodalite cage building units [1-2]. Due to the incorporation of aluminum in the framework, LTA also contains extra-framework cations. The cations also influence the effective pore size via a combination of partial pore-blocking, occupancy, and electrostatic effects. Zeolite LTA with Na^+ as the extraframework intracrystalline cation (referred to as zeolite 4A in the literature) has a pore size of ~0.4 nm, which is very close to the kinetic diameter of several gas molecules, as shown in Table 3.1. So far, substantial work on mixed matrix membranes has been done using zeolite LTA for O_2/N_2 and CO_2/CH_4 separation, which are industrially very important gas separations [3-9].

It is known that the permeability of light gases in zeolite 4A is well matched with that of commercial glassy polymers such as Ultem® so that one can observe enhancement in both permeabilities and selectivities in mixed matrix membranes [6, 10]. The estimated separation performance for the LTA-Ultem® nanocomposite, as calculated by the Maxwell model, is shown in Fig. 3-2. A significant improvement in CO_2/CH_4 separation appears to be achievable. It is also predicted that a more modest improvement in O_2/N_2 separation will occur, because of the smaller difference in kinetic diameter

between O_2 and N_2.

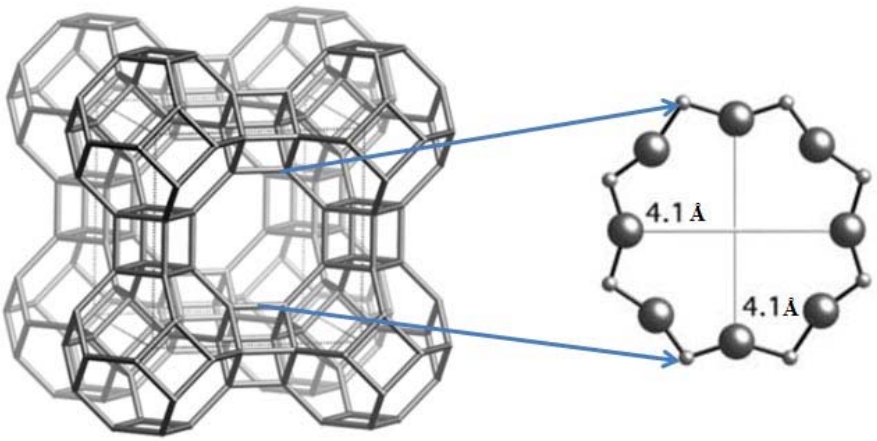

Fig. 3-1 The framework structure of zeolite LTA [2].

Table 3-1 Lennard-Jones kinetic diameters of gas molecules [11].

Molecules	Kinetic diameter (Å)
O_2	3.46
N_2	3.64
CO_2	3.30
CH_4	3.80

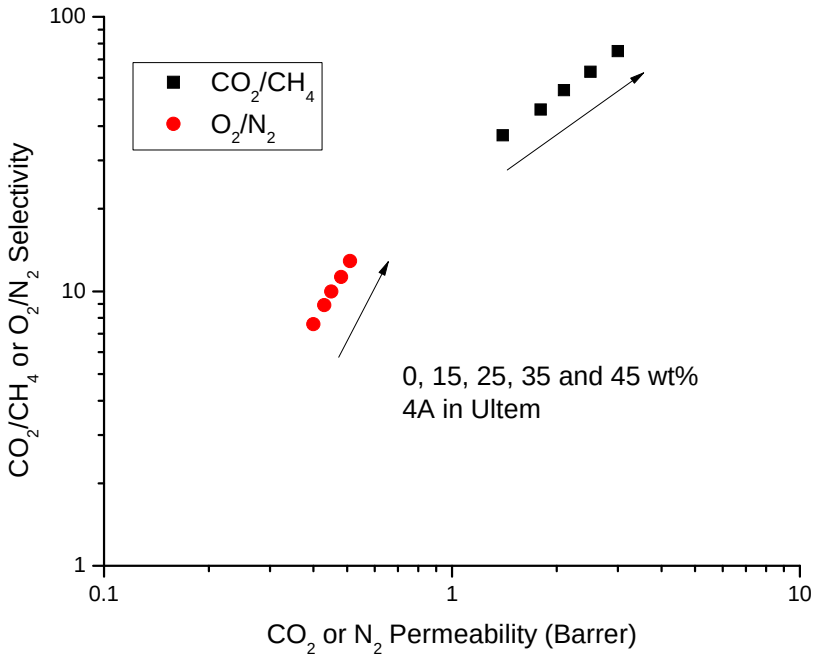

Fig. 3-2 Gas separation performance of 4A/Ultem® mixed matrix membranes calculated by Maxwell model; 4.5 atm upstream pressure at 35 ^{o}C.

Zeolite LTA can also be used in other molecular separations, since the size of the pores is tunable depending on the types of extra-framework intracrystalline cations. For example, LTA zeolites with K^{+} and Ca^{2+} as extra-framework cations are referred as zeolite 3A and 5A, respectively, due to their different pore dimensions. The properties of three different types of zeolite LTAs, viz, 3A, 4A and 5A, are summarized in Table 3-2. Zeolite 5A is a good candidate for butane isomer separation since it selectively adsorbs n-butane whereas iso-butane cannot get into the pore channels. Thus successful surface treatment of zeolite LTA is very beneficial since the potential applications of mixed matrix membranes containing zeolite LTA are wide-ranging.

In this Chapter, we discuss the surface functionalization of zeolite LTA, which presents challenges not encountered in the previous work on the functionalization of zeolite MFI. Zeolite LTA of two different particle sizes were hydrothermally synthesized and used as substrates. Initially the solvothermal treatment used in MFI functionalization was applied to the aluminosilicate LTA surfaces. Then the treatment conditions were modified to further tune the size/shape of the $Mg(OH)_2$ nanostructures on the LTA surfaces. The structural properties of these modified zeolites relevant to their application in mixed matrix membranes were thoroughly investigated.

Table 3-2 Characteristics of zeolites according to extraframework intracrystalline cations [1, 12].

Zeolite	Pore size (nm)	Cation	Micropore volume (cm^3/g)
3A	0.28	K^+	0.20
4A	0.40	Na^+	0.20
5A	0.49	Ca^{2+}	0.28

3.2 Experimental Section

3.2.1 Materials

The following chemicals were commercially available and were used as received: tetramethylammonuim hydroxide (TMAOH, 25% in water, Sigma-Aldrich),

ethylenediamine (EDA, 99%, Sigma-Aldrich), diethylenetriamine (DETA, 99%, Sigma-Aldrich), dichloromethane (DCM, 99.5%, Sigma-Aldrich), colloidal silica (Ludox HS-30, Sigma-Aldrich), aluminumisopropoxide ($Al(OiPr)_3$, 97%, Sigma-Aldrich), and magnesium sulfate heptahydrate (Acros). Ultem® 1000 (SABIC) was used as polymer matrix for mixed matrix membrane fabrication.

3.2.2 Synthesis of Zeolite LTA

LTA particles were synthesized hydrothermally based on the procedure published by Larlus et al [13]. Colloidal silica (Ludox HS-30) and aluminum isopropoxide were used as silicon and aluminum sources, respectively, and the structure directing agent was TMAOH. For 300 nm particle synthesis, clear precursor solution with molar ratio of $0.2NaOH$: $1SiO_2$: $1Al(OiPr)_3$: $4TMAOH$:$170H_2O$ was prepared at room temperature and treated hydrothermally at 60 ^oC for 1day, and at 100 ^oC for 1 day, correspondingly. Large crystal LTA, approximately 1-2 μm in diameter, was also prepared from the solution with molar ratio of $0.2NaOH$: $1SiO_2$: $1Al(OiPr)_3$: $2.4TMAOH$:$250H_2O$. The hydrothermal reaction was conducted at 120 ^oC for 4 days. After the reaction, the zeolite particles were washed with DI water by repetitions of centrifugation and dispersion at least 5 times and dried at 80 ^oC. Calcination was performed at 550 ^oC for 8 hr in air.

3.2.3 Solvothermal Treatment

After dispersing 0.2 g of zeolites in 10 ml of ethylenediamine (EDA) by sonication, 1 ml of 1 M aqueous $MgSO_4$ solution was added dropwise to the dispersion

while applying vigorous stirring. After further stirring for 1hr, the mixture was transferred to a Teflon-lined autoclave and the solvothermal treatment was performed at 160 ^{o}C in the synthesis oven for 12 hr. The particles were washed with DI water by several repetitions of sonication and centrifugation and dried at 80 ^{o}C.

Zeolite LTA was also treated with diethylenetriamine (DETA) as an organic base. In this method, $MgSO_4$ powder was used as the magnesium source. After dispersing 0.2 g LTA in 10 ml DETA placed in 23 ml volume Teflon cup, 1 mmol of $MgSO_4$ powder was added. The mixture was further sonicated for 1 min using a sonication horn and transferred to an autoclave reactor after adding 1 ml of DI water. The solvothermal reaction was conducted at 180 ^{o}C in the synthesis oven for 12 hr then the particles were washed with DI water by several repetitions of sonication and centrifugation. To remove residual DETA from the zeolites, more intense washing was often needed. For example, surface treated LTA crystals were further washed by stirring in water at 80 ^{o}C for 1 day.

3.2.4 Mixed-Matrix Composite Membrane Fabrication

Zeolite/polymer composite films were prepared using a solution casting technique. Zeolite particles were dispersed in DCM using a sonication horn. Polymer (polyetherimide, Ultem®) was added to the suspension, which was then stirred overnight. After pouring the solution on a glass plate, a nascent film was cast using a "doctor's knife". Finally, a dense film was obtained after drying at room temperature.

3.2.5 Characterization

Morphologies of both zeolite particles and mixed matrix membranes were observed with a scanning electron microscope (SEM, LEO 1530). To prevent any morphological change, the zeolite particles were observed without coating with gold. On the other hand, to observe cross-sections, mixed matrix membranes were coated with gold after being cryogenically fractured in liquid nitrogen. Energy dispersive X-ray spectroscopy (EDS) was used to investigate the elemental composition of zeolites. Micropore volume by t-plot method and BET (Brunauer-Emmett-Teller) surface area were calculated from nitrogen physisorption measurements performed on a Micromeritics ASAP 2020 or 2010. Powder X-ray diffraction (XRD) patterns were obtained on a Philips X'pert diffractometer equipped with X'celerator using Cu Kα radiation. To measure the mass fraction of $Mg(OH)_2$ in the solvothermally treated LTA crystals, differential scanning calorimetry (DSC) and thermogravimetric analysis (TGA) were performed on a Netzsch STA409. The detailed method for the calculation of mass fraction of $Mg(OH)_2$ is described in the Chapter 2.

3.2.6 Permeation Tests

Single gas permeation tests were performed in a constant volume apparatus. In this system, the feed and permeate reservoirs were separated by a cell that holds the membrane. It includes appropriate instrumentation for measuring the pressure in both reservoirs and the necessary valves, all within a constant temperature box. The detailed experimental procedure is described in the literature [14]. Permeation tests were performed with 4.5 atm upstream pressure at 35 °C. Numerous measurements were

performed for the thickness of each sample by using a micrometer, and their arithmetic average values were used for permeation data analysis.

3.3 Results and Discussion

3.3.1 Synthesis of LTA

The results of the hydrothermal synthesis of LTA are shown in the SEM images of the as-synthesized particles in Fig. 3-3. Well-defined cubic shape crystals with ~300 nm and ~1.5 μm average sizes were prepared. The zeolite LTA crystals have broader size distributions than the MFI crystals shown in Chapter 2. Powder XRD pattern revealed that both types of zeolite crystals had LTA frameworks (Fig. 3-4).

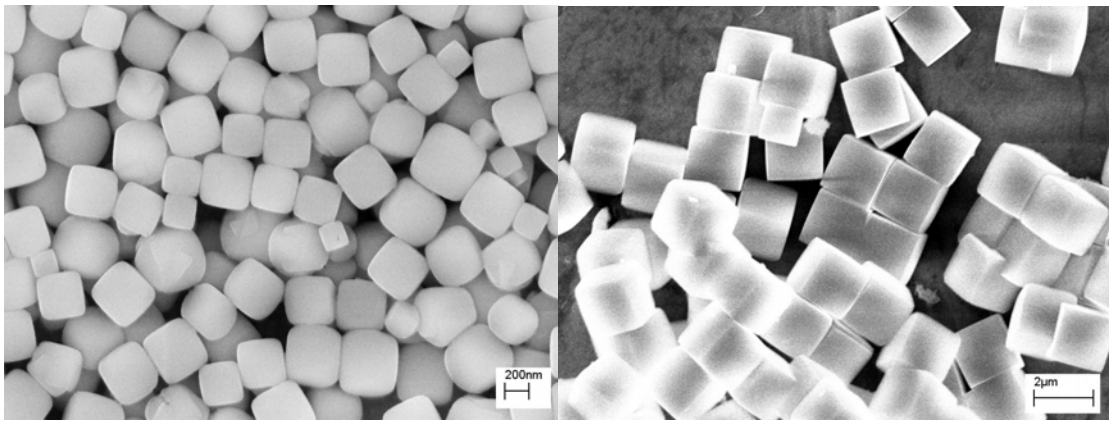

(a) (b)

Fig. 3-3 SEM images of zeolite LTA particles; (a) 300 nm and (b) 1-2μm large crystals

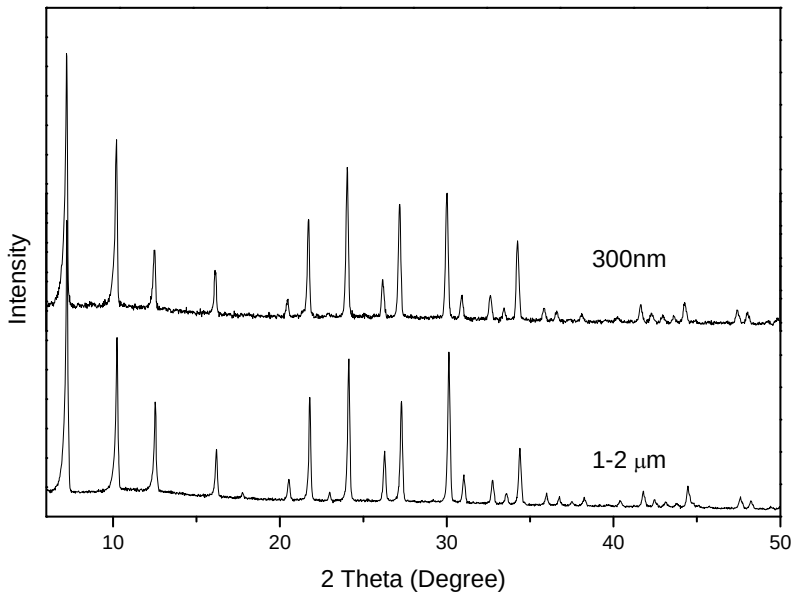

Fig. 3-4 Powder XRD patterns of zeolite LTA crystals.

3.2.2 Morphology of Surface Treated LTA

As in the case of MFI, solvothermal treatment using ethylenediamine (EDA) as an organic base was performed on LTA crystals. For 1-2 μm crystals, 0.5M $MgSO_4$ was used so the amount of magnesium would be half of that used for treatment of 300 nm crystals. As shown in Fig. 3-5, the smooth surfaces of zeolite LTA became highly roughened by the $Mg(OH)_2$ whiskers, so that the particles look like "cotton balls". This result indicates that solvothermal treatment with EDA may allow a perhaps general method to create inorganic nanostructures on various oxide surfaces such as pure silica (Chapter 2) and aluminosilicate surfaces (Chapter 3).

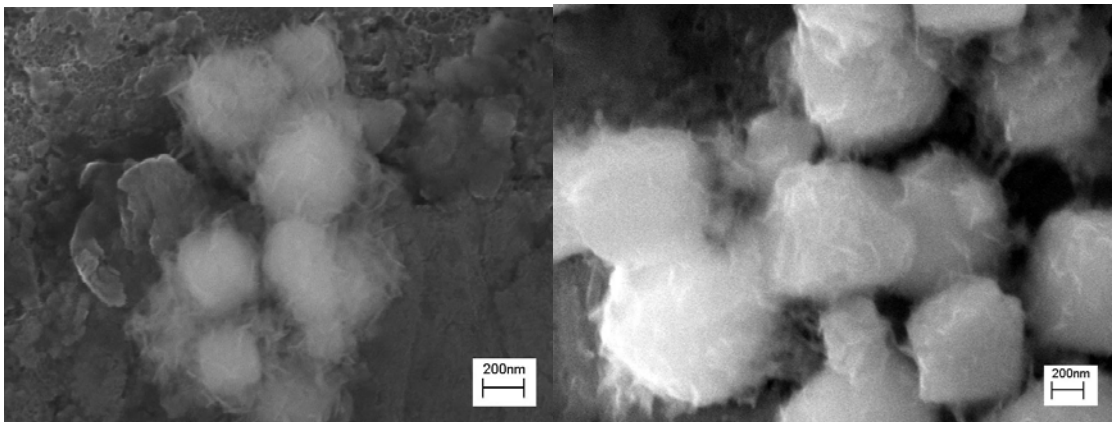

(a) (b)

Fig. 3-5 SEM images solvothermally treated LTA crystals in EDA/water mixture; (a) 300 nm Solvo-EDA, (b) 1-2 μm Solvo-EDA

In a previous study, $Mg(OH)_2$ nanorods or nanoneedles were solvothermally synthesized in EDA/water mixtures, and the authors have proposed that the controlled growth of $Mg(OH)_2$ nanorods originates from the formation of complexes of Mg^{2+} and two EDA ligands followed by their linear alignment and condensation [15-16]. Also they found that a high EDA/water ratio was essential for the formation of nanorods or "nanoneedles". In this study, a high volumetric ratio (~10) of EDA to water was used. Control experiments revealed that low EDA/water ratios caused homogeneous precipitation of $Mg(OH)_2$ and poor quality surface functionalization. For example, an EDA/water ratio of 1 resulted in thin, flat layers of $Mg(OH)_2$ on 2 μm MFI surfaces, whereas 1-2 μm LTA crystals were hardly functionalized (Fig. 3-6a and c). As shown in Fig. 3-6b and d, homogeneous precipitation was also observed independent of zeolite crystals.

Solvothermal treatment was also performed with DETA as an organic base. The powder form of $MgSO_4$ was directly used in this treatment instead of an aqueous solution. For 1-2 μm LTA crystals, 0.5 mmol of $MgSO_4$ powder (half of the amount used for 300 nm LTA) was added to 0.2 g LTA. As shown in Fig. 3-7, the surface treatment was successful and the resulting LTA crystals looked like "cotton-balls" due to the formation of $Mg(OH)_2$ nanowhiskers on the surfaces.

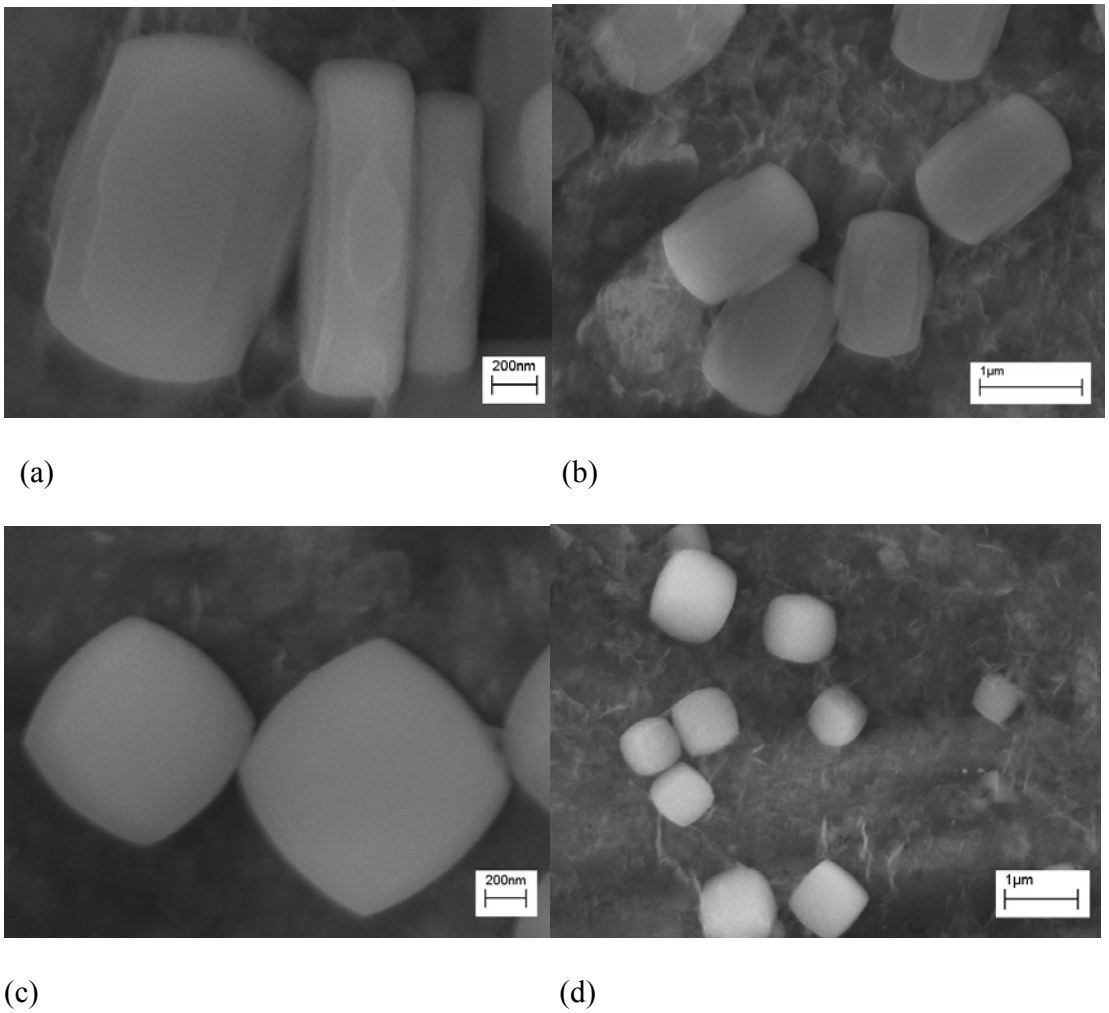

Fig. 3-6 Solvothermally treated zeolites at EDA to water ratio of 1; (a) and (b) 2 μm MFI; (c) and (d) 1-2 μm LTA.

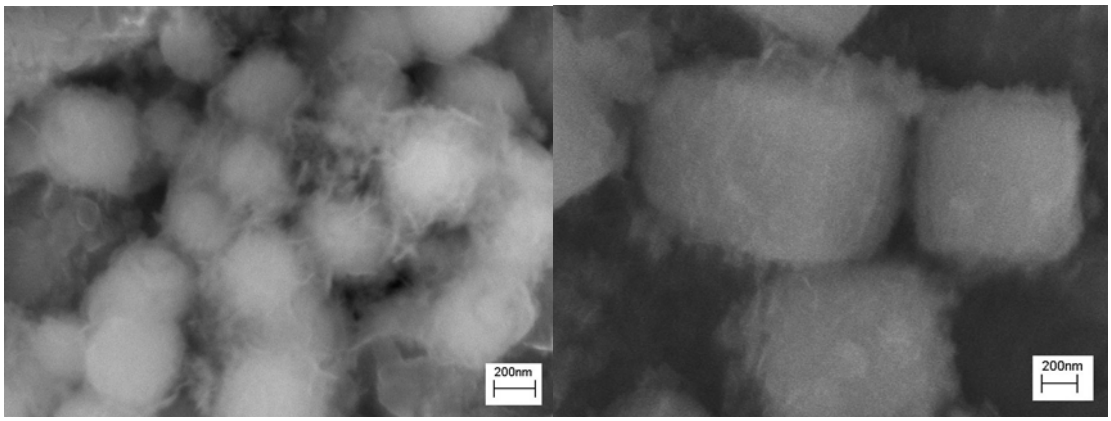

(a) (b)

Fig. 3-7 SEM images solvothermally treated LTA crystals in DETA/water mixture; (a) 300 nm Solvo-DETA and (b) 1-2 μm Solvo-DETA

3.2.3 Characterization of Surface Treated LTA Crystals

Powder XRD measurements revealed that the LTA structure was retained after both treatments (Fig. 3-8) and the XRD patterns for both materials were almost identical. A weak and broad reflection at 18^{o}, as well as a stronger peak at 38^{o}, were observed in the 300 nm samples, presumably due to $Mg(OH)_2$ nanostructures. The intensity of both peaks were weaker in 1-2 μm LTA crystals since the amount of the magnesium source was reduced to half of that was used in treatment of the 300 nm crystals,

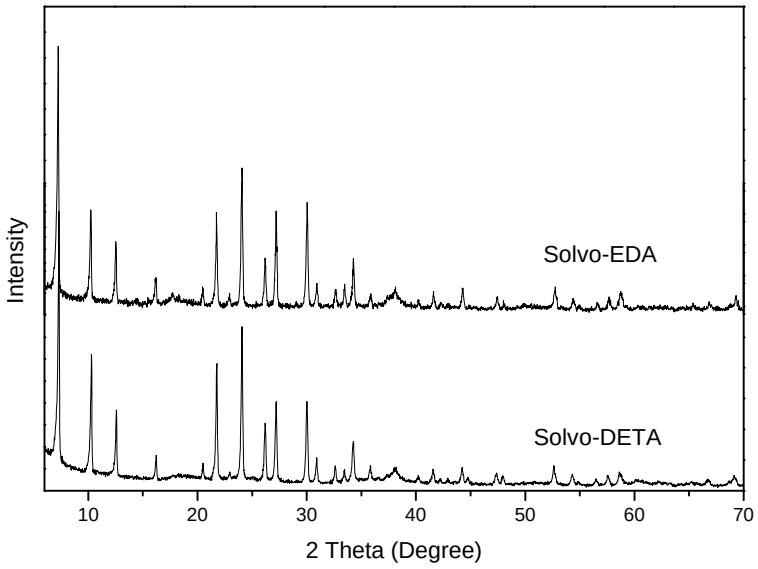

(a)

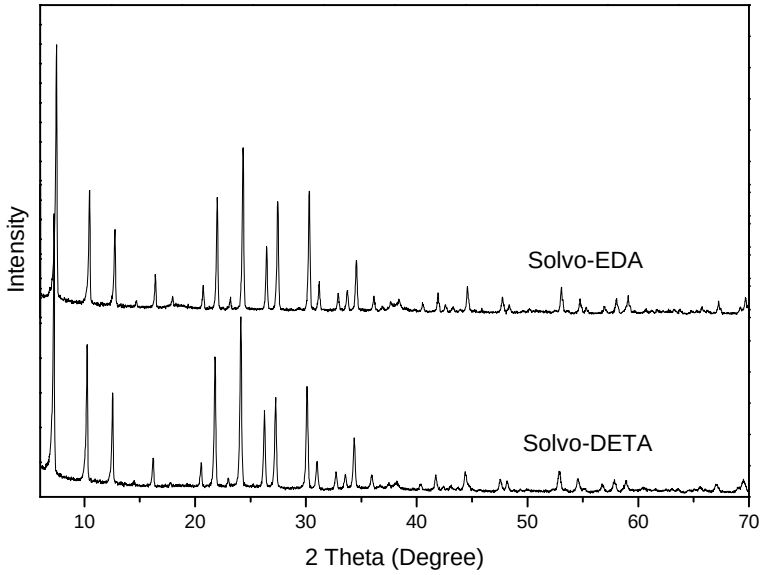

(b)

Fig. 3-8 XRD patterns of surface treated zeolite LTA; (a) 300 nm and (b) 1-2 μm crystals.

The $Mg(OH)_2$ mass fraction in the surface treated 300 nm LTA crystals was estimated by TGA and the results are shown in Table 3-3. The reaction yield was very high and the mass fraction was close to the stoichiometric maximum for solvothermal treatments using either EDA or DETA. However, since even the uncalcined zeolite LTA has some microporosity, unlike uncalcined MFI, the method used for MFI shown in Chapter 2 could not be applied directly (Fig. 3-9). Instead, the BET external surface area calculated by a t-plot of the data from the nitrogen physisorption measurement on calcined LTA was used to estimate the external surface area. Fig. 3-10 shows nitrogen physisorption isotherms of 300 nm untreated (bare) and surface treated zeolite LTA crystals. The corresponding BET external surface areas are summarized in Table 3-3. All numbers were normalized by masses of zeolite and $Mg(OH)_2$ respectively. It is clear that the surface roughness of zeolite LTA dramatically increased after deposition of $Mg(OH)_2$ whisker structures. Interestingly, solvothermal treatment with DETA gave rise to a higher surface area per unit mass of $Mg(OH)_2$ than when using the EDA route, indicating that smaller/finer nanostructures were created using DETA. Furthermore, it is advantageous to use the milder reaction conditions of the DETA route. In this case, the reaction temperature is lower than the boiling point of the solvent (hence reducing the vapor pressure in the reactor).

Table 3-3 Micropore volumes and t-plot external surface area of 300 nm LTA crystals.

	$Mg(OH)_2$ mass fraction (%)	Micropore volume cm^3/g zeolite	External surface area	
			m^2/g zeolite	m^2/g $Mg(OH)_2$
Untreated	-	0.17	15	-
Solvo-EDA	22 (21*)	0.21	100	360
Solvo-DETA	20 (21*)	0.20	160	620

*Theoretical calculations based on Mg source input assuming $Mg(OH)_2$ reaction yield is 100%.

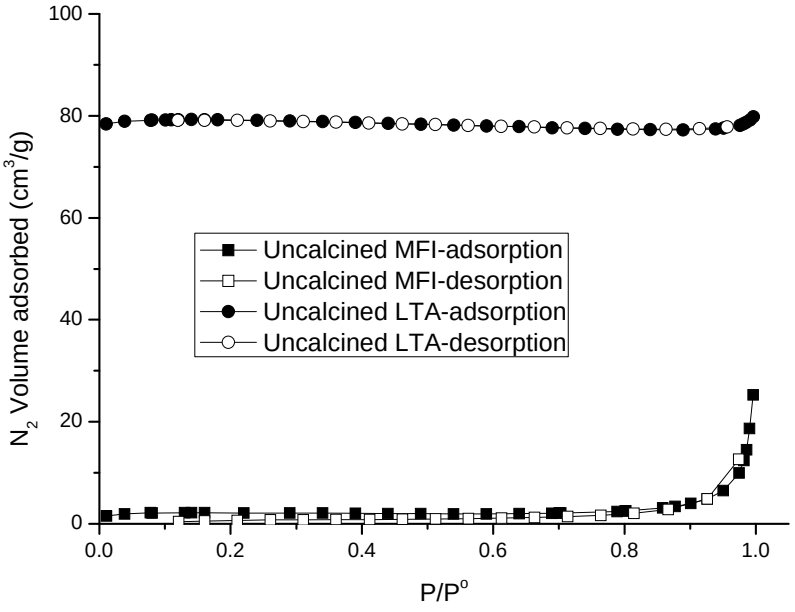

Fig. 3-9 Nitrogen physisorption isotherms of uncalcined PS-MFI and LTA particles. 300 nm PS-MFI and 1-2 μm LTA crystals were used for measurements. The t-plot micropore volumes of the uncalcined MFI and LTA crystals were 0.00 and 0.12cm^3/g, respectively.

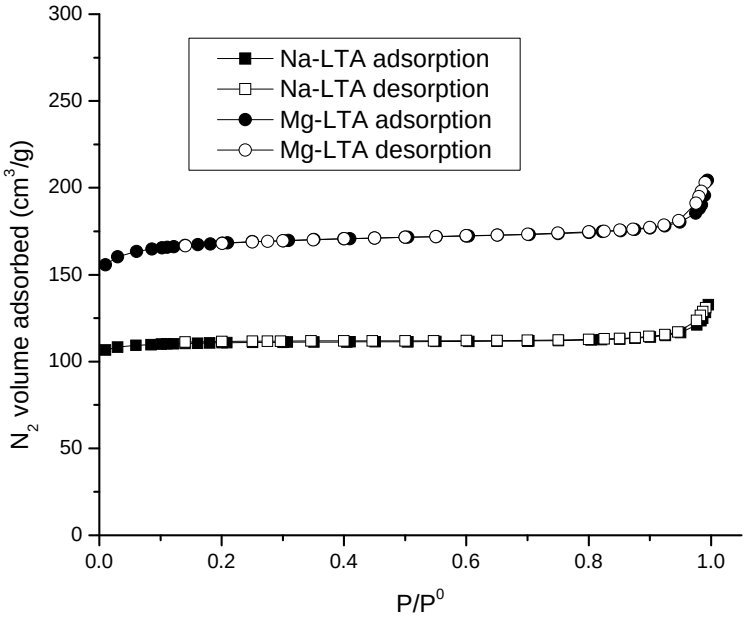

(a)

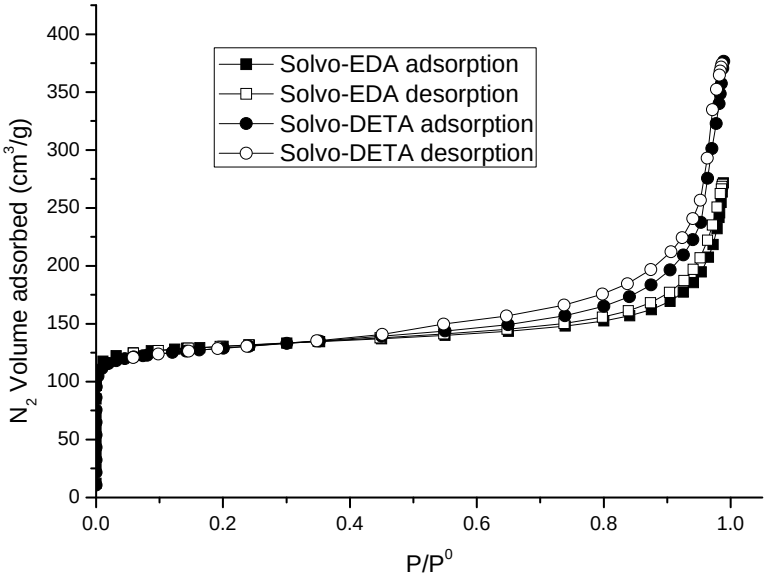

(b)

Fig. 3-10 N_2 physisorption isotherms of (a) 300 nm untreated LTA and (b) 300 nm surface treated LTA.

Elemental compositions of both untreated and treated LTA were measured by energy dispersive spectroscopy (EDS) and the results are shown in Table 3-4. After the surface treatment, the Na/Al ratio dramatically decreased, presumably due to ion exchange of extraframework intracrystalline Na^+ in LTA with Mg^{2+} from the reactant solution. This hypothesis is further supported by nitrogen physisorption measurements. Unlike the case of MFI, surface treatments gave rise to substantial micropore volume changes in LTA. As shown in Table 3-3, solvothermally treated LTA showed higher micropore volume than the original Na-LTA. A control experiment revealed that ion-exchanged Mg-LTA has a higher pore volume than Na-LTA. Since two Na^+ ions are replaced by a Mg^{2+} ion, the micropore volume increased from 0.17 to 0.24 cm^3/g (Fig. 3-10a). Micropore volumes of surface-treated LTA crystals were 2.1 and 2.0 cm^3/g zeolite, by the EDA and DETA routes respectively. These values are intermediate between those of Na-LTA and Mg-LTA, indicating a partial ion exchange of Na^+ with Mg^{2+}. Thus, the molecular sieving/transport properties of LTA could be altered because it is well known that the effective size of the micropores in LTA can be varied by ion-exchange. For example, Ca-LTA ("5A") has 0.5 nm pore size in contrast to 0.4 nm for Na-LTA ("4A"). Finally, it must be mentioned that the EDS measurements (spuriously) indicate a higher magnesium content than the possible stoichiometric maximum, since the technique emphasizes the contribution of elements on the surface over those in the underlying bulk material. However, the comparison of elements existing in the same region (surface or bulk) as described above, is reliable.

Table 3-4 Elemental composition of 300 nm zeolite LTA measured by EDS.

Atomic %	O	Na	Mg	Al	Si	Na/Al
Na-LTA	61.4	11.1	-	13.6	14.0	0.82
Solvo-LTA (EDA)	49.8	3.3	18.6	14.2	14.1	0.23
Solvo-LTA (DETA)	66.7	1.5	12.1	9.4	10.4	0.16

3.2.4 Mixed Matrix Composite Membranes

To investigate the adhesion of the surface-treated LTA particles with polymers, mixed matrix films were prepared using Ultem® as a polymeric matrix. Fig. 3-11 shows cross sections of membranes made with Ultem®/untreated LTA and Ultem®/solvothermal-LTA. Untreated LTA/Ultem® films showed a typical "sieve-in-a-cage" morphology, with voids at the interfacial regions. Furthermore – and especially for the 300 nm LTA crystals - the particles also formed clusters in the polymer matrix, resulting in a non-uniform distribution. In contrast, mixed matrix membranes fabricated with solvothermally treated LTAs were uniformly free of interfacial voids, and the individual particles were well distributed in the polymer matrix due to their improved interactions with the polymer. Since these characteristics are prerequisites for good membrane performance [6, 14], I consider these results as promising for the pursuit of applications for these surface-nanostructured materials in gas separations.

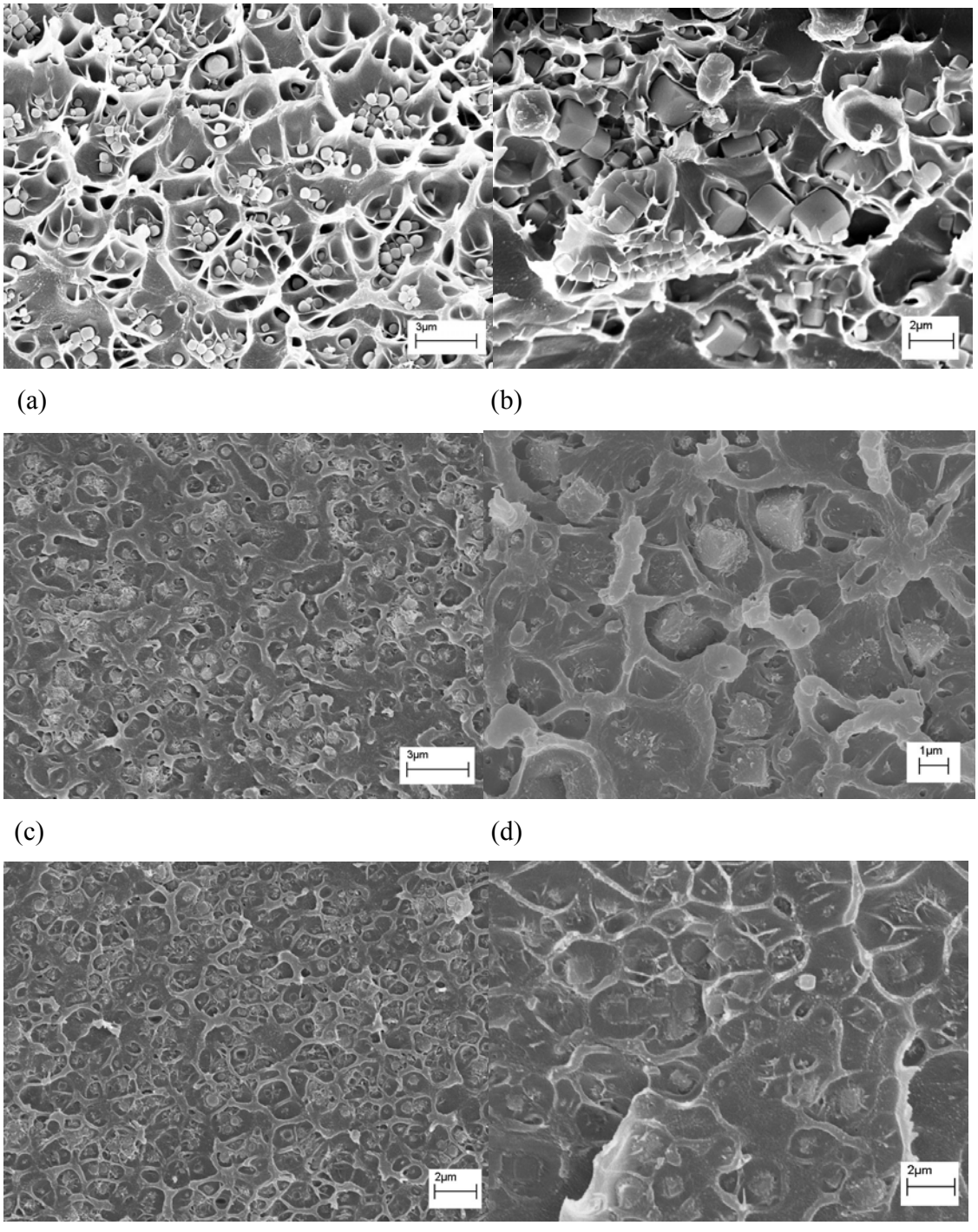

Fig. 3-11 SEM images of cross sections of mixed matrix membranes containing 20 wt % molecular sieve loading in Ultem®; (a) 300 nm bare, (b) 1-2 µm bare, (c) 300 nm Solvo-EDA, (d) 1-2 µm Solvo-EDA, (e) 300 nm Solvo-DETA, and (f) 1-2 µm Solvo-DETA.

3.2.5 Gas Permeation

As discussed in Section 3.2.4, the DETA route results in more roughened LTA surfaces than reaction in EDA/water mixtures. However, right after the treatment, LTA pores was plugged with DETA molecules and intracrystalline extraframework Na^+ ions are also replaced Mg^{2+} ions. To obtain a molecular sieve suitable for CO_2/CH_4 separation, the surface treated LTA was stirred in 1M $NaNO_3$ solution at 60 ^oC for 12 hr to remove DETA residue in the pores and also replace the Na^+ ions in zeolite structure after the treatment. After the ion-exchange, the Na/Al ratio increased from 0.16 to 0.55 by EDS. However, the ratio didn't increase noticeably further, even though the ion-exchange was repeated several times more. The micropore volume (0.20 cm^3/g zeolite) was also higher than the untreated bare LTA. This result may imply that some Mg^{2+} ions were preferentially bound to framework and not replaced with Na^+ ions.

The gas permeation propertis of mixed matrix membranes fabricated with two types of surfaces modified 300 nm LTAs and Ultem® were measured, and the results are shown in Table 3-5. Mixed matrix membranes containing surface modified LTAs showed a slight enhancement in both CO_2 permeability and CO_2/CH_4 selectivity. The performance of membranes with surface treated LTA was totally different from a membrane containing untreated zeolites. As shown in Table 2-5 in Chapter 2, the CO_2/CH_4 selectivity of a mixed matrix membrane with untreated zeolite was lower than that of the pure polymeric membrane due to the non-selective gas flow through the zeolite/polymer and zeolite/zeolite interfacial defects. A theoretical prediction by the Maxwell model was conducted. For the calculation, the permeability information of

zeolite 4A was adopted from the literature [10]. As shown in Table 3-5, the CO_2/CH_4 selectivity of the mixed matrix membranes was lower than the theoretical prediction by the Maxwell model.

Table 3-5 Pure-component gas permeation properties of mixed matrix membranes containing 20 wt% of 300 nm solvothermally treated LTA crystals at 35°C and 4.5 atm upstream pressure[(a)].

Membranes	CO_2 permeability (Barrer)	CH_4 permeability (Barrer)	CO_2/CH_4 selectivity
Pure Ultem[(b)]	1.4±0.1	0.036±0.001	38±1
Solvo-LTA (EDA)/Ultem	1.5±0.1	0.037±0.002	42±3
Solvo-LTA (DETA)/Ultem	1.6±0.1	0.038±0.002	42±3
Theoretical prediction[(c)]	1.8	0.033	47

[(a)] measured by Junqiang Liu in Dr. Koros research group
[(b)] averaged value from the literature [6, 17-18]
[(c)] by the Maxwell model; density of dehydrated LTA: 1.52g/cm^3; density of Ultem: 1.27g/cm^3

Although the results show improvement in membrane performance upon incorporation of surface-functionalized LTA, there are a number of possible reasons for the somewhat lower CO_2/CH_4 selectivity of mixed matrix membranes with surface treated LTA in comparison with the theoretical predictions. Firstly, the transport properties of the surface modified zeolites may be different from Na-LTA. The Na/Al

ratio of the surface treated LTA was ~0.5, and the micropore volume was higher than that of 4A. Since the surface treated zeolite has both Mg^{2+} and Na^{+} as extra-framework cations, the sizes of the pores in LTA could be distributed over a range of values. This may result in lower CO_2/CH_4 selectivity than when using 4A. Secondly, the LTA/polymer adhesion properties may still not be ideal as assumed in the Maxwell model. However, nanometer-scale gaps can still be present at the zeolite/$Mg(OH)_2$ layer or the $Mg(OH)_2$ layer/polymer interfaces, and cannot be observed by SEM. The surface properties of aluminosilicate LTA are different from those of pure silica MFI, and the quality of the surface treatments may also be different in both cases. For example, $Mg(OH)_2$ adhesion to LTA may be weaker than the PS-MFI case. In this case, during membrane fabrication, nanometer scale gaps can be formed between the zeolite and $Mg(OH)_2$ layers, due to the stress generated by solvent evaporation. Furthermore, LTA nanoparticles (300 nm) were used as fillers in this study. The control of the interfacial morphology was even harder due to the larger interfacial area compared to bigger LTA crystals. It is also possible that the Maxwell model overpredicted the performance of the mixed matrix membrane. The transport properties of the Na-LTA used in the calculation (CO_2/CH_4 selectivity = 340) may not be accurate, since it is based on several assumptions [10]. For the calculation, the diffusion coefficient and sorption capacity reported in the literature were used [19-22]. However, the values, especially, the diffusion coefficients in zeolites, can vary depending on the measurement methods. If another CH_4 diffusion coefficient reported in a different literature paper was used for the calculation, the CO_2/CH_4 selectivity of 4A would drop to130 [10]. Finally, it is noted that the permeabilities being measured in the Ultem®-based membranes here quite small, and can be affected by the variability of the sample

preparation procedures. The error bars reported in the Table only refer to the least count (systematic error) of the measurement apparatus, and not the statistical (random) errors as estimated from measurements with several different samples.

3.4 Conclusions

LTA zeolite crystals were hydrothermally synthesized and treated by solvothermal methods to deposit inorganic nanostructures on their surfaces. Solvothermal deposition of inorganic nanostructures was successfully applied to aluminosilicate LTA surfaces. However, concurrent ion exchange took place between the Na^+ ions in the LTA pores and the Mg^{2+} ions in the reactant solution. Solvothermal treatment of LTA was tuned to deposit smaller/finer $Mg(OH)_2$ nanostructures, resulting in a more highly roughened zeolite surface. Characterization of particles and mixed matrix membranes revealed that the solvothermally surface-treated LTA particles were promising for application in mixed matrix membranes. The CO_2/CH_4 separation properties were enhanced in a mixed matrix membrane containing solvothermally modified LTA, but the CO_2/CH_4 selectivity was lower than the Maxwell model prediction. Several potential reasons for this result have been given, and the true caused should be the subject of ongoing investigations.

3.5 References

[1] S.M. Auerbach, K.A. Carrado and P.K. Dutta (Editors), Handbook of zeolite science and technology, Marcel Dekker, 2003.

[2] C. Baerlocher, Atlas of zeolite framework types, Published on behalf of the Structure Commission of the International Zeolite Association by Elsevier, Amsterdam ;, 2007.

[3] R. Mahajan and W.J. Koros, Ind. Eng. Chem. Res., 39 (2000) 2692.

[4] R. Mahajan and W.J. Koros, Polym. Eng. Sci., 42 (2002) 1420.

[5] R. Mahajan and W.J. Koros, Polym. Eng. Sci., 42 (2002) 1432.

[6] S. Shu, S. Husain and W.J. Koros, J. Phys. Chem. C, 111 (2007) 652.

[7] T.-S. Chung, L.Y. Jiang, Y. Li and S. Kulprathipanja, Prog. Polym. Sci., 32 (2007) 483.

[8] Y. Li, T.-S. Chung, C. Cao and S. Kulprathipanja, J. Membr. Sci., 260 (2005) 45.

[9] Y. Li, H.-M. Guan, T.-S. Chung and S. Kulprathipanja, J. Membr. Sci., 275 (2006) 17.

[10] T.T. Moore, Chem. Eng. PhD thesis, University of Texas, 2004.

[11] R. Szostak, Molecular Sieves; principles of synthesis and identification, Van Nostrand Reinhold, New York, 1989.

[12] S. Basu, A.L. Khan, A. Cano-Odena, C.Q. Liu and I.F.J. Vankelecom, Chem. Soc. Rev., 39 (2010) 750.

[13] O. Larlus, S. Mintova and T. Bein, Micropor. Mesopor. Mater., 96 (2006) 405.

[14] T.T. Moore and W.J. Koros, J. Mol. Struct., 739 (2005) 87.

[15] Y. Ding, G.T. Zhang, H. Wu, B. Hai, L.B. Wang and Y.T. Qian, Chem. Mater., 13 (2001) 435.

[16] Y.D. Li, M. Sui, Y. Ding, G.H. Zhang, J. Zhuang and C. Wang, Adv. Mater., 12 (2000) 818.

[17] D.Q. Vu, W.J. Koros and S.J. Miller, J. Membr. Sci., 211 (2003) 335.

[18] T.A. Barbari, W.J. Koros and D.R. Paul, J. Membr. Sci., 42 (1989) 69.

[19] H. Yucel and D.M. Ruthven, J. Colloid Interface Sci., 74 (1980) 186.

[20] H. Yucel and D.M. Ruthven, J. Chem. Soc. Faraday Trans., 76 (1980) 60.

[21] N. Haq and D.M. Ruthven, J. Colloid Interface Sci., 112 (1986) 154.

[22] R.J. Harper, G.R. Stifel and R.B. Anderson, Can. J. Chem., 47 (1969) 4661.

CHAPTER 4

ION-EXCHANGE-INDUCED GROWTH OF INORGANIC NANOSTRUCTURES ON ZEOLITE SURFACES FOR MIXED MATRIX MEMBRANE FABRICATION

4.1 Introduction

In the previous two chapters, a facile solvothermal treatment to deposit $Mg(OH)_2$ nanostructures on zeolite surfaces is presented. Especially in Chapter 2, it is shown that improved gas separation performance was observed with resultant mixed matrix dense film membranes and good zeolite/polymer adhesion properties were also rigorously measured. From economic and environmental perspectives, however, it is more beneficial to perform the surface treatment of the molecular sieves in the aqueous phase. It is also desirable to create more strongly bound inorganic structures on zeolite surfaces, in order to better withstand the high shear forces generated during phase separation processes occurring in the fabrication of commercially viable asymmetric membranes such as hollow fibers.

Several studies have demonstrated synthesis of $Mg(OH)_2$ with various morphologies via aqueous phase reaction at moderate temperatures [1-4] or hydrothermal processes [5-8]. However, these methods cannot be used for the treatment of zeolites directly, as the reaction conditions strongly prefer homogeneous precipitation in the bulk phase rather than nucleation/growth on a zeolite substrate. A special methodology is required to create nanostructured morphologies in a controlled manner and with high

yield on the surfaces of zeolites, limiting precipitation in solution independent of the zeolite surfaces.

In this chapter, an ion-exchange-induced growth of $Mg(OH)_2$ nanostructures on zeolite LTA is presented. The reaction scheme is shown in Fig. 4-1. In this method, the magnesium source for the formation of $Mg(OH)_2$ structures is supplied from inside the zeolite particles. It is hypothesized that such a method will allow supersaturation to be generated only in the vicinity of the zeolite surface, whereas the bulk solution would contain only a low concentration of Mg^{2+} ions. Thus, the nucleation and growth of nanostructures would be confined to the surface of the zeolite, and potentially with a higher adhesion to the zeolite than solvothermally deposited nanostructures. Initially, LTA with magnesium as an extraframework cation (Mg-LTA) was prepared by ion exchange of Na-LTA with $MgCl_2$ aqueous solution. This Mg-LTA was hydrothermally treated in basic solution contacting Na^+ ions. During the treatment, ion-exchange happened between intracrystalline extraframework Mg^{2+} ions and Na^+ ions in basic solution. As the free Mg^{2+} ions diffuse out from the micropore channels of the zeolites, $Mg(OH)_2$ was formed at the LTA surfaces by the reaction between free Mg^{2+} ions and hydroxyl ions in bulk solution. As the reaction went on, the $Mg(OH)_2$ structures were continuously grown at the surface of the zeolites. The treatment conditions were then systematically modified to tune the size, shape and amount of $Mg(OH)_2$ nanostructures on the zeolite surface. Gas permeation properties were also measured for mixed matrix membranes containing surface-modified zeolite crystals.

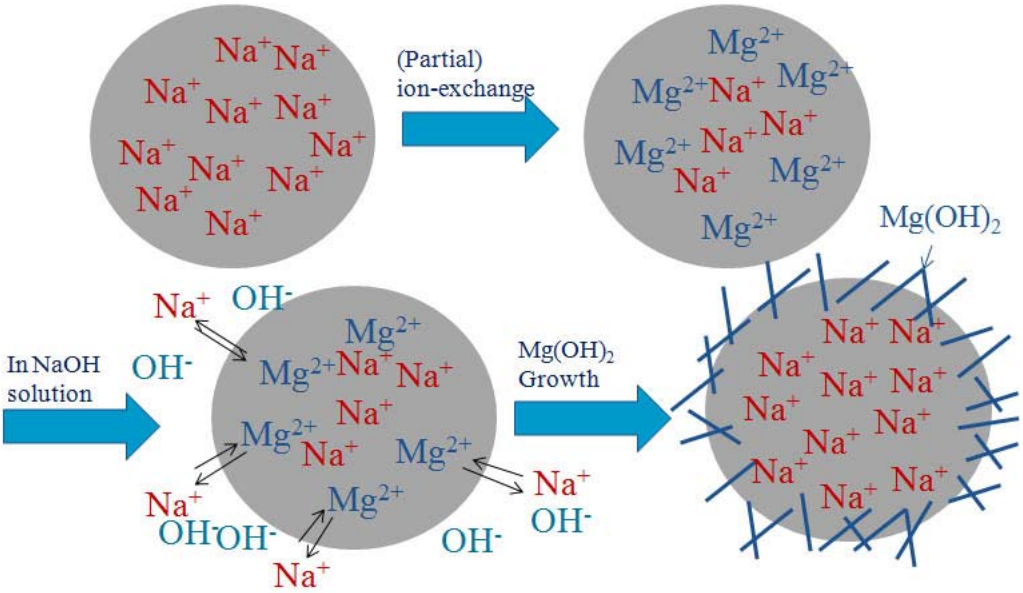

Fig. 4-1 Reaction scheme of ion-exchange induced growth of $Mg(OH)_2$ on the zeolite LTA surface.

4.2 Experimental Section

4.2.1 Materials

The following chemicals were commercially available and were used as received: tetramethylammonuim hydroxide (TMAOH, 25% in water, Sigma-Aldrich), magnesium chloride hexahydrate (Sigma-Aldrich), calcium nitrate tetrahydrate (Sigma-Aldrich), sodium hydroxide (Sigma-Aldrich), sodium nitrate (Sigma-Aldrich), dichloromethane (DCM, 99.5%, Sigma-Aldrich), colloidal silica (Ludox HS-30, Sigma-Aldrich), and aluminumisopropoxide ($Al(OiPr)_3$, 97%, Sigma-Aldrich). 6FDA-DAM polyimide (6FDA: 2,2-bis (3,4-carboxyphenyl) hexafluoropropane dianhydride and DAM: diaminomesitylene), synthesized in-house, was used for mixed matrix membrane fabrication. The chemical structure of 6FDA-DAM is shown in Fig. 4-2, and its properties are described elsewhere [9].

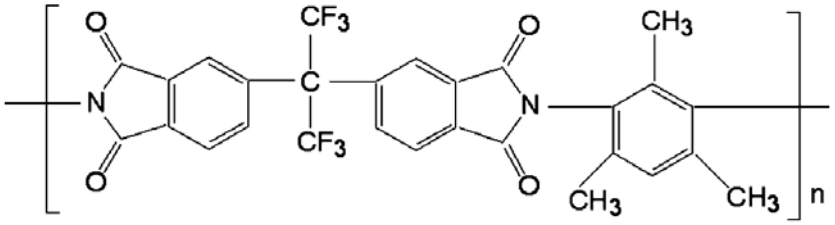

Fig. 4-2 Chemical structure of 6FDA-DAM polyimide.

4.2.2 Synthesis of Zeolite LTA

LTA particles were synthesized hydrothermally based on the procedure published by Larlus et al [10]. Colloidal silica (Ludox HS-30) and aluminum isopropoxide were used as silicon and aluminum sources, respectively, and the structure directing agent was TMAOH. For 300 nm particle synthesis, a clear precursor solution with molar ratio of 0.2NaOH: 1SiO_2: 1$Al(OiPr)_3$: 4TMAOH:170H_2O was prepared at room temperature and treated hydrothermally at 60 ^oC for 1 day, and at 100 ^oC for 1 day, correspondingly. Large crystal LTA, approximately 1-2 μm, was also prepared from a solution with a molar ratio of 0.2NaOH: 1SiO_2: 1$Al(OiPr)_3$: 3TMAOH:170H_2O. The hydrothermal reaction was conducted at 120 ^oC for 4 days. After the reaction, the zeolite particles were washed with DI water by repetitions of centrifugation and dispersion at least 5 times and dried at 80 ^oC. Calcination was performed at 550 ^oC for 8hr in air.

4.2.3 Zeolite Surface Treatment

To control the amount of $Mg(OH)_2$ in the final product, two types of Mg-LTA were prepared. High Mg content LTA was prepared by stirring 2 g Na-LTA in 100 ml of 1 M $MgCl_2$ solution at room temperature for 8 hr. In contrast, to prepare low Mg content

LTA, 2 g of Na-LTA was stirred in 0.1 M $MgCl_2$ solution at room temperature for 1hr. Three different treatments were performed on the zeolites and the reaction conditions are summarized in Table. 4-1. In the first surface treatment (IE-1), 0.1 g of high Mg-LTA was dispersed in 10 ml of 0.1 M NaOH (~13 of pH) using a sonication horn. Then the mixture was transferred to a Teflon lined autoclave reactor (23 ml total volume) and hydrothermally treated at 160 ^{o}C for 12 hr. In the second treatment (IE-2), the reaction was performed with 0.1 M $NaNO_3$ solution at pH = 9.5 adjusted using a very dilute aqueous NaOH solution. All the other conditions are the same as those in IE-1. In the third treatment (IE-3), the low Mg-LTA was used as a substrate and the method was the same with IE-2.

Table 4-1 Reaction conditions for the zeolite LTA surface treatment.

Treatment	Mg occupancy in LTA*	pH of solution	Concentration of Na^+ in solution	Temperature and time
IE-1	62 %	~13	0.1 M	160 ^{o}C, 12hr
IE-2	62 %	9.5	0.1 M	160 ^{o}C, 12hr
IE-3	38 %	9.5	0.1 M	160 ^{o}C, 12hr

* 2 x Mg/Al; elemental composition was measured by EDS

4.2.4 Mixed Matrix Membrane Fabrication

Mixed matrix dense films were prepared using a solution casting technique. Zeolite particles were dispersed in DCM then sonicated using a sonication horn and stirred at room temperature for 8 hr to break up particle aggregates. Polymer was added

to the suspension, which was then further stirred overnight. A nascent film was cast with the dope solution using a "doctor's knife" in a glove bag saturated with DCM vapor to delay solvent evaporation from the fabricated nascent membrane. The membrane on a glass plate was taken out of the glove bag after 8 hrs, and then further dried at room temperature in air. Annealing was performed at 230 ^{o}C for 1 day before gas permeation measurement.

4.2.5 Characterization

Morphologies of the zeolite particles and mixed matrix membranes were observed with a scanning electron microscope (SEM, LEO 1530). To prevent any morphological changes, the zeolite particles were observed without coating with gold. On the other hand, to observe cross-sections, mixed matrix membranes were coated with gold after being cryogenically fractured in liquid nitrogen. The morphology of surface treated zeolite particles was also observed with a transmission electron microscope (TEM, Hitachi HF-2000). Energy dispersive X-ray spectroscopy (EDS) connected to the SEM instrument was used to investigate the elemental composition of the zeolites. The t-plot micropore volume and BET (Brunauer-Emmett-Teller) surface area were calculated from nitrogen physisorption measurements performed on a Micromeritics ASAP 2020. To quantify the surface roughness of the surface treated zeolites, the BET external surface area was also calculated by extracting the contribution of the internal micropores of the zeolite to total BET surface area using the t-plot method. Powder X-ray diffraction (XRD) patterns were obtained on a Philips X'pert diffractometer equipped with X'celerator using Cu Kα radiation. To measure the mass fraction of $Mg(OH)_2$ in surface

treated LTA crystals, differential scanning calorimetry (DSC) and thermogravimetric analysis (TGA) were performed on a Netzsch STA409. The detailed method for the calculation of $Mg(OH)_2$ mass fraction is described in Chapter 2.

4.2.6 Gas Permeation Tests

Single gas permeation tests were performed in a constant volume apparatus. In the system, feed and permeate reservoirs were separated by a cell that holds the membrane. The apparatus includes appropriate instrumentation for measuring the pressure in both reservoirs and the necessary valves, all within a constant temperature box. The detailed experimental procedure is described in the literature [11]. Permeation tests were performed at 2 atm upstream pressure and 25 °C. Numerous measurements were performed to estimate the thickness of each sample using a micrometer, and their arithmetic average values were used for permeation data analysis.

4.3 Results and Discussion

4.3.1 Zeolite Synthesis and Surface Treatments

As shown in Fig. 4-3a and 4-3b, well defined cubic-shape LTA crystals were hydrothermally synthesized. Two different sizes of LTA crystals, 300nm and 1-2 μm, were prepared by controlling the composition of the reagent mixtures, and the crystallization temperature and time. Surface treatments were performed on these LTA crystals and the SEM images of surface treated LTA crystals are shown in Fig.4-3c-h. Smooth surfaces of untreated LTA crystals were changed into roughened surfaces by the formation $Mg(OH)_2$ nanostructures on the surface of particles. For all three treatments,

the presence of nanostructures on LTA surfaces is distinguishable in SEM images, although the precise $Mg(OH)_2$ structure is not clear in some cases, due to the resolution limit of the SEM instrument. A morphological evolution of particles was observed according to the systematic modification of reaction conditions from IE-1 to IE-3. Using a high pH treatment (IE-1), relatively big nanostructures were formed compared to the $Mg(OH)_2$ structures created by lower pH treatments (IE-2 and IE-3). The 300 nm LTA crystals treated by IE-2 and IE-3 showed "cotton-ball" like morphologies due to the formation of fine nanostructures on the surfaces. However, the shape of the individual nanostructures on the 300 nm LTA crystals is not clearly seen in SEM images. IE-2 treatment gave rise to more roughened surfaces than IE-3, as the amount of the magnesium source in the LTA substrate of IE-2 was higher than that of IE-3.

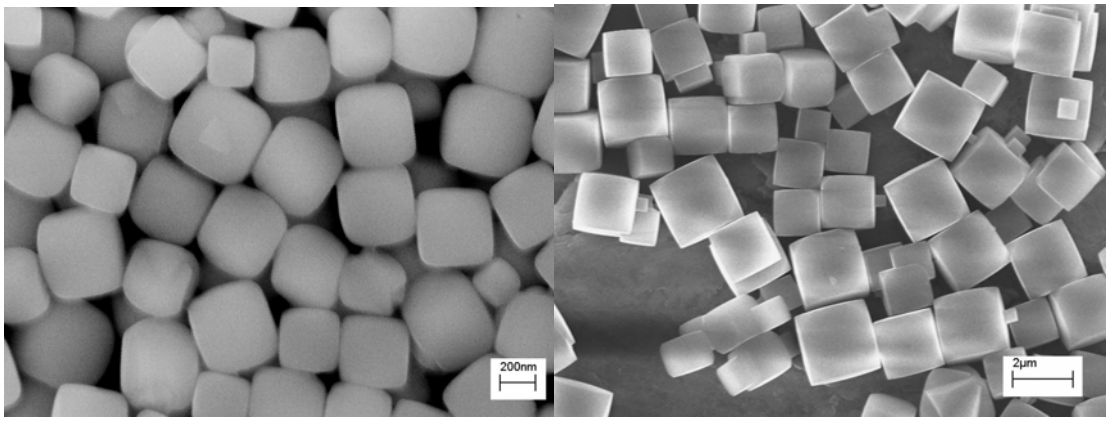

(a) (b)

Fig. 4-3 SEM images of LTA crystals; (a) bare_300 nm, (b) bare_1-2 μm (c) IE-1_300 nm, (d) IE-1_1-2 μm, (e) IE-2_300 nm, (f) IE-2_1-2 μm, (g) IE-3_300 nm and (h) IE-3_1-2 μm

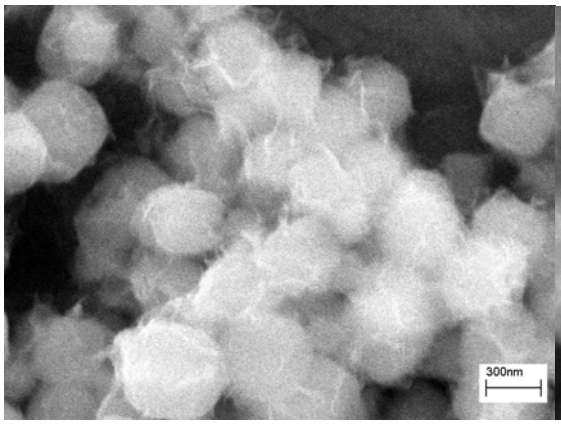

(c)

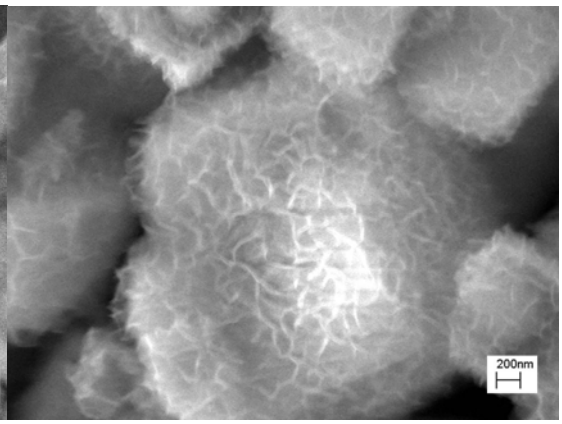

(d)

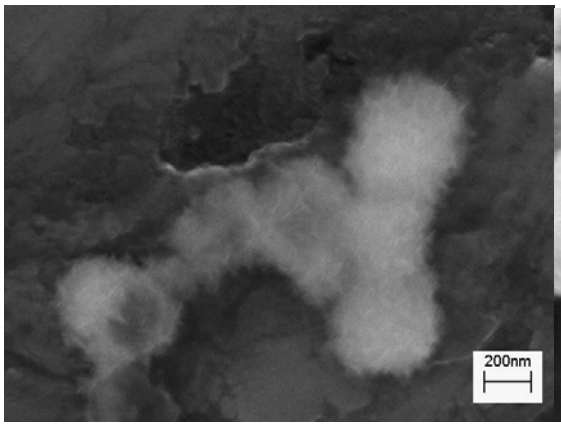

(e)

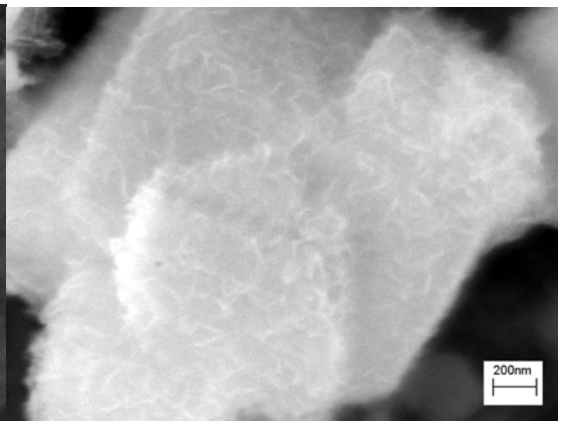

(f)

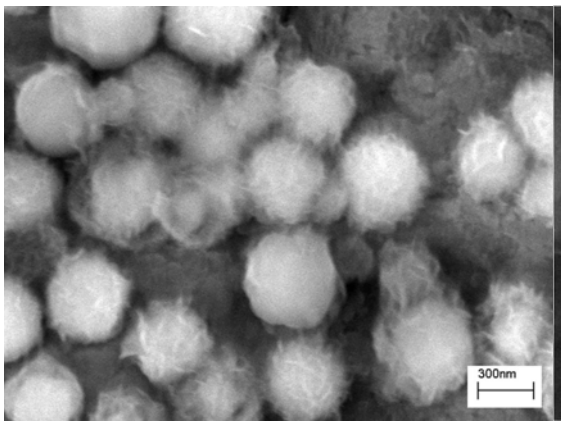

(g)

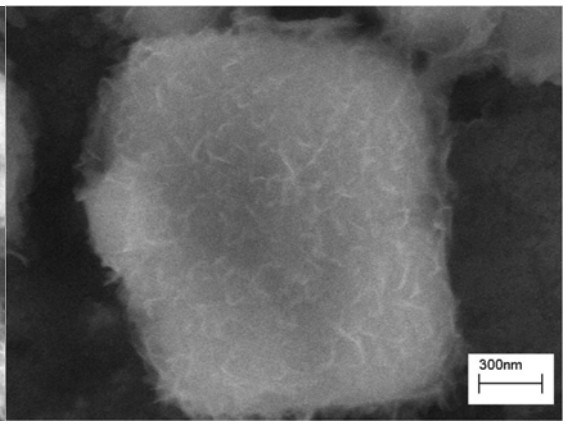

(h)

continued

4.3.2 Characterization of Surface Treated LTA Particles

Fig. 4-4 shows the XRD patterns of untreated and surface treated LTA crystals. For both the 300 nm and 1-2 μm crystals, LTA frameworks were retained after the treatments. The majority of the aluminosilicate LTA crystals were robust to the treatment conditions, a basic environment at high temperature. Initially, it was expected peaks from $Mg(OH)_2$ to be visible in the XRD pattern along with LTA peaks. However, no distinguishable peaks were observed in any case. It is possible that the $Mg(OH)_2$ structures formed on the LTA surfaces were mostly amorphous or they have very low crystallinity compared to the LTA crystals. The content of $Mg(OH)_2$ was also very low compared to LTA substrate. Detailed investigation of these inorganic structures is needed in the future. At present, there is no indication of the respective advantages of amorphous versus crystalline surface nanostructures.

The $Mg(OH)_2$ mass fraction of the surface treated LTA particles is shown in Table 4-2. The reaction yield was lowest in the high pH treatment (IE-1). However, at pH=9.5, the efficiency was so high that almost all the magnesium ions in the zeolite participated in $Mg(OH)_2$ formation. This result indicates that the amount of $Mg(OH)_2$ nanostructures in the final product is readily tunable by adjusting the initial magnesium content in the LTA particles and the reaction condition.

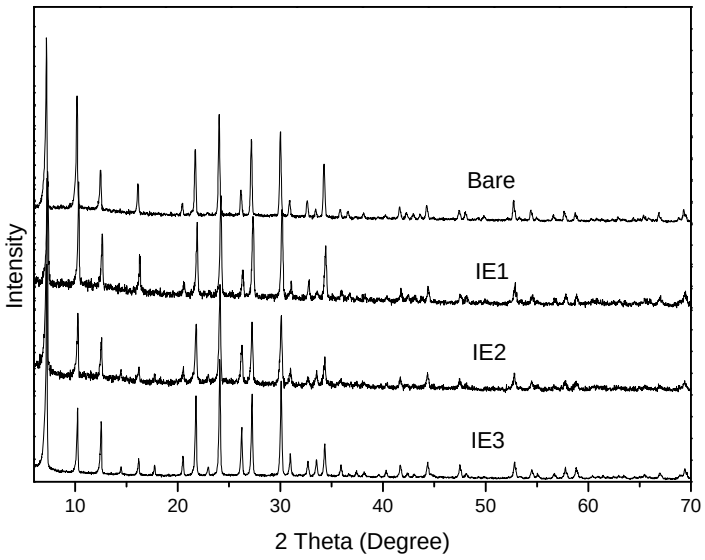

(a)

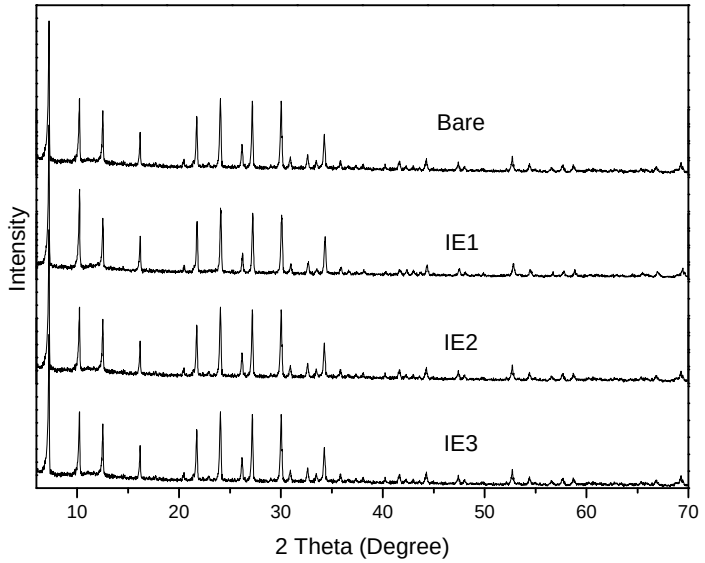

(b)

Fig. 4-4 XRD patterns of untreated and surface treated LTA crystals. (a) 300 nm and (b) 1-2 μm.

For application in gas separation membranes, the porosity of the modified LTA should remain high after the treatment. To investigate the effect of the surface treatments on the microporosity of the LTA crystals, the miropore volume of the zeolite was measured before and after the treatment. N_2 physisorption isotherms of surface treated 300 nm LTA crystals are shown in Fig. 4-5 and the t-plot micropore volume calculated from the measurements is summarized in Table 4-2. Only the mass of zeolite was taken into account in the calculations for a clear comparison between samples. The micropores of IE-1-LTA were almost fully blocked and the shape of the adsorption curve was typical of what is seen with nonporous materials as shown in Fig. 4-5. However, as shown in Fig 4-4, the treated particles still retain the LTA framework. These results may imply that the external region of the LTA particles was partially dissolved at such high pH (~13) and temperature (160 ^{o}C) and a non-porous layer covered the remaining LTA particle. Or, a dense layer of $Mg(OH)_2$ may block the micropores. When the samples were treated at lower pH (IE-2), the LTA particles retained some of their microposity. However, the micropore volume (0.11 cm^3/g zeolite) was still much lower than that of untreated LTA (0.17 cm^3/g), indicating that pore plugging by the $Mg(OH)_2$ formation may occur during the reaction. When the amount of magnesium source was reduced in the substrate (IE-3), the microporosity of the surface treated LTA was much improved so that the micropore volume of the product was close to that of the untreated LTA. Consequently, as the treatment conditions were systematically modified from IE-1 to -3, the micropore volume of the product was gradually increased and a good candidate for application in gas separation was obtained in the last treatment (IE-3).

Table 4-2 $Mg(OH)_2$ mass fraction and mircopore volumes of surface-treated zeolites.

Zeolite	$Mg(OH)_2$ mass fraction (%)		micropore volume
	Maximum*	Measurement	(cm^3/g zeolite)
LTA			0.17
IE-1	13	6	0.01
IE-2	13	14	0.11
IE-3	9	8	0.18

*Theoretical calculations based on Mg source input assuming $Mg(OH)_2$ reaction yield is 100%.

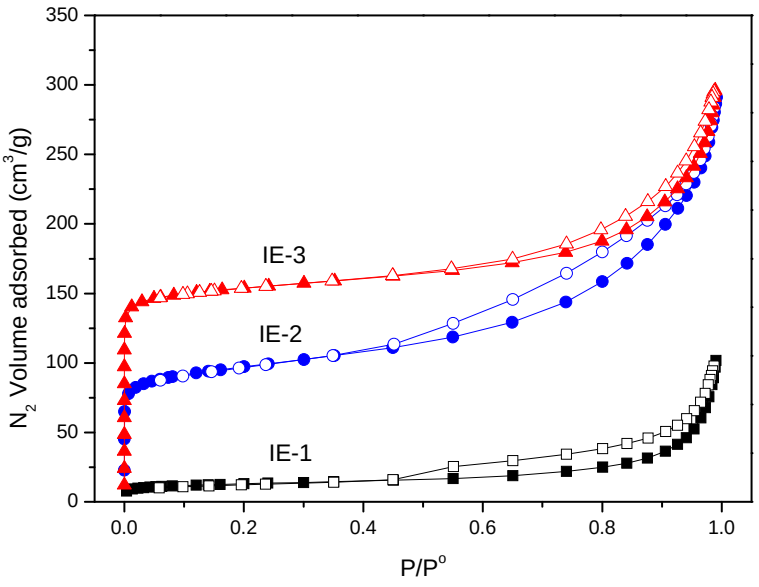

Fig. 4-5 Nitrogen physisorption isotherms of surface treated 300 nm LTA crystals.

Even though the bulk morphology of each batch of particles was observed with SEM, the shape of the individual inorganic nanostructures was not clearly seen in some cases. To observe the individual inorganic nanostructures on LTA surface, TEM images of the surface treated particles were taken at high magnification (Fig. 4-6). After the IE-1 treatment, the surface of the LTA crystals were uniformly covered with sheet-like $Mg(OH)_2$ layers, as shown in Fig.4-6a. When the pH was reduced to 9.5, the size/shape of the inorganic nanostructures on the LTA was changed. The small platelet and needle like $Mg(OH)_2$ structures were uniformly grown on the surface of IE-2-LTA, as shown in Fig. 4-6b. The size of the nanostructures created by IE-2 looked smaller than those of IE-1-LTA. The surface of IE-3-LTA was also uniformly covered with platelet and needle-like $Mg(OH)_2$ nanostructures. However, the density of the $Mg(OH)_2$ structures on the LTA surface was lower than that on IE-2-LTA.

To quantify both the surface roughness of the particles and the size of the inorganic nanostructures on the LTA crystals, the t-plot BET external surface area was calculated from nitrogen adsorption measurements and the values were normalized by the masses of the zeolites and $Mg(OH)_2$, respectively. As shown in Table 4-3, the surface area per unit mass of zeolite increased after the treatment, indicating a surface roughening by the treatments. The external surface area of the zeolite moderately increased from 15 to 27 m^2/g zeolite after the treatment with IE-1. In contrast, IE-2 LTA showed a huge increase in surface roughness so that the BET external surface area was 10 times higher than that of the untreated LTA. IE3-LTA also showed a substantial increase in surface

roughness. Normalization of the surface area by the mass of $Mg(OH)_2$ showed that the size of nanostructures is biggest on IE-1-LTA. The values from IE-2 and IE-3 were close to each other (930 and 890 m^2/g $Mg(OH)_2$, respectively), indicating the main difference between the two particles was the amount or density of the $Mg(OH)_2$ nanostructures on the LTA rather than the size of the nanostructures. The results from the surface roughness study are well matched with the TEM observations.

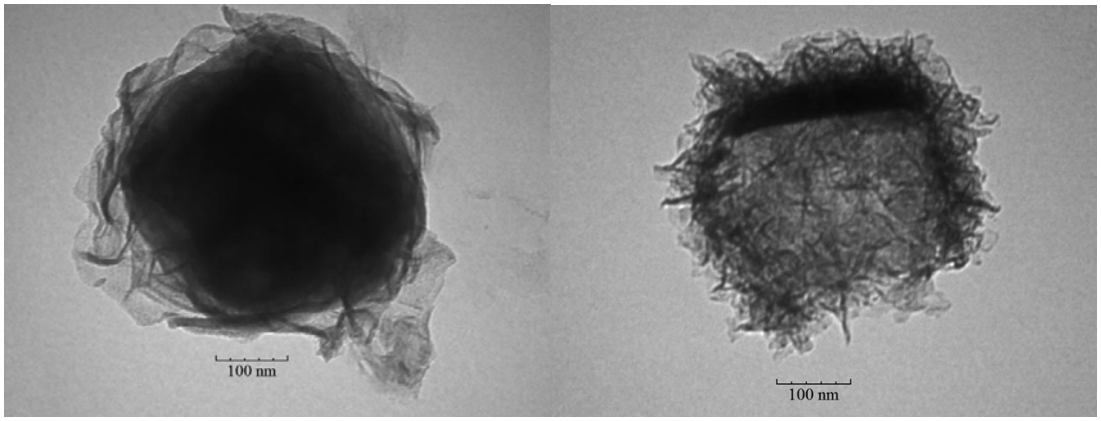

(a) (b)

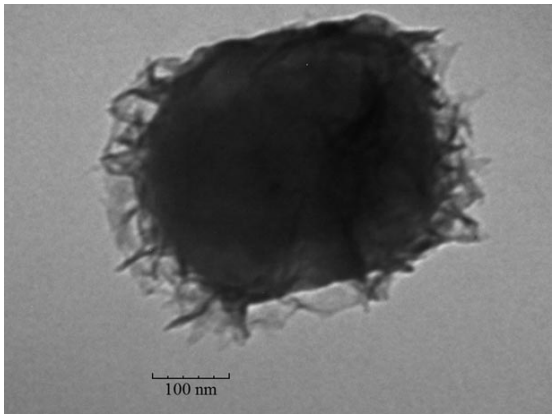

(c)

Fig. 4-6 TEM images of surface treated 300 nm LTA crystals; (a) IE-1, (b) IE-2 and (c) IE-3.

Table 4-3 The t-plot BET external surface area of LTA normalized by masses of both zeolite and $Mg(OH)_2$.

Zeolite	t-plot BET external surface area	
	m^2/g zeolite	m^2/g $Mg(OH)_2$
LTA	15	-
IE-1	26	440
IE-2	150	930
IE-3	81	890

4.3.3 Surface Treated Zeolite 5A

The micropore volume and size of the pore windows are tunable in zeolite LTA, according to the type of extraframework cations included in the pores. Zeolite LTA with Ca^{2+} as an extraframework cation (zeolite 5A) has a larger pore size (~0.5 nm) and pore volume (~0.28 cm^3/g) than the original Na-LTA (zeolite 4A), and hence its transport properties may be better matched with highly permeable polymers in mixed matrix membranes. To prepare surface-treated zeolite 5A, the remaining cations in the pores of the zeolite were exchanged with Ca^{2+} after the surface treatment, by stirring 0.5 g IE-3-LTA in 50 ml of 0.5 M $Ca(NO_3)_2$ at 60 ^oC for 4 hr. The ion-exchange was repeated twice to ensure that most of the extra-framework cations (Na^+, H^+, and residual Mg^{2+}) were replaced with Ca^{2+} ions.

Fig. 4-7 shows the morphology of the surface modified 1-2 μm zeolite 5A crystals. Particles have uniformly highly roughened surfaces, as the $Mg(OH)_2$ nanostructures on the LTA surfaces were retained after the ion-exchange at 60 ^{o}C. This result indicates the ion-exchange conditions are mild, since the nanostructures were stably bound onto the LTA surfaces. The elemental composition was measured with EDS and results are shown in Fig. 4-7. After the ion-exchange, the amount of Na^{+} in the product was negligible and 70 % of extraframework cation sites in the zeolite LTA (estimated by 2 x Ca/Al) were occupied with Ca^{2+} ions, indicating that the ion-exchange was effective in creating a material with the characteristics of zeolite 5A. Table 4-4 shows the t-plot micropore volumes of zeolite LTA. The micropore volume of IE-3-5A was intermediate between zeolites 4A and 5A. However, the value was closer to that of untreated zeolite 5A.

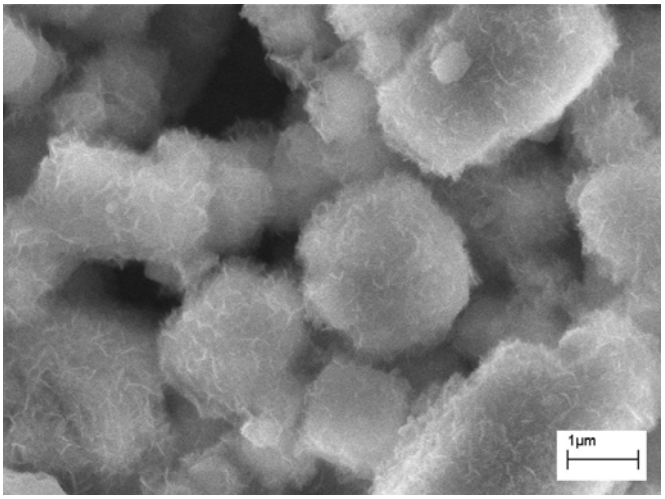

Fig. 4-7 SEM image of surface treated 1-2 μm zeolite 5A.

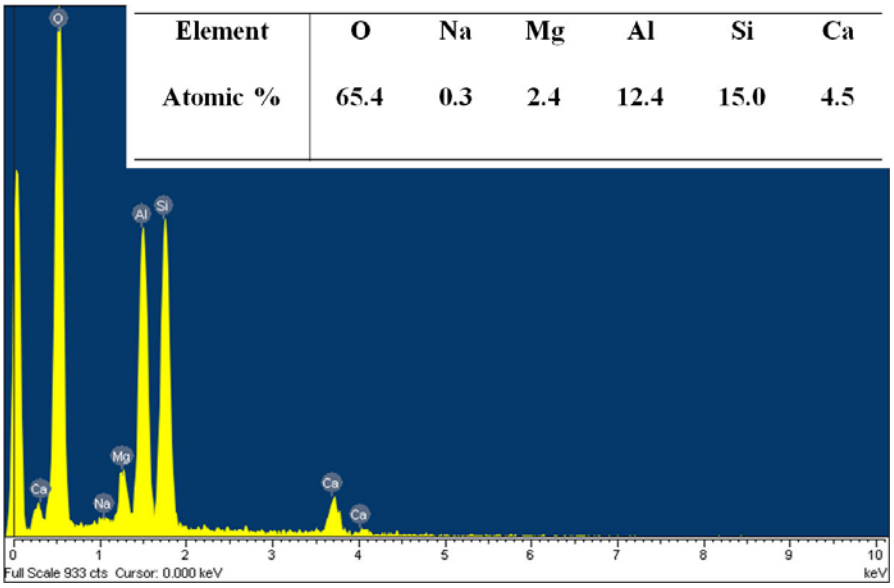

Fig. 4-8 EDS analysis of surface treated 1-2 μm zeolite 5A.

Table 4-4 The t-plot micropore volume of zeolite LTA.

LTA	Micropore volume (cm^3/g zeolite)
Zeolite 4A	0.17
Zeolite 5A	0.24
IE-3-5A	0.22

4.3.4 Mixed Matrix Membranes

Fig. 4-9 shows the morphology of mixed matrix membranes containing untreated and surface treated 5A crystals. As shown in Fig. 4-9a, the surface treated 5A showed

good adhesion with 6FDA-DAM presumably due to the improved physical interaction between the highly roughened zeolite surface and the polymer. In contrast, interfacial voids are clearly seen in the mixed matrix membrane containing untreated 5A (Fig. 4-9b).

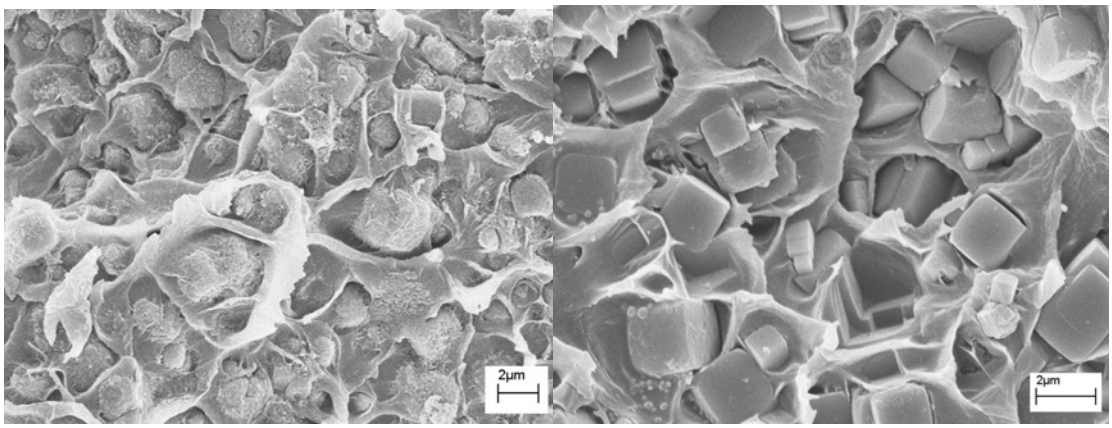

(a) (b)

Fig. 4-9 SEM images of cross-section of mixed matrix matrix membranes;
(a) IE-3-5A in 6FDA-DAM and (b) untreated 5A in 6FDA-DAM.

The CO_2/CH_4 transport properties of the mixed matrix membranes are shown in Fig. 4-10. The CO_2 permeability of the IE-3-5A/6FDA-DAM membrane increased significantly, with slight enhancement in the CO_2/CH_4 selectivity, compared to a pure polymeric membrane. In contrast, the membrane containing untreated 5A showed lower CO_2/CH_4 selectivity than the pure polymer, presumably due to non-selective gas flow through interfacial voids. This result indicates that the zeolite/polymer adhesion properties were improved by the zeolite surface modification. No significant enhancement in the CO_2/CH_4 selectivity might be due to the low CO_2/CH_4 selectivity of zeolite 5A. The pore size of zeolite 5A (~0.5 nm) is much bigger than both CO_2 (~0.33 nm) and CH_4 (~0.38 nm). This result does not ensure that the IE-3-5A/6FDA-DAM

adhesion properties are ideal, since it was not assessed by more rigorous mean as was done in Chapter 2. The positive effect of the surface treatment on the interfacial morphology, however, was clearly shown, since the CO_2/CH_4 selectivity of membrane containing surface treated 5A was much higher than that of the untreated 5A mixed matrix membrane.

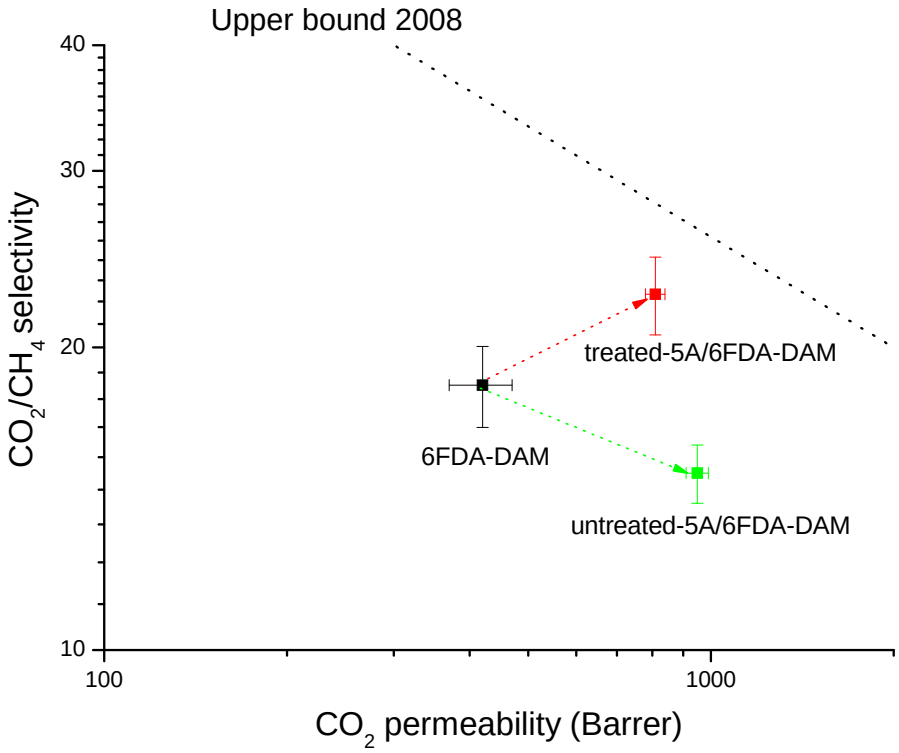

Fig. 4-10 Pure-component gas permeation properties of mixed matrix membranes containing 30 wt% LTA in 6FDA-DAM; measurement at 25 °C and 2atm upstream pressure.

4.4 Conclusions

Zeolite LTA materials with highly roughened surfaces were successfully prepared by a new method: the ion-exchange-induced growth of $Mg(OH)_2$ nanostructures using the

zeolite as the source of Mg^{2+} ions. The size, shape and mass of the inorganic nanostructures were tuned by adjusting several parameters such as the pH of the reagent solution and the amount of the magnesium in substrates and modification of reaction conditions led to a good molecular sieve (IE-3-LTA) for application in mixed matrix membranes. The structural properties of the surface treated LTAs were then thoroughly investigated with combined characterization of SEM, TEM, XRD and nitrogen physisorption. The zeolite/polymer adhesion properties in mixed matrix membranes were improved after the surface treatment compared to the membrane made with untreated bare LTA, based on SEM observation. The IE-3-5A/6FDA-DAM mixed matrix membrane showed significant enhancement in CO_2 permeability, with a slight increase in the CO_2/CH_4 selectivity, as compared to the pure polymer membrane. The CO_2/CH_4 selectivity of the membrane containing the surface treated zeolite 5A was much higher than that of the membrane made with untreated zeolite 5A.

4.5 References

[1] J. Lv, L.Z. Qu and B.J. Qu, J. Cryst. Growth, 267 (2004) 676.

[2] H. Yan, J.M. Wu, X.C. Zhang, Y. Zhang, L.Q. Wei, X.G. Liu and B.S. Xu, J. Mater. Res., 22 (2007) 2544.

[3] C. Henrist, J.P. Mathieu, C. Vogels, A. Rulmont and R. Cloots, J. Cryst. Growth, 249 (2003) 321.

[4] J.P. Hsu and A. Nacu, Colloids Surf. A, 262 (2005) 220.

[5] L. Yan, J. Zhuang, X.M. Sun, Z.X. Deng and Y.D. Li, Mater. Chem. Phys., 76 (2002) 119.

[6] Y. Ding, G.T. Zhang, H. Wu, B. Hai, L.B. Wang and Y.T. Qian, Chem. Mater., 13 (2001) 435.

[7] X.T. Lv, B. Hari, M.G. Li, X.K. Ma, S.S. Ma, Y. Gao, L.Q. Tang, J.Z. Zhao, Y.P. Guo, X. Zhao and Z.C. Wang, Colloids Surf. A., 296 (2007) 97.

[8] C.L. Yan, D.F. Xue, L.J. Zou, X.X. Yan and W. Wang, J. Cryst. Growth, 282 (2005) 448.

[9] J.Q. Liu, T.H. Bae, W.L. Qiu, S. Husain, S. Nair, C.W. Jones, R.R. Chance and W.J. Koros, J. Membr. Sci., 343 (2009) 157.

[10] O. Larlus, S. Mintova and T. Bein, Micropor. Mesopor. Mater., 96 (2006) 405.

[11] T.T. Moore and W.J. Koros, J. Mol. Struct., 739 (2005) 87.

CHAPTER 5

SYNTHESIS OF SUB-MICRON CRYSTALS OF A ZEOLITIC IMIDAZOLATE FRAMEWORK AND THEIR APPLICATION IN GAS SEPARATION MEMBRANES

5.1 Introduction

Zeolite particles have been a mainstay as inorganic components for mixed matrix membrane fabrication. However, only a limited number of zeolites (particularly, small pore zeolites) are suitable for application in gas separation membranes. More importantly, the compatibility between inorganic zeolite particles and organic polymer is generally so poor that defects can be formed at zeolite/polymer interfaces. Membranes with this non ideal morphology usually result in poor gas separation performance since most gas molecules take non-selective bypass around the zeolite particles instead of permeation through the micropore channels in zeolites [1-5]. New methods for surface functionalization of zeolites have been extensively discussed in this thesis. These methods were found to be quite effective in obtaining significantly improved membrane microstructures and performance, but will obviously increase the cost and complexity of membrane manufacture to some extent.

In this chapter, we explore a somewhat different perspective, viz. the use of non-zeolitic porous materials that may allow a wide range of gas separations to be carried out, while being exempt from the requirement for surface functionalization of zeolites. In particular, metal organic frameworks (MOFs) are a new class of nanoporous materials

comprising metal centers connected by various organic linkers to created 1-D, 2-D and 3-D pore structures. So far, several thousand MOF materials have been synthesized, and their numbers continue to grow rapidly [6-7]. In their early stages of development, the poor thermal and chemical stability of MOFs was a significant issue limiting their applications. However, many structurally robust MOF materials have been reported recently.

MOFs have a wide range of potential applications such as selective gas adsorption [8-9], hydrogen storage [10], catalysis [11] and sensors [12] due to their large pore volume, surface area and tunable chemical properties. MOF materials are also highly attractive for application in gas separation membranes. Recently, several thin continuous MOF films have been fabricated for various potential applications [12]. MOF membranes have also been fabricated as films on porous substrates, but their performance is not yet satisfactory. Liu et al. fabricated a MOF-5 thin film on an alumina support by a solvothermal method, but the membranes were not selective and showed a Knudsen diffusion behavior [13]. Yoo et al. also fabricated a MOF-5 film by seeded growth, and also observed Knudsen diffusion of gases[14]. Guo et al. reported a HKUST-1 ($Cu_3(BTC)_2$) membrane exhibiting a rather modest selectivity of 7 for H_2/N_2 [15]. However, neither MOF-5 nor HKUST-1 are appropriate choices for gas separation, since they have relatively large pores (0.5-0.9 nm) [16]. On the other hand, Ranjan et al. fabricated a continuous membrane with Cu(hfipbb)(H_2hfipbb)$_{0.5}$, a MOF having a narrow 1-d pore channel comparable to a small-pore zeolite [17]. However, the permeance of the membrane was very low. This was hypothesized to be a result of incorrect orientation of

the 1-d micropore channels in the membrane. Most recently, continuous ZIF-8 films have been fabricated on titania supports by a microwave-assisted solvothermal method [18]. However, the membrane showed very low CO_2/CH_4 selectivity (~3) even through the pore size of ZIF-8 is 0.34 nm, which is in between kinetic diameters of CO_2 and CH_4. This poor gas separation performance may indicate that the resultant membrane had defects allowing non-selective gas flow. Unlike zeolite films made with silicates or aluminosilicates, the fabrication of pure MOF membranes of high quality seems not readily achievable at present.

MOF mixed matrix membranes are very attractive since they may offer a technically viable option to make high quality membranes incorporating various MOF materials. Furthermore, MOFs as fillers in mixed matrix membranes have several potential advantages over zeolites. In general, MOFs have higher pore volumes than zeolites, so that the molecular sieving effect can be greater for the same amount of particles in the polymer matrix. Furthermore, the control of MOF/polymer interfacial morphology may not be required (or be much easier than that of zeolite/polymer interface), since the organic linkers in MOFs will likely have a better affinity with organic polymer chains and the surface of MOFs can be further tuned by organic functionalization via various well-known reactions, if required [19]. Recently several MOF mixed matrix membranes have been reported. Addition of Cu-BPY-HFS (Cu-4,40-bipyridine hexafluorosilicate,) to Matrimid® increased CO_2 permeability but decreased ideal CO_2/CH_4 selectivity [20]. Car et al. reported that a polysulfone membrane containing 10 % HKUST-1 showed a substantial increase in CO_2 permeability with a

significant loss in CO_2/CH_4 selectivity. [21]. A Matrimid®/MOF-5 mixed matrix membrane showed increased CO_2 permeability with no significant change in CO_2/CH_4 selectivity by pure gas permeation tests [22], but a mixed gas permeation measurement showed lower CO_2/CH_4 selectivity than the pure polymer. Most recently, Adams et el. fabricated a defect-free polyvinylacetate (PVAc) membrane containing 15 wt% Cu-TPA (terephthalic acid) [23]. The membrane showed enhanced separation performance, with a 34 % increase in CO_2 permeability and a 16 % increase in CO_2/CH_4 selectivity. This moderate gas separation enhancement is proposed to be due to both the molecular sieving effect from the relatively small-pore MOF (~0.52 nm pore window) and good filler/polymer adhesion properties. However, from a practical viewpoint, PVAc is not a useful membrane polymer due to its physical properties. PVAc has a very low Tg and cannot be processed into hollow fibers, a commercially viable membrane module. Overall, the previous works imply that the selection of appropriate MOFs, as well as good MOF/polymer adhesion, are both indispensable for successful fabrication of mixed matrix membranes. The importance of the 'matching' of MOF and polymer in mixed matrix membranes has been emphasized by Keskin et al. recently [24].

ZIF-90 is a very attractive MOF material for application in CO_2 selective mixed matrix membranes. ZIF-90 has a sodalite cage-like structure with 0.35 nm pore windows, through which accurate size exclusion of CO_2 and CH_4 is possible (Fig. 5-1). Furthermore, ZIF-90 is constructed with an imidazole linker containing a carbonyl functional group, which is known to have a good chemical interaction with a CO_2 molecule [25]. So far, ZIF-90 crystals have been synthesized by the conventional

solvothermal method. However, the size of crystals obtained by solvothermal synthesis (~100 μm) is too large to be used in thin mixed matrix membranes (which require submicron crystals) [26].

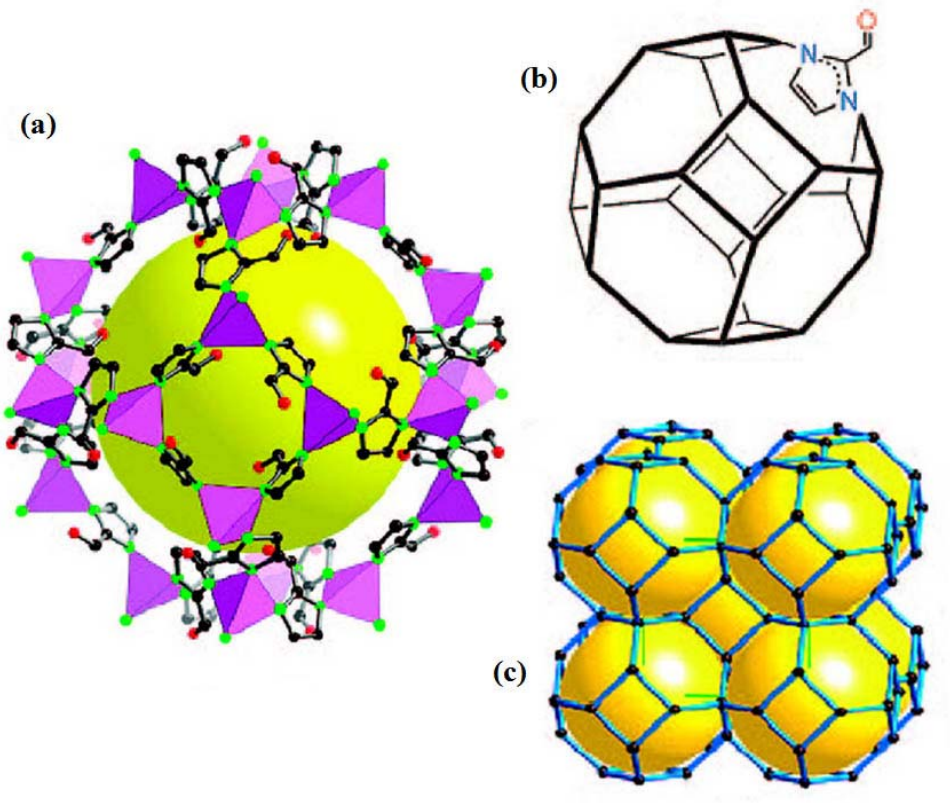

Fig. 5-1 (a) Crystal structure of ZIF-90 (C, black; N, green; O, red), (b) carbonyl group in the imidazole linker and (c) the structure of sodalite cage (SOD) [26].

In the present work, a synthesis of submicron ZIF-90 crystals by a new method, namely "nonsolvent-induced crystallization" is described. The ZIF-90 crystals prepared by this method were thoroughly characterized and compared with solvothermally synthesized ZIF-90. Mixed matrix membranes were then fabricated using various

polyimides as the polymer matrix, and their CO_2/CH_4 transport properties were investigated. It is shown that membranes containing ZIF-90 have unprecedented high performance for CO_2/CH_4 separation.

5.2 Experimental Section

5.2.1 Materials

The following chemicals were commercially available and were used as received: zincnitrate hexahydrate (98%, Sigma-Aldrich), imidazole-2-carboxaldehyde (97%, Alfa Aesar), N,N-dimethylformamide (DMF, anhydrous, Sigma-Aldrich), Methanol (MeOH, HPLC grade, J.T. Baker) and dichloromethane (DCM, 99.5%, Sigma-Aldrich). A house-made 6FDA-DAM polyimide (6FDA: 2,2-bis (3,4-carboxyphenyl) hexafluoropropane dianhydride and DAM: diaminomesitylene) and two commercially available polyimides, Ultem® 1000 (SABIC) and Matrimid® 5218 (Vantico), were chosen as the polymer matrix for mixed matrix membrane fabrication. The properties of 6FDA-DAM are described in elsewhere [27].

5.2.2 Synthesis of ZIF-90

$Zn(NO_3)_2 \cdot 6H_2O$ (5 mmol) and imidazole-2-carboxaldehyde (20 mmol) were added to 50 ml of DMF in 250 ml round bottom flask. To obtain a clear solution, the mixture was stirred at 80 ^oC for 4 hr. After the solution cooled down to room temperature, 50 ml of nonsolvent was quickly poured into the solution while applying vigorous stirring. After further stirring at room temperature for 30 min, particles were separated by centrifuge and washed with methanol by several repetitions of a sonication-centrifugation

cycle. To remove the remaining DMF from the MOF material, the particles were stirred in MeOH for 1 day. After drying at room temperature, the ZIF-90 crystals were evacuated at 170 ^{o}C under high vacuum.

5.2.3 Mixed Matrix Membrane Fabrication

ZIF-90/polymer composite films were prepared using a solution casting technique. ZIF-90 particles were dispersed in DCM and the mixture was sonicated with a sonication horn to break up particle aggregates. Polymer was added to the suspension, which was then further stirred overnight. A nascent film was cast with the solution on a glass plate using a "doctor's knife" in a glove bag previously saturated with DCM vapor to delay solvent evaporation from the nascent membrane. The membrane on a glass plate was taken out of the glove bag after 8 hrs then further dried at room temperature in air. All membranes were annealed before gas permeation measurements; at 170 ^{o}C for 16 hr for Ultem®, at 230 ^{o}C for 16 hr for Matrimid®, and at 230 ^{o}C for 1 day for 6FDA-DAM based membranes, respectively.

5.2.4 Characterization

Morphologies of the ZIF-90 particles and the mixed matrix membranes were observed with a scanning electron microscope (SEM, LEO 1530). All samples were coated with gold before SEM measurements. To observe cross-sections, mixed matrix membranes were cryogenically fractured in liquid nitrogen prior to the coating with gold. BET (Brunauer-Emmett-Teller) and Langmuir surface areas, the total pore volume, and the t-plot micropore volume were calculated from nitrogen physisorption measurements

performed on an ASAP 2020 (Micromeritics). Thermogravimetric analyses (TGA) were performed on a Netzsch STA409. Samples were heated under a nitrogen-diluted air stream from 30 to 900 °C at a rate of 10 °C/min. Powder X-ray diffraction (XRD) patterns were obtained on a PAnalytical X'pert diffractometer operating with Cu Kα radiation and equipped with an X'celerator detector. In situ powder XRD was also performed on the same instrument. The powder sample was placed in an Anton Paar TTK 450 temperature-control chamber. The sample was heat-treated at a desired temperature for 1 hr under a vacuum of 7.5 militorr and high-resolution diffraction data were then rapidly collected with an X'Celerator detector. The particle size of ZIF-90 crystals was assessed with dynamic light scattering (DLS, Dynapro, Wyatt Technology). The particles were dispersed in DI water and measurements were performed 20 times for each sample then the results were averaged.

5.2.5 Gas Permeation Tests

Single gas permeation tests were performed in a constant volume apparatus. In the system, feed and permeate reservoirs were separated by a cell that holds the membrane. It includes appropriate instrumentation for measuring the pressure in both reservoirs and necessary valves, all within a constant temperature box. The detailed experimental procedure is described in the literature [2]. Permeation tests were performed at 35 °C and 4.5 atm upstream pressure for Matrimid® and Ultem® membranes and at 25 ^{o}C and 2 atm upstream pressure for 6FDA-DAM membranes. Numerous measurements were performed for the thickness of each sample by using a micrometer, and their arithmetic average values were used for permeation data analysis.

5.3 Results and Discussion

5.3.1 Synthesis and Characterization of ZIF-90 Crystals

The morphologies of the ZIF-90 crystals are shown in Fig. 5-2. Two nonsolvents, MeOH and DI water were used in this study for room temperature crystallization of ZIF-90. In both cases, well defined crystals were prepared by a rapid reaction at room temperature. As shown in Fig. 5-2a, the size of most of the ZIF-90 particles formed in the DMF/MeOH mixture (ZIF-90A) were smaller than 1 μm. Particles with broader size distribution, up to 2-3 μm, were made in the DMF/water mixture (ZIF-90B), as shown in Fig. 5-2b. The mean particle diameters measured by DLS are approximately 800 nm and 2 μm for ZIF-90A and ZIF-90B, respectively (Table 5-1). The sizes of crystals in this work were much smaller than ZIF-90 crystals made by a conventional solvothemal method (~100 μm) [26].

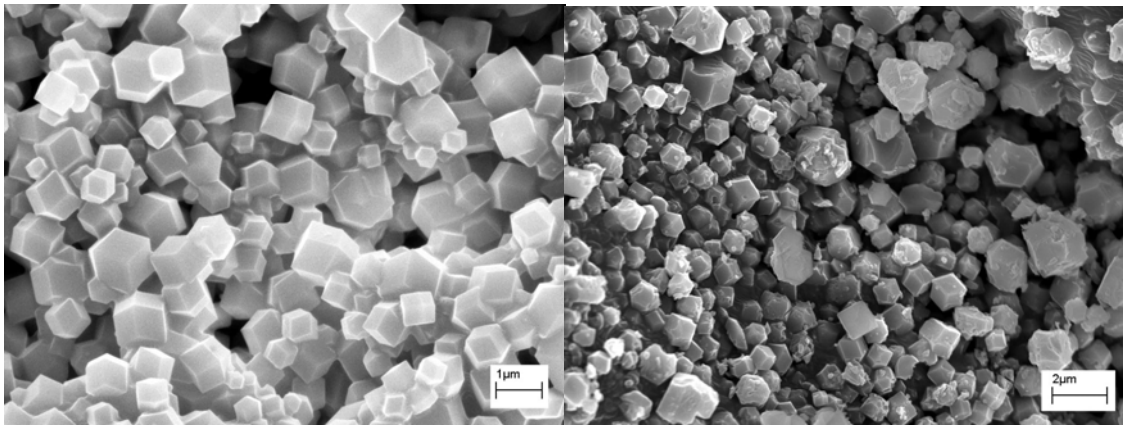

(a) (b)

Fig. 5-2 SEM images of ZIF-90 particles; (a) ZIF-90A synthesized using MeOH as nonsolvent; (b) ZIF-90B synthesized using DI water as nonsolvent.

Table 5-1 Particle size of ZIF-90 crystals measured by DLS.

Particle	Diameter (nm)
ZIF-90A	810±50
ZIF-90B	2000±660

The particle size of zeolites is relatively easy to control by adjusting reaction conditions, such as the composition of the reagent mixture, synthesis temperature and reaction time. In general, to synthesize smaller crystals, the reaction conditions should be favorable to nucleation over crystal growth. Unlike zeolite synthesis, however, the particle size control of MOFs is very difficult yet especially in solvothermal synthesis since the mechanism of crystal formation is not well understood. In this work, ZIF-90 particles were crystallized at room temperature by the addition of nonsolvent to the reagent solution. The precursors in solution became highly supersaturated immediately after the addition of nonsolvent. As a result, a large number of nuclei can be formed instantaneously at the beginning of the reaction, leading to the formation of a large number of small crystals.

To investigate the crystallinity and framework type of the synthesized particles, power XRD patterns were measured. The XRD patterns of the particles synthesized are shown in Fig. 5-3. Both materials have good crystallinity and were identified as a sodalite

type of ZIF material, such as ZIF-8, ZIF-65 and ZIF-90, indicating successful preparation of ZIF-90 crystals within a very short reaction time (30 min). Fig. 5-4 shows the nitrogen physisorption isotherms of the ZIF-90 crystals. The shape of isotherms for the ZIF-90 crystals was somewhat different from that of typical microporous zeolites. The curve reached a first plateau region after N_2 adsorption up to a p/p^0 of ca. 0.2. The curve then reached a second plateau region after a step-wise increase. This phenomenon was also reported in the previous work on solvothermal synthesis of ZIF-90 crystals [26]. This nitrogen adsorption behavior may be an inherent property of ZIF-90. Interestingly, ZIF-90B crystals showed a hysteresis loop between adsorption and desorption paths in the step-wise jump region, indicating nitrogen molecules are more strongly bound in some area of ZIF-90B. The pore volume and surface area calculated from the nitrogen physisorption measurements are summarized in Table 5-2. For comparison, the properties of ZIF-90 synthesized by the typical solvothermal reaction were taken from the literature. The particles synthesized in this work have good porosity, and both pore volume and surface area were close to those of the solvothermally synthesized ZIF-90. This result implies the precipitation of amorphous materials is strongly inhibited under the reaction condition and ZIF-90 crystals were rapidly crystallized at room temperature induced by nonsolvent addition. ZIF-90B showed a slightly higher pore volume than ZIF-90A but the difference was marginal, indicating the effect of the nonsolvent on the porosity of the product was not significant.

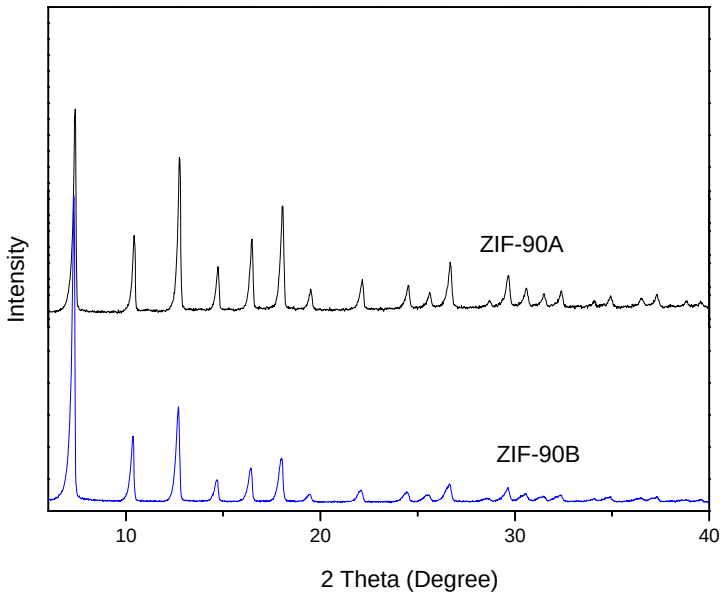

Fig. 5-3 XRD patterns of ZIF-90 crystals.

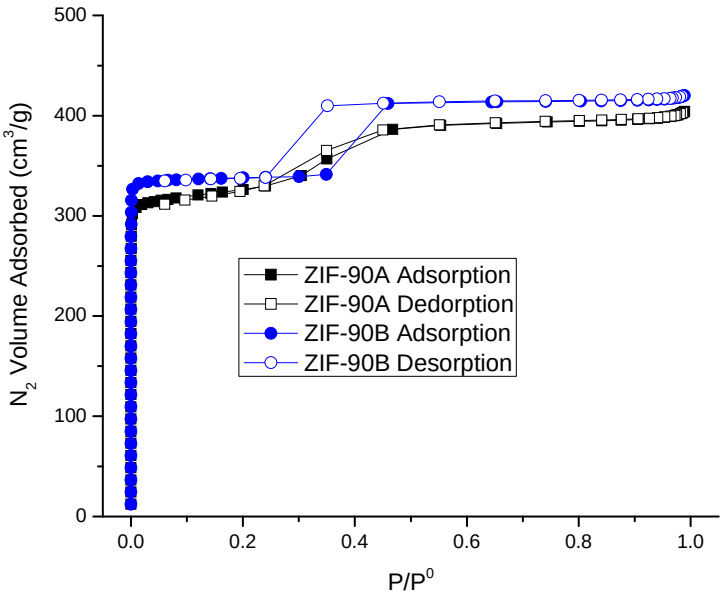

Fig. 5-4 Nitrogen physisorption isotherms of ZIF-90 particles.

Table 5-2 Surface area and pore volume measured by nitrogen physisorption.

ZIF-90	Langmuir surface area (m^2/g)	BET surface area (m^2/g)	Total pore volume (cm^3/g)	t-plot micropore volume (cm^3/g)
ZIF-90A	1410	1180	0.62	0.44
ZIF-90B	1470	1230	0.65	0.50
ZIF-90* [26]	1320	1270	0.58	0.48

* solvothermally synthesized crystals

Fig. 5-5 shows the TGA curves for the ZIF-90 crystals. The weight loss for ZIF-90A started at ~290 ^{o}C while ZIF-90B crystal was stable up to 400 ^{o}C. It was reported that solvothermally synthesized ZIF-90 crystals (when pores were previously evacuated) start to lose weight at ~250 ^{o}C. The ZIF-90A and B crystals are more thermally stable than solvothermally synthesized crystals. This may imply that the ZIF-90A and B crystals have better framework integrity and fewer defects than the solvothermally synthesized ZIF-90. Especially, ZIF-90B showed outstanding thermal stability. Many ZIF materials have been reported to be thermally stable up to 400 ^{o}C due to the strong chemical bonds between the imidazole linkers and the zinc metal centers [28]. Thus, it is possible to make more stable ZIF-90 crystals if the frameworks are constructed with superior integrity.

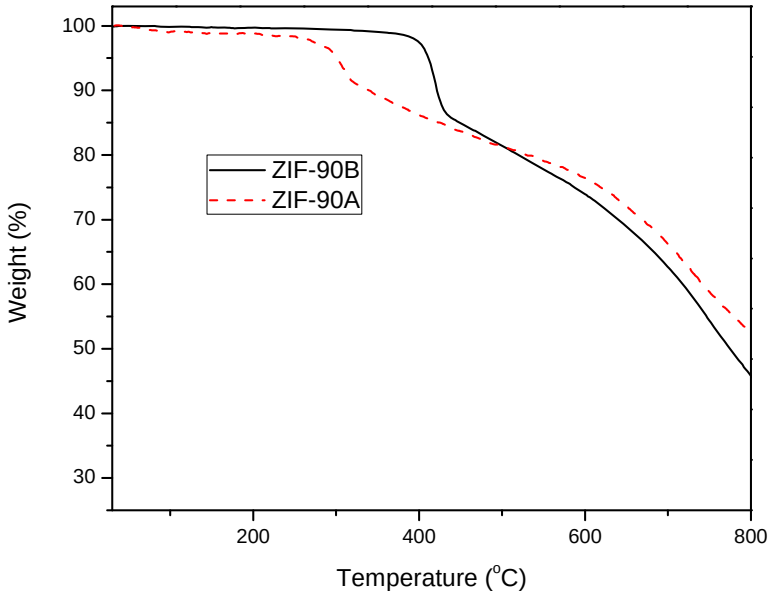

Fig. 5-5 TGA curves of ZIF-90 particles; micropores were evacuated at 170 °C under vacuum prior to the measurement.

Temperature programmed in-situ XRD was conducted to investigate the framework integrity of ZIF-90B at high temperature (Fig. 5-6). There was no significant change in the XRD pattern up to 300 °C. At 350 °C, the intensity of the first peak at 8° of 2θ was decreased, whereas the intensities of the other peaks remained stable. At 400 °C, where the weight loss started in TGA, the intensities of all peaks were decreased, indicating a loss of crystallinity of the ZIF-90. After the whole temperature programmed measurement from room temperature to 450 °C, the XRD pattern of the sample was measured again at room temperature. Although the particles still showed the characteristic XRD pattern of ZIF-90, the intensity of all peaks was weaker than that of the original sample, indicating a permanent change in crystallinity was induced at high temperature.

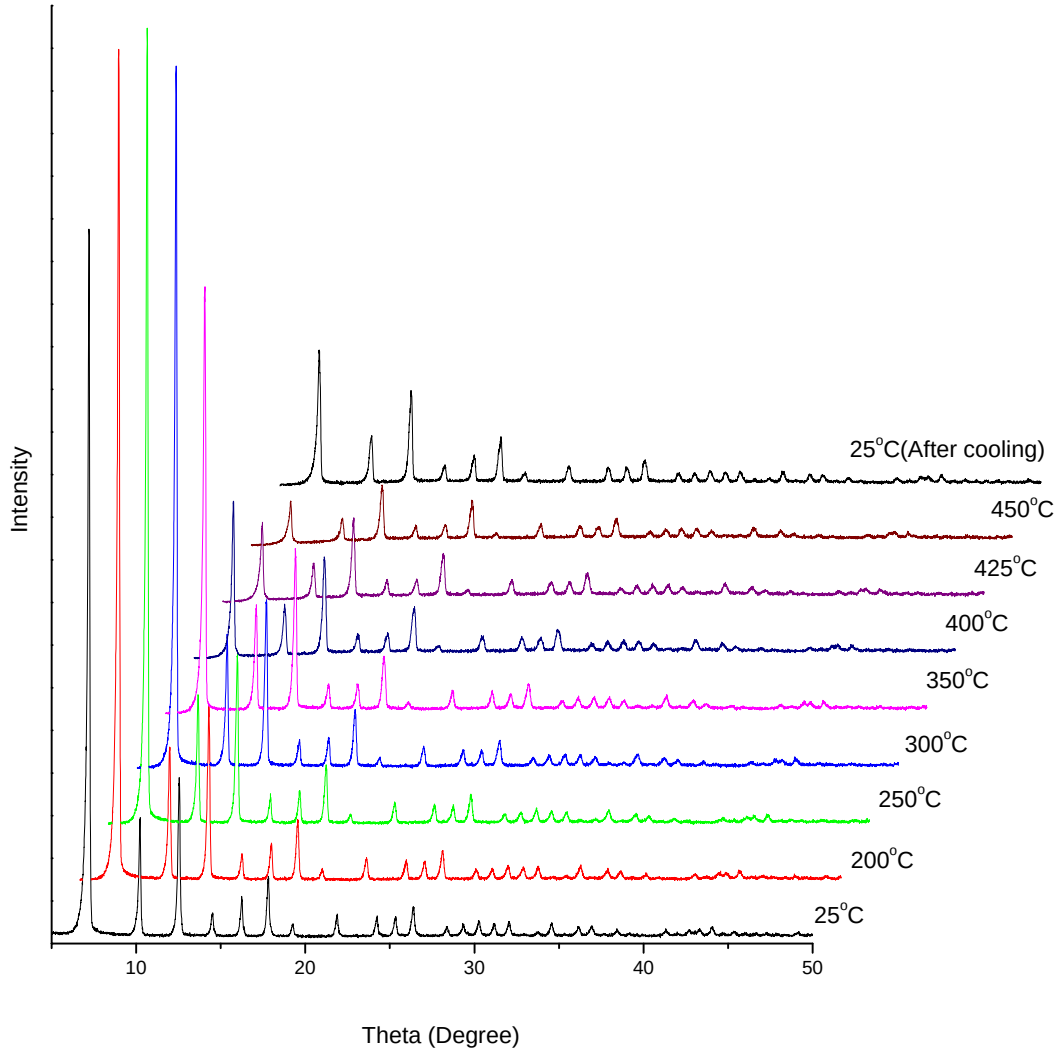

Fig. 5-6 Temperature-programmed in situ XRD of ZIF-90B crystal.

5.3.2 ZIF-90 Mixed Matrix Membranes

The morphologies of the cross-section of the mixed matrix membranes are shown in Fig. 5-7. Without any additional compatibilization, the ZIF-90 crystals and polymers showed good adhesion. Interfacial voids were hardly seen in the images and the individual particles were well surrounded with polymers in all cases.

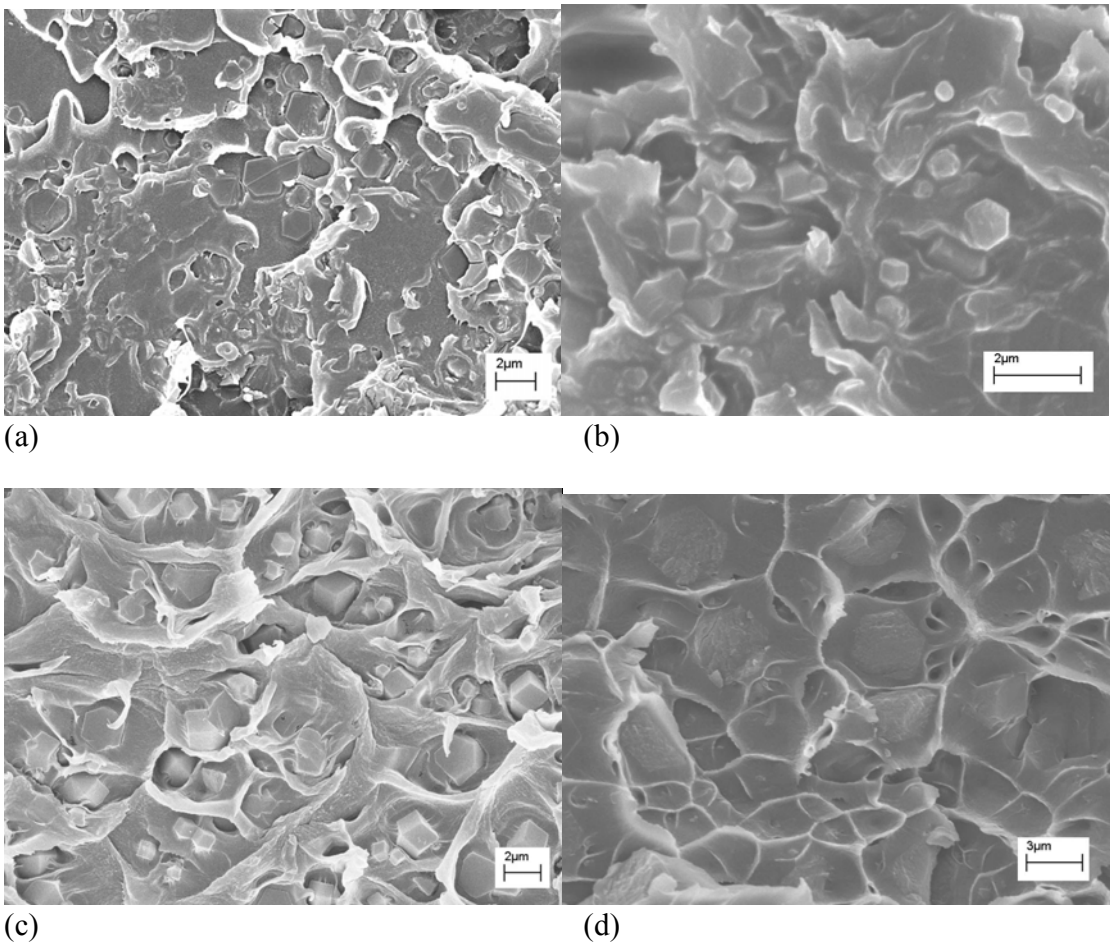

(a) (b)

(c) (d)

Fig. 5-7 SEM images of cross-section of mixed matrix membranes containing ZIF-90 crystals; (a) ZIF-90A/Ultem®, (b) ZIF-90A/Matrimid®, (c) ZIF-90A/6FDA-DAM and (d) ZIF-90B/6FDA-DAM.

Fig. 5-8 shows the CO_2/CH_4 gas transport properties of mixed matrix membranes with ZIF-90 crystals. Ultem® and Matrimid® mixed matrix membranes showed significantly enhanced CO_2 permeability without a loss in CO_2/CH_4 selectivity. The lack of significant change in selectivity is due to the mismatch between the permeabilities of ZIF-90 and polymers. According to the Maxwell model, if the difference in gas permeability between the two phases is large, one cannot observe an enhancement in gas selectivity even if the molecular sieve has a higher gas selectivity than the polymer matrix. The commercial polyimides used in this study, Ultem® and Matrimid®, have very low CO_2 permeabilities, as shown in the Fig. 5-8. However, this result, enhanced permeability without a decrease in selectivity, is still very attractive since the CO_2 throughput (permeability) of membrane increased significantly (e.g., from 1.4 to 2.9 for Ultem®) while preserving the great advantage of the commercial polyimides, a high CO_2/CH_4 selectivity. Moreover, mixed matrix membranes with a highly permeable 6FDA-DAM showed significant enhancement in both permeability and selectivity, indicating a better permeability match between the two phases. Both ZIF-90A and ZIF-90B gave rise to a good separation enhancement, but a slightly better result was obtained from a membrane with the smaller particles, ZIF-90A. The performance of ZIF-90/6FDA-DAM mixed matrix membranes clearly transcends the polymer upper bound drawn in 1991, and reaches the technologically attractive region. To my knowledge, this is the best result among any MOF-containing membrane reported so far.

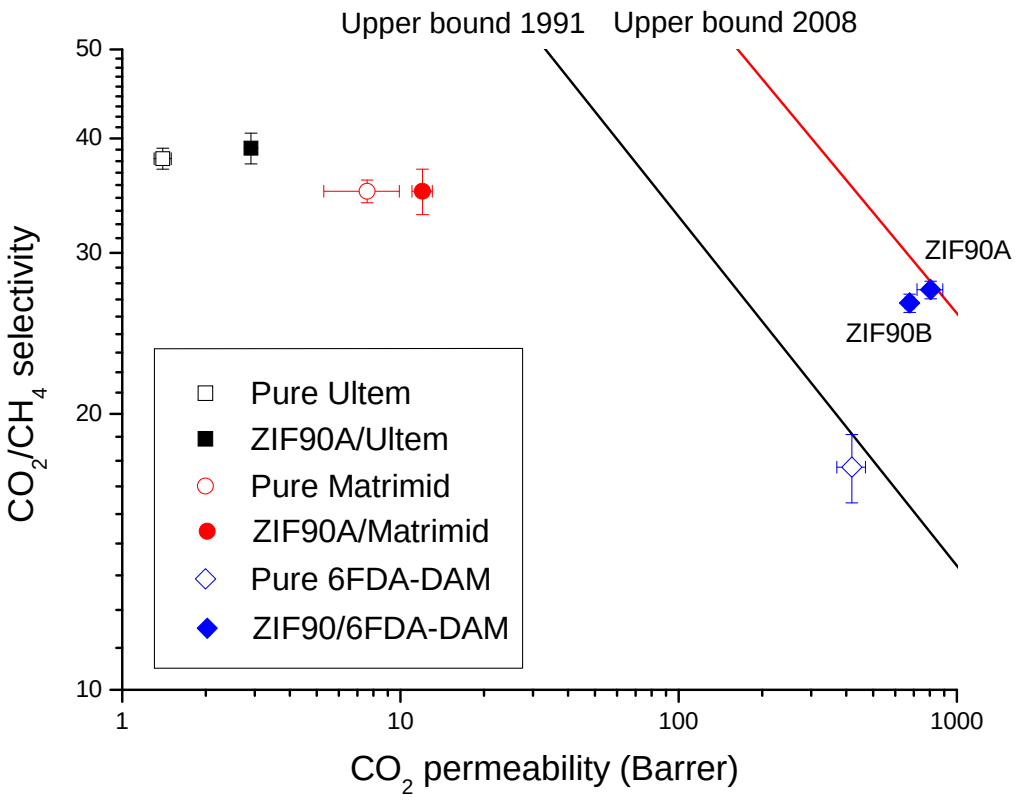

Fig. 5-8 Pure-component gas permeation properties of mixed matrix membranes containing 15 wt% of ZIF-90 crystals; measurements performed at 35 °C and 4.5 atm upstream pressure for Ultem® and Matrimid® membranes and at 25 °C and 2 atm upstream pressure for 6FDA-DAM membranes. The performance of pure Ultem® and Matrimd® are averaged values from the literature [29-31].

5.4 Conclusions

ZIF-90 crystals with submicron and 2-μm sizes were successfully synthesized by a nonsolvent induced crystallization technique. Characterization by XRD, TGA and nitrogen physisorption revealed that the ZIF-90 particles synthesized by this method have high crystallinity, microporosity and good thermal stability. The ZIF-90 particles showed good adhesion with polymers in mixed matrix membranes without any compatibilization.

A significant increase in CO_2 permeability was observed without sacrificing CO_2/CH_4 selectivity when Ultem® and Matrimd® were used as the polymer matrices. In contrast, mixed matrix membranes with a highly permeable polymer such as 6FDA-DAM showed substantial enhancement in both permeability and selectivity, as the transport properties of the two phases were more closely matched.

5.5 References

[1] T.-S. Chung, L.Y. Jiang, Y. Li and S. Kulprathipanja, Prog. Polym. Sci., 32 (2007) 483.

[2] T.T. Moore and W.J. Koros, J. Mol. Struct., 739 (2005) 87.

[3] R. Mahajan and W.J. Koros, Ind. Eng. Chem. Res., 39 (2000) 2692.

[4] R. Mahajan and W.J. Koros, Polym. Eng. Sci., 42 (2002) 1420.

[5] R. Mahajan and W.J. Koros, Polym. Eng. Sci., 42 (2002) 1432.

[6] A.K. Cheetham, G. Ferey and T. Loiseau, Angew. Chem. Int. Ed., 38 (1999) 3268.

[7] J.R. Long and O.M. Yaghi, Chem. Soc. Rev., 38 (2009) 1213.

[8] J.R. Li, R.J. Kuppler and H.C. Zhou, Chem. Soc. Rev., 38 (2009) 1477.

[9] S. Choi, J.H. Drese and C.W. Jones, ChemSusChem, 2 (2009) 796.

[10] L.J. Murray, M. Dinca and J.R. Long, Chem. Soc. Rev., 38 (2009) 1294.

[11] J. Lee, O.K. Farha, J. Roberts, K.A. Scheidt, S.T. Nguyen and J.T. Hupp, Chem. Soc. Rev., 38 (2009) 1450.

[12] D. Zacher, O. Shekhah, C. Woll and R.A. Fischer, Chem. Soc. Rev., 38 (2009) 1418.

[13] Y.Y. Liu, Z.F. Ng, E.A. Khan, H.K. Jeong, C.B. Ching and Z.P. Lai, Micropor. Mesopor. Mater., 118 (2009) 296.

[14] Y. Yoo, Z. Lai and H.-K. Jeong, Micropor. Mesopor. Mater., 123 (2009) 100.

[15] H.L. Guo, G.S. Zhu, I.J. Hewitt and S.L. Qiu, J. Am. Chem. Soc., 131 (2009) 1646.

[16] S.S.Y. Chui, S.M.F. Lo, J.P.H. Charmant, A.G. Orpen and I.D. Williams, Science, 283 (1999) 1148.

[17] R. Ranjan and M. Tsapatsis, Chem. Mater., 21 (2009) 4920.

[18] H. Bux, F.Y. Liang, Y.S. Li, J. Cravillon, M. Wiebcke and J. Caro, J. Am. Chem. Soc., 131 (2009) 16000.

[19] Z.Q. Wang and S.M. Cohen, Chem. Soc. Rev., 38 (2009) 1315.

[20] Y.F. Zhang, I.H. Musseman, J.P. Ferraris and K.J. Balkus, J. Membr. Sci., 313 (2008) 170.

[21] A. Car, C. Stropnik and K.V. Peinemann, Desalination, 200 (2006) 424.

[22] E.V. Perez, K.J. Balkus, J.P. Ferraris and I.H. Musselman, J. Membr. Sci., 328 (2009) 165.

[23] R. Adams, C. Carson, J. Ward, R. Tannenbaum and W. Koros, Micropor. Mesopor. Mater., 131 (2010) 13.

[24] S. Keskin and D.S. Sholl, Energy Environ. Sci., 3 (2010) 343.

[25] P. Raveendran, Y. Ikushima and S.L. Wallen, Acc. Chem. Res., 38 (2005) 478.

[26] W. Morris, C.J. Doonan, H. Furukawa, R. Banerjee and O.M. Yaghi, J. Am. Chem. Soc., 130 (2008) 12626.

[27] J.Q. Liu, T.H. Bae, W.L. Qiu, S. Husain, S. Nair, C.W. Jones, R.R. Chance and W.J. Koros, J. Membr. Sci., 343 (2009) 157.

[28] R. Banerjee, A. Phan, B. Wang, C. Knobler, H. Furukawa, M. O'Keeffe and O.M. Yaghi, Science, 319 (2008) 939.

[29] S. Shu, S. Husain and W.J. Koros, J. Phys. Chem. C, 111 (2007) 652.

[30] D.Q. Vu, W.J. Koros and S.J. Miller, J. Membr. Sci., 211 (2003) 335.

[31] T.A. Barbari, W.J. Koros and D.R. Paul, J. Membr. Sci., 42 (1989) 69.

CHAPTER 6

SUMMARY AND FUTURE WORK

6.1 Summary

The main theme of this dissertation is to engineer nanoporous materials and nanostructured surfaces for applications in membrane separations. I have developed a set of tunable methods to create inorganic hydroxide nanostructures on zeolite surfaces, and used them to control the inorganic/polymer interfacial morphology in zeolite/polymer composite membranes. The study of the structure-property relationships in this material system showed that appropriate tuning of the surface modification methods leads to quite promising structural and permeation properties of the membranes made with the modified zeolites. Moreover, the use of metal organic framework (MOF) materials in mixed matrix membranes has been explored. A MOF/polymer composite membrane synthesized in this work was shown to exhibit technologically attractive permeation properties.

6.1.1 Solvothermal Deposition of Inorganic Nanostructures on Zeolites

In Chapter 2, a facile, high-yield, and inexpensive solvothermal deposition process to prepare roughened inorganic nanostructures on zeolite (MFI) crystal surfaces was presented. SEM characterization showed that the smooth surfaces of the zeolite crystals were altered to roughened surfaces by the formation of nanostructures on the zeolite surfaces after the treatments. The degree of surface roughness was quantified by external surface area measurements and the solvothermally treated particles showed significantly higher roughness than Grignard treated particles. N_2 physisorption

measurements revealed that the micropore volume reduction of the zeolite by the surface treatment was marginal or negligible.

The functionalized zeolite crystals were used in high-quality 'mixed matrix' membranes, wherein the zeolite crystals were used well-adhered to the polymeric matrix. To demonstrate examples of enhanced gas separation in mixed matrix membranes, the pure-component CO_2 and CH_4 gas permeation performance of membranes made with solvothermally modified MFI were measured. High-quality membranes of this type would give large increases in throughput with modest enhancement in selectivity. To rigorously show that the enhanced gas separation performance was due to the high quality of the polymer/modified-MFI interface, gas permeation measurements were used with nonporous (uncalcined) MFI crystals, employing O_2 and N_2 as probes. Experimental results from membranes made with solvothermally treated MFI were well matched with the theoretical predictions, indicating excellent adhesion and no significant interfacial polymer rigidification. The overall results clearly showed that the solvothermal deposition process substantially enhanced polymer/particle adhesion, and is a promising route for processing functional inorganic crystals for membrane applications.

In Chapter 3, the solvothermal treatment was applied to aluminosilicate zeolite LTA, a very good candidate for the separation of CO_2/CH_4. After synthesizing well-defined LTA crystals with 300 nm and 1-2 μm sizes, the solvothermal treatment using ethylenediamine (EDA) as an organic base was performed on LTA crystals. To tune the size/shape of the inorganic nanostructures on the surface of the zeolites, solvothermal

treatment was also performed with diethylenetriamine (DETA) as an organic base. The surface treatments were successful and the resulting LTA crystals had highly roughened surfaces due to the formation of $Mg(OH)_2$ nanostructures on the surfaces. The reaction yield was very high and the mass fraction was close to the stoichiometric maximum for both EDA and DETA routes. The surface roughness of the samples was quantified with the BET external surface area (calculated by a t-plot) using data from the nitrogen physisorption measurements. It was clear that surface roughness of zeolite LTA dramatically increased after deposition of $Mg(OH)_2$ whisker structures. Interestingly, solvothermal treatment with DETA gave rise to higher surface area per unit mass of $Mg(OH)_2$ than the EDA route, indicating that smaller/finer nanostructures were created using DETA. Elemental compositions of both untreated and treated LTA were measured by EDS. After the surface treatment, the Na/Al ratio dramatically decreased, presumably due to ion exchange of extraframework intracrystalline Na^+ in LTA with Mg^{2+} from the reactant solution. This hypothesis is further supported by nitrogen physisorption measurements, as micropore volumes of solvothermally treated LTAs were intermediate between those of Na-LTA and Mg-LTA, indicating a partial ion exchange of Na^+ with Mg^{2+}.

SEM observation revealed that mixed matrix membranes fabricated with solvothermally treated LTAs were uniformly free of interfacial voids and the individual particles were well distributed in polymer matrix due to their improved interaction with the polymer. In contrast, membranes with untreated LTA showed a typical sieve-in-a-cage morphology. The CO_2/CH_4 separation performance was measured with the membranes

containing 20 wt% of surface treated LTA. Both CO_2 permeability and CO_2/CH_4 selectivity were slightly enhanced compared to the pure polymer but the performance was lower than the theoretical prediction.

6.1.2 Ion-Exchange Induced Growth of Inorganic Nanostructures on Zeolites

To create inorganic nanostructures on the surface of LTA in a controlled manner by an aqueous phase reaction, the inherent ion-exchange chemistry of zeolites was used. In this method, the amount of $Mg(OH)_2$ in the final product was simply controlled by changing the loading of Mg^{2+} ions in the zeolite when Mg-LTA was initially prepared. It was also found that the size/shape of the nanostructures could be tuned by adjusting the pH of the aqueous solution. For example, when a high pH solution, such as 0.1M NaOH, was used, relatively bigger nanostructures were formed. The micropore volume of this material, however, was very low compared to the original LTA, presumably due to partial dissolution of the external region of the LTA particles at such a high pH and temperature (160 ^{o}C). Reaction at pH 9.5 gave rise to fine nanostructures and the reaction yield was much higher than the previous method. XRD analysis showed that the LTA framework was retained after the treatment, but a significant micropore volume reduction compared to original LTA was observed, presumably due to partial pore blocking by the high density of nanostructures. However, the pore blocking problem was solved by optimizing the initial amount of the magnesium source in the zeolite substrate. This systematic modification of the reaction conditions led to a good candidate for application in mixed matrix membranes.

According to SEM observations, the zeolite/polymer adhesion in mixed matrix membranes was improved after the surface treatment compared to a typical "sieve-in-a-cage" morphology of untreated, bare LTA mixed matrix membranes. IE-3-5A/6FDA-DAM mixed matrix membrane showed significant enhancement in CO_2 permeability with a slight increase in the CO_2/CH_4 selectivity compared to pure polymer membrane. The CO_2/CH_4 selectivity of the membrane containing surface modified zeolite was much higher than that of membrane with untreated 5A.

6.1.3 Metal Organic Framework Mixed Matrix Membranes

Based on recent computational results, ZIF-90 was selected as a promising material for the fabrication of CO_2-selective mixed matrix membranes. To obtain ZIF-90 crystals suitable for application in such membranes, a novel synthesis method was developed, namely nonsolvent induced crystallization. The sizes of the resulting crystals were 800 nm or 2 μm when methanol and DI water were used as the nonsolvent, respectively. The structural investigation revealed that the ZIF-90 crystals had a good crystallinity and microporosity, even though they were rapidly formed at room temperature. Furthermore, the thermal stability was better than that of the traditional solvothermally synthesized particles.

SEM observation revealed that the ZIF-90 particles showed good adhesion with polymers in mixed matrix membranes without any compatibilization treatment. A significant increase in CO_2 permeability was observed without sacrificing CO_2/CH_4 selectivity when polymers with low permeability, such as Ultem® and Matrimd®, were

used as the polymer matrix. No enhancement in selectivity may indicate a mismatch of the permeabilities of the two phases. In contrast, mixed matrix membranes with highly permeable polymers, such as 6FDA-DAM, showed substantial enhancement in both permeability and selectivity, as the permeabilities of the two phases were more closely matched. As the best example, the performance of 15 wt% of 800 nm ZIF-90/6FDA-DAM was excellent and was located beyond the upper bound limit of polymer membranes.

6.2 Future Works

The present work leads to a number of interesting avenues for further research, some of which are described below.

6.2.1 Application of Surface Treatment to Other Zeolites

Zeolites PS-MFI and LTA have an extensive literature and were used as model zeolites in this thesis. However, they are not necessarily the best available molecular sieves for application in gas separations. There are several zeolites that can be used in the fabrication of potential high performance mixed matrix membranes, such as DDR and CHA. The surface treatments developed in this study can be applied to the surfaces of these zeolites to control the interfacial morphology in mixed matrix membranes. This is one of the potential advantages of the methods developed in this thesis over compatibilization using silane chemistry.

Zeolite DDR is an excellent molecular sieve for CO_2/CH_4 separation, and several

DDR membranes (continuous film) have been reported [1-4]. The zeolite DDR has a two-dimensional pore structure with a small pore window (0.36 x 0.44 nm) constructed by an 8-membered ring (Fig. 6-1) [5]. A recent simulation study predicted an excellent CO_2/CH_4 selectivity for pure silica DDR [6]. Thus, mixed matrix membranes containing DDR are potential high performance CO_2 selective membranes if the control of interfacial morphology is successful. First of all, DDR with appropriate sizes for the mixed matrix membrane fabrication should be synthesized. The pure silica DDR surface can be then treated by the solvothermal method described in Chapter 2. Since both PS-MFI and PS-DDR have the same chemical composition, the treatment may be applied to the DDR surface without any expected issues. As shown in the Chapter 3, the solvothermal treatment was already applied to aluminosilicate LTA surfaces that have much different surface properties.

Ion-exchange induced surface treatment described in Chapter 4 can be applied to zeolite CHA, which is also a good molecular sieve for CO_2 separation [7-9]. The zeolite CHA has three-dimensional pore structure with a small pore window (0.38 x 0.38 nm) constructed by an 8-membered ring (Fig. 6-2) [5]. CHA has been synthesized in both aluminosilicate (SSZ-13) and silicoaluminophosphate (SAPO-34) forms. Both molecular sieves contain extraframework cations which are reversibly exchangeable. The reaction conditions used in the LTA treatment may be modified while monitoring the morphology of the nanostructures and the framework integrity of zeolites. The reaction conditions should be mild so that the framework of zeolites can be retained after the treatment.

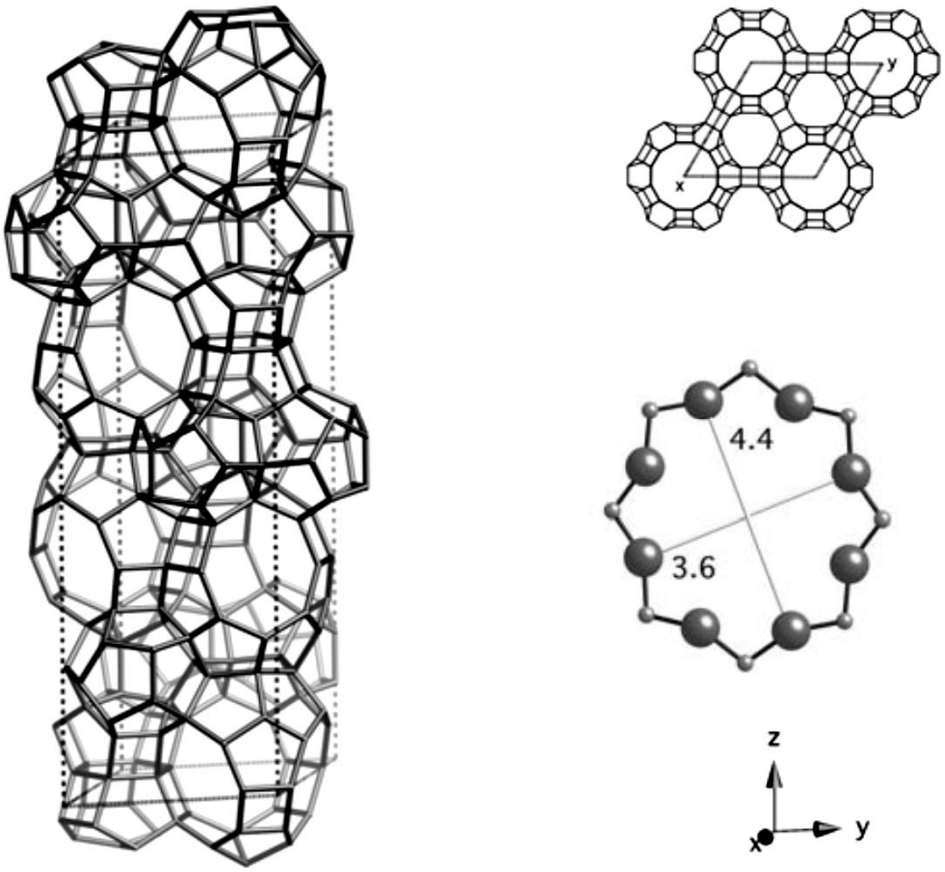

Fig. 6-1 The framework structure of zeolite DDR; left: framework viewed normal to [001], upper right: projection down [001], lower right: dimension of 8-membered ring in Å. [5]

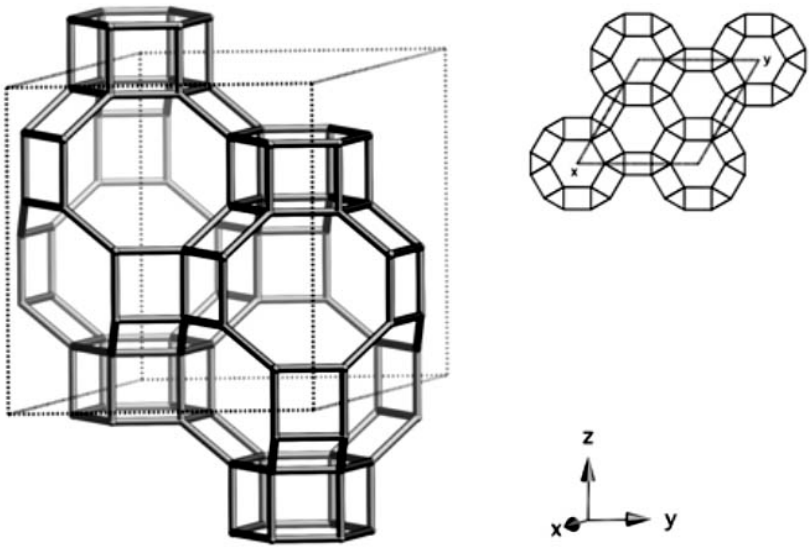

Fig. 6-2 The framework structure of zeolite CHA; left: framework viewed normal to [001], upper right: projection down [001] [5].

6.2.2 Inorganic Nanostructures with Various Materials

In this thesis, $Mg(OH)_2$ nanostructures were used for roughening zeolite surfaces. Other inorganic materials can also be used for this purpose, and will broaden the range of surface properties that can be achieved. Metal hydroxides such as $Ca(OH)_2$ and $Al(OH)_3$ are good starting materials for generalization of the methods developed in this thesis, since the formation mechanism may be similar with $Mg(OH)_2$. Fig. 6-3a shows a preliminary synthesis of $Ca(OH)_2$ nanostructures on the surface of 5 μm PS-MFI created by solvothermal deposition. $CaCl_2$ and ethylenediamine were used as the calcium source and the organic base, respectively. The $Ca(OH)_2$-surface-roughened PS-MFI crystals also showed improved adhesion with Ultem® as shown in Fig. 6-3b. Ion-exchange induced treatment can potentially be used to form $Ca(OH)_2$ on zeolite surfaces by loading Ca^{2+}

ions in substrates instead of Mg^{2+}. The solubility of $Ca(OH)_2$ in the solution will be an important parameter. The reaction conditions, especially pH, should be tuned accordingly for successful zeolite surface treatments.

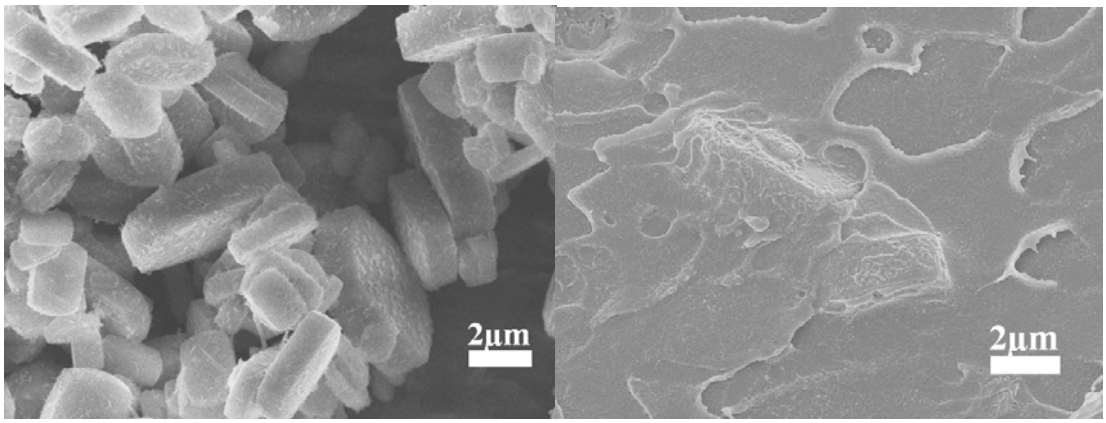

(a) (b)

Fig. 6-3 Solvothermal-based $Ca(OH)_2$ nanostructure fabrication on the surfaces of pure-silica MFI; (a) surface-treated pure-silica-MFI and (b) cross section of mixed matrix dense film made with surface treated MFI and Ultem®.

Metal oxides are also potential candidates for creating roughened surfaces on zeolites. They generally have better mechanical strength and thermal/chemical stability than hydroxides. Numerous studies on preparation of metal oxide nanostructures have been reported so far. However, most of studies have dealt with nanostructure formation in the homogeneous phase and not on growth on substrates. Thus, a new methodology should be developed to create metal oxides on the zeolite surface rather than in bulk solution. The ion-exchange induced treatment in Chapter 4 is a good example for a possible surface-mediated growth of the inorganic nanostructures.

6.2.3 Fabrication of Asymmetric Hollow Fiber Membranes

All membranes described in this thesis were fabricated in dense film form. This is a prototype membrane suitable for the investigation of inherent transport properties of membrane materials. However, for industrial applications, membranes should be processed into an asymmetric structure, wherein a thin, dense skin layer exists on a porous support layer. This ensures a high flux by minimizing the mass transport resistance. For example, the asymmetric hollow fiber is a widely used membrane form in many fields. Fig 6-4 shows a schematic description of mixed matrix hollow fiber membranes. The dual layer spinning technique allows the creation thin mixed matrix skin layers on a porous support that is usually made of inexpensive polymers [10].

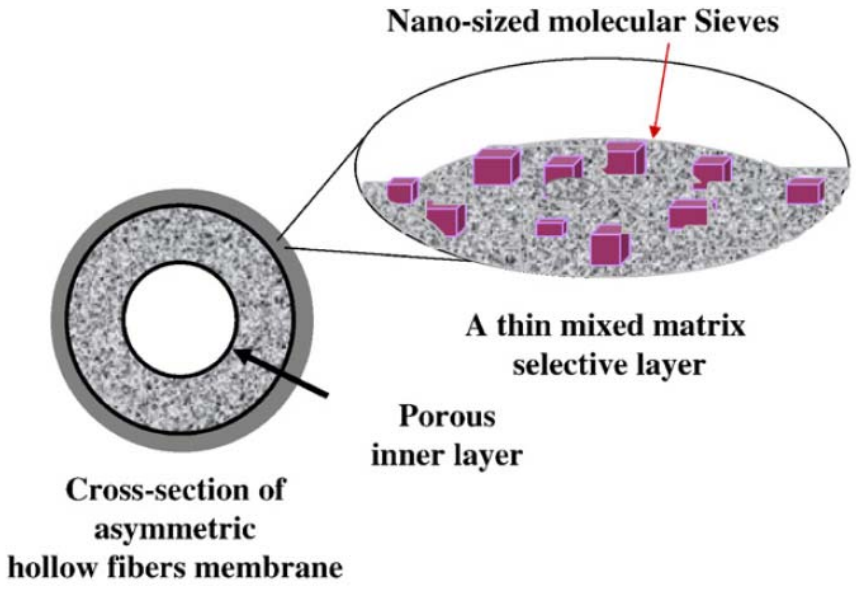

Fig. 6-4 Schematic cross-section morphology of a hollow fiber with a polymer/zeolite mixed matrix skin [10].

Several zeolite surface treatments were developed in this work for the control of the interfacial morphology in mixed matrix dense films. However, the membrane formation mechanism in hollow fiber spinning is different from that of dense films. In general, stress generated at the zeolite/polymer interfaces induced by wet precipitation is higher than that by solvent evaporation. In future work targeted towards high-performance membrane fabrication, the zeolite/polymer adhesion and gas transport properties should be investigated in hollow fiber membranes. The gas transport properties of metal organic framework mixed matrix hollow fiber membranes should also be investigated.

6.3 References

[1] S. Himeno, T. Tomita, K. Suzuki, K. Nakayama, K. Yajima and S. Yoshida, Ind. Eng. Chem. Res., 46 (2007) 6989.

[2] M. Kanezashi, J. O'Brien-Abraham, Y.S. Lin and K. Suzuki, AIChE J., 54 (2008) 1478.

[3] T. Tomita, K. Nakayama and H. Sakai, Micropor. Mesopor. Mater., 68 (2004) 71.

[4] J. van den Bergh, A. Tihaya and F. Kapteijn, Micropor. Mesopor. Mater., 132 (2010) 137.

[5] C. Baerlocher, Atlas of zeolite framework types, Published on behalf of the Structure Commission of the International Zeolite Association by Elsevier, Amsterdam ;, 2007.

[6] S.E. Jee and D.S. Sholl, J. Am. Chem. Soc., 131 (2009) 7896.

[7] Y. Hasegawa, H. Hotta, K. Sato, T. Nagase and F. Mizukami, J. Membr. Sci., 347 (2010) 193.

[8] H. Kalipcilar, T.C. Bowen, R.D. Noble and J.L. Falconer, Chem. Mater., 14 (2002) 3458.

[9] H. Lee and P.K. Dutta, Micropor. Mesopor. Mater., 38 (2000) 151.

[10] T.-S. Chung, L.Y. Jiang, Y. Li and S. Kulprathipanja, Prog. Polym. Sci., 32 (2007) 483.